Eur. Phys. J. C (2023) 83:515
https://doi.org/10.1140/epjc/s10052-023-11434-w

THE EUROPEAN PHYSICAL JOURNAL C

Regular Article - Experimental Physics

Searches for new phenomena in events with two leptons, jets, and missing transverse momentum in 139 fb^{-1} of $\sqrt{s} = 13$ TeV pp collisions with the ATLAS detector

ATLAS Collaboration[⋆]

CERN, 1211 Geneva 23, Switzerland

Received: 28 April 2022 / Accepted: 5 September 2022 / Published online: 19 June 2023

Abstract Searches for new phenomena inspired by supersymmetry in final states containing an e^+e^- or $\mu^+\mu^-$ pair, jets, and missing transverse momentum are presented. These searches make use of proton–proton collision data with an integrated luminosity of 139 fb^{-1}, collected during 2015–2018 at a centre-of-mass energy $\sqrt{s} = 13$ TeV by the ATLAS detector at the Large Hadron Collider. Two searches target the pair production of charginos and neutralinos. One uses the recursive-jigsaw reconstruction technique to follow up on excesses observed in 36.1 fb^{-1} of data, and the other uses conventional event variables. The third search targets pair production of coloured supersymmetric particles (squarks or gluinos) decaying through the next-to-lightest neutralino ($\tilde{\chi}_2^0$) via a slepton ($\tilde{\ell}$) or Z boson into $\ell^+\ell^-\tilde{\chi}_1^0$, resulting in a kinematic endpoint or peak in the dilepton invariant mass spectrum. The data are found to be consistent with the Standard Model expectations. Results are interpreted using simplified models and exclude masses up to 900 GeV for electroweakinos, 1550 GeV for squarks, and 2250 GeV for gluinos.

Contents

1 Introduction

Supersymmetric (SUSY) [1–6] extensions to the Standard Model (SM) have the potential to resolve the SM gauge hierarchy problem, explain the origin of dark matter [7,8], and lead to a grand unified theory of nature [9–12]. Partner particles, called sparticles, differ from their SM counterparts by half a unit of spin. The scalar partners of quarks and leptons are squarks ($\tilde{q}$) and sleptons ($\tilde{\ell}$) respectively. Gluinos ($\tilde{g}$) are the fermionic partners of gluons. Charginos ($\tilde{\chi}_i^{\pm}$) and neutralinos ($\tilde{\chi}_i^0$) are the mass eigenstates of the mixing between the SUSY partners of the Higgs (higgsinos) and electroweak bosons, where i runs from the lightest to heaviest mass. If R-parity is conserved [13], then the lightest SUSY particle (LSP) is stable and a good candidate for dark matter.

This paper reports on searches for electroweak and strong production of sparticles in events with exactly two same-flavour (SF) opposite-sign (OS) electrons or muons, jets, and missing transverse momentum ($\vec{p}_{\mathrm{T}}^{\,\mathrm{miss}}$, with magnitude $E_{\mathrm{T}}^{\mathrm{miss}}$). The full Run 2 dataset of 13 TeV proton–proton collisions collected by the ATLAS detector [14] at the Large Hadron Collider (LHC) [15] is used, corresponding to an integrated luminosity of 139 fb^{-1}. The same-flavour lepton

⋆ e-mail: atlas.publications@cern.ch

final state is used in order to make use of the dilepton system's invariant mass ($m_{\ell\ell}$) as a discriminant to search for events in models with leptonic Z boson decays or models where the $m_{\ell\ell}$ distribution has a kinematic endpoint. Two searches targeting electroweak production of sparticles and one targeting strong production are considered. The first consists of two signal regions (SRs), using recursive-jigsaw reconstruction (RJR) variables [16] targeting electroweak production, which check whether previously observed excesses of 2.0σ and 1.4σ above the SM expectations in the 36 fb^{-1} 13 TeV dataset collected during 2015–2016 [17] persist with more data. This is referred to as the RJR search, and only model-independent upper limits are presented for it. The same 36 fb^{-1} 13 TeV analysis also included three-lepton regions which had 3.0σ and 2.1σ excesses above the Standard Model expectations, which were not observed with more data [18]. This previous search, and this update, used RJR variables designed to target electroweak production of SUSY particles. The second targets electroweak (EWK) production of chargino–neutralino pairs decaying to W and Z bosons along with two $\tilde{\chi}_1^0$ neutralinos, and also includes a new search inspired by gauge-mediated SUSY breaking (GMSB) [19–21] targeting the pair production of higgsino next-to-lightest SUSY particles (NLSPs) decaying into a ZZ or Zh pair and gravitino LSPs. This is referred to as the EWK search, and it follows a methodology similar to that used in the two-lepton channel in a previous search [22] using the 36 fb^{-1} 13 TeV dataset, but with optimizations for the full Run 2 dataset and a new region targeting off-shell Z boson decays. The third, the Strong search, targets the production of gluino or squark pairs that produce lepton pairs from $\tilde{\chi}_2^0 \to \ell^+\ell^-\tilde{\chi}_1^0$ decays and follows a methodology similar to that in a previous search [23] based on 36 fb^{-1} of 13 TeV data, also with optimizations for the full Run 2 dataset. These updated EWK and Strong searches benefit from a larger dataset and an optimization of the analysis, generally resulting in tighter selection requirements for signal-like events. The EWK search now includes additional binning of the SRs, further improving sensitivity to the considered signal models.

The EWK and Strong searches interpret the results with simplified models, described in the next section, by performing separate model-dependent profile likelihood fits [24] in their respective regions. All three searches also report upper limits on possible beyond-the-SM (BSM) event yields from model-independent fits to single-bin regions, where the BSM signal is assumed to only populate the SR.

The EWK search presented here extends the sensitivity to GMSB models with $\tilde{\chi}_1^0$ masses in the 400–500 GeV range, between the limits from ATLAS searches in a four-lepton final state [25] and an all-hadronic final state [26]. It also reaches higher $\tilde{\chi}_1^0$ masses around chargino masses of 600 GeV for the C1N2 model described in Table 1, between the limits from ATLAS searches in a three-lepton final state [18] and the same electroweak all-hadronic search. The Strong search has a gluino mass sensitivity similar to that of an ATLAS search in a single-lepton final state [27]. The zero-lepton ATLAS search [28] has sensitivity to gluinos a few hundred GeV heavier than in both of these searches, but the Strong search presented here has sensitivity to higher $\tilde{\chi}_1^0$ masses. A strong all-hadronic search also has sensitivity to squarks a few hundred GeV heavier than in the Strong search. Unlike the EWK searches targeting the same model with different SM boson decays, the decay chains of the gluinos and squarks differ between the various strong searches. Thus each analysis complements each other by testing different assumptions of the SUSY particle spectra.

Similar searches have been performed by the CMS Collaboration with the full Run 2 dataset. For electroweak production, limits on chargino–neutralino production (C1N2 model in Table 1) were presented in Ref. [29] and on the GMSB model in Ref. [30], albeit with a different final state requiring same-charge leptons or more than two leptons. For strong production, limits on similar models but with different parameterizations were presented in Ref. [29].

This paper is organized with the common aspects of the searches preceding sections with the details specific to each search. Section 2 describes the SUSY signal models targeted in this paper. Section 3 describes the ATLAS detector. Section 4 describes the data and simulated samples used to guide the analysis strategy and estimate background and signal yields. Section 5 describes the event reconstruction and criteria used to identify the physics objects used in the searches. Section 6 describes the event selections that define the various search regions in each search. Section 7 describes the background estimation for each search. Section 8 describes the uncertainties. Sections 9 and 10 present the results and interpretations of the results, respectively. The conclusions are presented in Sect. 11.

2 SUSY signal models

Simplified models [31–33] inspired by SUSY are used to guide the search strategy and interpret the results. Two classes of models that contain production of weakly interacting or strongly interacting SUSY particles are used. Each model is scanned over a two-dimensional space, varying the masses or decay branching ratios of sparticles. Table 1 summarizes the simplified models considered for analysis. As mentioned in Sect. 1, electrons or muons are required to be in the final state, including those from leptonic decays of τ-leptons. However, these will often fail SR requirements related to boson mass compatibility.

Two models of electroweak sparticle production are considered. The first is the production of a chargino ($\tilde{\chi}_1^\pm$) and the second-lightest neutralino ($\tilde{\chi}_2^0$), henceforth the C1N2 model,

Table 1 Summary of the simplified signal model topologies used in this paper. Here x and y denote the x–y plane across which the signal model masses, or branching fraction B, are varied to construct the signal grid. A dash (−) signifies the column is irrelevant for that model. For the gluino–slepton model, the masses of the superpartners of the left-handed leptons are given by $[m(\tilde{\chi}_2^0) + m(\tilde{\chi}_1^0)]/2$, while the superpartners of the right-handed leptons are decoupled. The gluino and squark decays have equal branching fractions for $q = u, d, c, s, b$

Model	Production mode	x	y	$[x+y]/2$
C1N2	$\tilde{\chi}_1^\pm\ \tilde{\chi}_2^0$	$m(\tilde{\chi}_1^\pm) = m(\tilde{\chi}_2^0)$	$m(\tilde{\chi}_1^0)$	–
GMSB	$\tilde{\chi}_1^0\ \tilde{\chi}_1^0$	$m(\tilde{\chi}_1^0)$	$B(\tilde{\chi}_1^0 \to h\tilde{G})$	–
Gluino–slepton	$\tilde{g}\tilde{g}$	$m(\tilde{g})$	$m(\tilde{\chi}_1^0)$	$m(\tilde{\chi}_2^0)$
Gluino–$Z^{(*)}$	$\tilde{g}\tilde{g}$	$m(\tilde{g})$	$m(\tilde{\chi}_1^0)$	$m(\tilde{\chi}_2^0)$
Squark–$Z^{(*)}$	$\tilde{q}\tilde{q}$	$m(\tilde{q})$	$m(\tilde{\chi}_1^0)$	$m(\tilde{\chi}_2^0)$

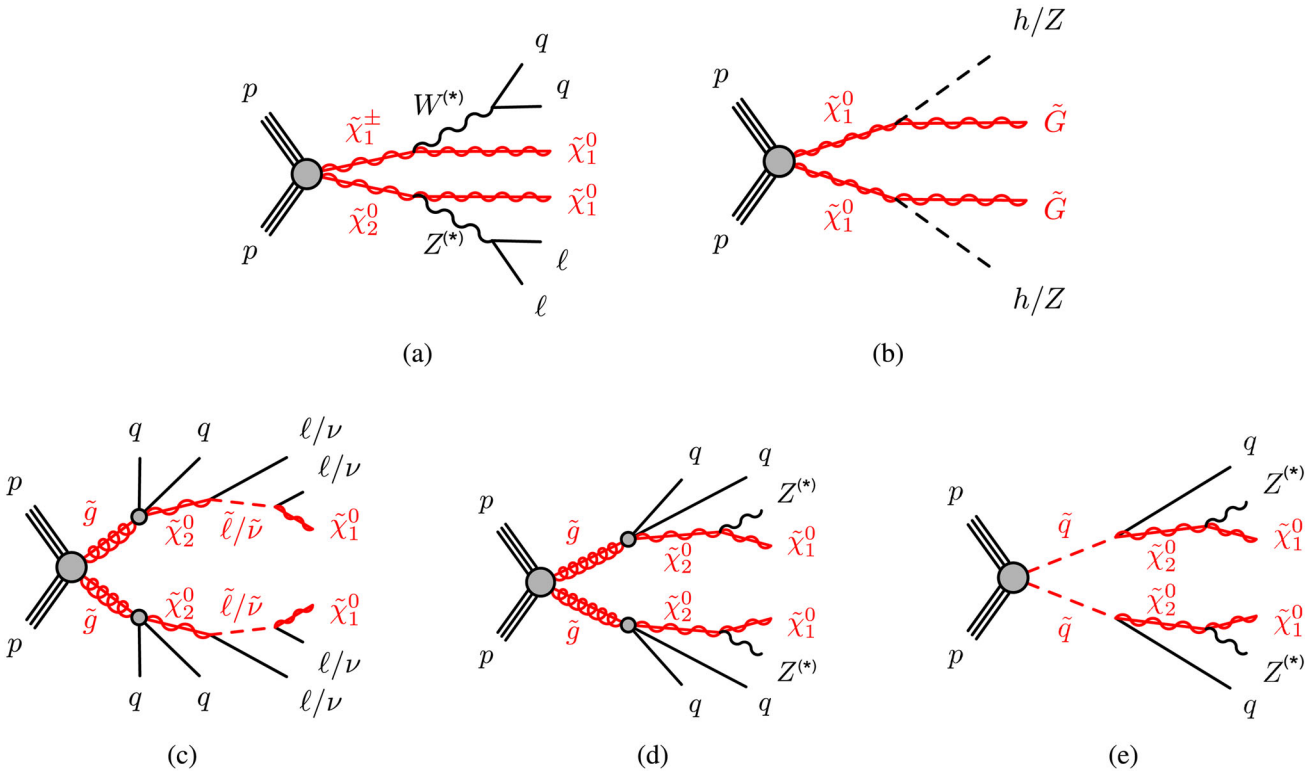

Fig. 1 Example decay topologies for the (top row) two electroweak SUSY models and (bottom row) three strong SUSY models considered in the analysis. Model (**a**) shows the process $\tilde{\chi}_2^0\tilde{\chi}_1^\pm \to W^{(*)}(jj)Z^{(*)}(\ell\ell) + E_{\mathrm{T}}^{\mathrm{miss}}$ and model (**b**) shows a gauge-mediated SUSY breaking model with a higgsino next-to-lightest SUSY particle and gravitino lightest SUSY particle. For the strong-production models, the left two decay topologies involve gluino pair production, with the gluinos following an effective three-body decay for $\tilde{g} \to q\bar{q}\tilde{\chi}_2^0$, with $\tilde{\chi}_2^0 \to \tilde{\ell}^\mp\ell^\pm/\tilde{\nu}\nu$ for the gluino–slepton model (**c**) and $\tilde{\chi}_2^0 \to Z^{(*)}\tilde{\chi}_1^0$ in the gluino–$Z^{(*)}$ model (**d**). The diagram (**e**) illustrates the squark–$Z^{(*)}$ model, where squarks are pair-produced, followed by the decay $\tilde{q} \to q\tilde{\chi}_2^0$, with $\tilde{\chi}_2^0 \to Z^{(*)}\tilde{\chi}_1^0$

which decay via a W boson and Z boson respectively into LSPs, $\tilde{\chi}_1^0$. The $\tilde{\chi}_1^\pm$ and $\tilde{\chi}_2^0$ are assumed to have equal masses and always decay into a W and Z boson respectively. A diagram of this model is shown in Fig. 1a. The second is the pair production of higgsino neutralinos ($\tilde{\chi}_1^0$), which decay into a Higgs or Z boson and a nearly massless gravitino ($\tilde{G}$). This model is inspired by GMSB [19–21] and referred to as the GMSB model. A diagram of this model is shown in Fig. 1b. The branching ratio of the $\tilde{\chi}_1^0$ to a Higgs boson, alternatively a Z boson, is varied from 0 to 100%.

Three models of strong sparticle pair production are considered. The choice of mass parameterization, namely setting intermediate particles halfway between the parent and child, enhances the topological differences between these simplified models and others with fewer intermediate particles in the decay chains [34] or very small mass differences between particles. Changing this assumption matters when interpreting the particle spectrum of a new signal, but does not affect the sensitivity of the analysis to generic kinematic endpoint features. In all three models, the gluino (or squark) and $\tilde{\chi}_1^0$ masses are varied to produce a two-dimensional grid of signal models for interpretation. The gluino and squark decays have equal branching fractions for $q = u, d, c, s, b$. The first strong-production model, shown in Fig. 1c, is referred to as the gluino–slepton model, and assumes that the sleptons are lighter than the $\tilde{\chi}_2^0$. The gluino decays via a $\tilde{\chi}_2^0$, which subsequently decays via a slepton or sneutrino ($\tilde{\nu}$) to the LSP ($\tilde{\chi}_1^0$). The two decay channels, $\tilde{\chi}_2^0 \to \tilde{\ell}^\mp \ell^\pm$ with $\tilde{\ell} \to \ell \tilde{\chi}_1^0$ or $\tilde{\chi}_2^0 \to \tilde{\nu}\nu$ with $\tilde{\nu} \to \nu \tilde{\chi}_1^0$, have equal probability. Only the superpartners of the left-handed leptons are allowed in the decays and they are taken to be mass degenerate, with a mass equal to the average of the $\tilde{\chi}_2^0$ and $\tilde{\chi}_1^0$ masses. The superpartners of the right-handed leptons are decoupled. In this model, a kinematic endpoint in the dilepton invariant mass forms near half of the difference between the gluino and $\tilde{\chi}_1^0$ masses, given by $m_{\ell\ell} = \sqrt{(m^2_{\tilde{\chi}_2^0} - m^2_{\tilde{\ell}})(m^2_{\tilde{\ell}} - m^2_{\tilde{\chi}_1^0})/m^2_{\tilde{\ell}}}$ [35]. This endpoint serves as an unambiguous signature of new physics that probes a wide variety of signal models, which can produce excesses over the entire $m_{\ell\ell}$ spectrum.

The second model, shown in Fig. 1d, is referred to as the gluino–$Z^{(*)}$ model, where the $\tilde{\chi}_2^0$ from the gluino decay then decays as $\tilde{\chi}_2^0 \to Z^{(*)}\tilde{\chi}_1^0$. The $\tilde{\chi}_2^0$ mass is set to the average of the gluino and $\tilde{\chi}_1^0$ masses.

The final model, shown in Fig. 1e, is referred to as the squark–$Z^{(*)}$ model, where the squark decays through a $\tilde{\chi}_2^0$ to a Z boson and the LSP ($\tilde{\chi}_1^0$). Similarly to the gluino–$Z^{(*)}$ model, the $\tilde{\chi}_2^0$ mass is set to the average of the $\tilde{q}$ and $\tilde{\chi}_1^0$ masses. Both of these models with decays to a Z boson result in a kinematic endpoint in the dilepton invariant mass if the mass-splitting between the $\tilde{\chi}_2^0$ and $\tilde{\chi}_1^0$ is smaller than the Z boson mass. If the mass-splitting is larger than the Z boson mass, the models result in a peak in $m_{\ell\ell}$ at the Z boson mass. The superpartners of $q = u, d, c, s, b$ are all set to the same mass, with the superpartner of the t-quark decoupled.

3 ATLAS detector

The ATLAS detector [14] is a multipurpose particle detector with a forward–backward symmetric cylindrical geometry and a near 4π coverage in solid angle.[1] It consists of an inner tracking detector surrounded by a thin superconducting solenoid providing a 2T axial magnetic field, electromagnetic and hadronic calorimeters, and a muon spectrometer. The inner tracking detector covers the pseudorapidity range $|\eta| < 2.5$. It consists of silicon pixel, silicon microstrip, and transition radiation tracking detectors. An additional layer of silicon pixels, the insertable B-layer [36,37], was installed before Run 2. Lead/liquid-argon (LAr) sampling calorimeters provide electromagnetic (EM) energy measurements with high granularity. A steel/scintillator-tile hadron calorimeter covers the central pseudorapidity range ($|\eta| < 1.7$). The endcap and forward regions are instrumented with LAr calorimeters for both the EM and hadronic energy measurements up to $|\eta| = 4.9$. The muon spectrometer surrounds the calorimeters and is based on three large superconducting air-core toroidal magnets with eight coils each. The field integral of the toroids ranges between 2.0 and 6.0 Tm across most of the detector. The muon spectrometer includes a system of precision chambers for tracking and fast detectors for triggering. A two-level trigger system is used to select events. The first-level trigger is implemented in hardware and uses a subset of the detector information to accept events at a rate below 100 kHz. This is followed by a software-based trigger that reduces the accepted event rate to 1 kHz on average depending on the data-taking conditions. An extensive software suite [38] is used in the reconstruction and analysis of real and simulated data, in detector operations, and in the trigger and data acquisition systems of the experiment.

4 Data and simulated samples

The LHC pp collision data used in this analysis were collected by the ATLAS detector during 2015–2018 at a centre-of-mass collision energy of 13 TeV. After imposing requirements for beam and detector conditions and data quality

[1] ATLAS uses a right-handed coordinate system with its origin at the nominal interaction point (IP) in the centre of the detector and the z-axis along the beam pipe. The x-axis points from the IP to the centre of the LHC ring, and the y-axis points upwards. Cylindrical coordinates (r, ϕ) are used in the transverse plane, ϕ being the azimuthal angle around the z-axis. The pseudorapidity is defined in terms of the polar angle θ as $\eta = -\ln\tan(\theta/2)$. Angular distance is measured in units of $\Delta R \equiv \sqrt{(\Delta\eta)^2 + (\Delta\phi)^2}$.

[39], the dataset corresponds to an integrated luminosity of 139 fb^{-1}. The uncertainty in the combined 2015–2018 integrated luminosity is 1.7% [40], obtained using the LUCID-2 detector [41] for the primary luminosity measurements.

Data events were collected using dilepton triggers with p_{T} thresholds of 7–26 GeV varying with lepton flavour and data-taking period [42,43]. In 2017 and 2018, the asymmetric electron–muon trigger had thresholds of 26 and 8 GeV respectively, where 26 GeV is above the lepton p_{T} requirement used in the analysis. The p_{T} range below the trigger threshold is covered by an asymmetric muon–electron trigger with thresholds of 24 and 7 GeV respectively. The use of the electron–muon trigger compensates for trigger inefficiencies due to the first-level muon trigger as it is seeded only by the first-level electromagnetic trigger. The rest of the triggers used have thresholds of at most 24 GeV. Typical efficiencies for the muon part of a dilepton trigger requiring a single muon, including a Level-1 accept, is between 75 and 85% depending on the muon p_{T} and η. For electrons, the typical efficiency for a single part of a dilepton trigger is between 85 and 97% depending on the electron p_{T} and η.

Simulated event samples are used to help estimate the SM backgrounds, validate the analysis techniques, optimize the event selection, and provide predictions of the SUSY signal processes. The majority of the SM process samples were generated with Sherpa 2.2 [44] or with Powheg Box v2 [45–47] and Pythia 8 [48] for the simulation of the parton shower (PS), hadronization, and underlying event. The details of the matrix element (ME) generator, PS and parameter values (tune), parton distribution function (PDF) choice, and cross-section for the SM processes are listed in Table 2. The $t\bar{t}$ and Wt processes are referred to as 'Top' events. The VV processes, where $V = W$ or Z, are referred to as 'Diboson' events. The remaining smaller backgrounds, except Z/γ^*+jets, are referred to as 'Other' events. The Other events category also includes the fake and non-prompt (FNP) lepton background estimated from data as described in Sect. 7.

The signal samples were generated using MG5_aMC@NLO 2.2.3 [71] interfaced to Pythia 8.186 with the A14 tune for the modelling of the PS, hadronization and underlying event. The ME calculation was performed at tree level and includes the emission of up to two additional partons. The PDF set used for event generation was NNPDF2.3lo. The ME–PS matching used the CKKW-L prescription, with a matching scale set to a quarter of the mass of the initial SUSY particle.

For the C1N2 and GMSB signal models, cross-sections are calculated to next-to-leading order in the strong coupling constant, adding the resummation of soft gluon emission at next-to-leading-logarithm accuracy (NLO+NLL) [78–82]. The nominal cross-section and its uncertainty are taken from an envelope of cross-section predictions using different PDF sets and factorization and renormalization scales, as described in Ref. [83].

For the gluino and squark signal models, cross-sections are calculated to approximate next-to-next-to-leading order in the strong coupling constant, adding the resummation of soft gluon emission at next-to-next-to-leading-logarithm accuracy (approximate NNLO+NNLL) [84–91]. The nominal cross-section and its uncertainty are derived using the PDF4LHC15_mc PDF set, following the recommendations of Ref. [92].

The SM background Monte Carlo (MC) samples were passed through a full simulation of the ATLAS detector [93] using Geant4 [94]. A fast simulation [93] was used for the signal MC samples; it relies on a parameterization of the lateral and longitudinal shower shapes of single particles in the calorimeters, and on Geant4 elsewhere. The effect of multiple pp interactions per bunch crossing (pile-up) and detector-response effects due to interactions in neighbouring bunch crossings were included by overlaying the simulated hard-scattering events with additional inelastic pp collision events generated with Pythia 8.186.

5 Analysis object identification and selection

Leptons and jets selected for analysis are categorized as 'baseline' or 'signal' objects by using various quality and kinematic requirements. Baseline objects are used in the computation of the missing transverse momentum ($\vec{p}_{\mathrm{T}}^{\,\mathrm{miss}}$) and its magnitude ($E_{\mathrm{T}}^{\mathrm{miss}}$), to resolve ambiguities between closely spaced analysis objects, and to ensure orthogonality to other analyses. The signal objects used in the analysis selection are required to pass more stringent requirements.

Electron candidates are reconstructed using energy clusters in the electromagnetic calorimeter matched to inner-detector tracks. Baseline electrons are required to have $p_{\mathrm{T}} >$ 4.5 GeV, satisfy the 'loose likelihood' criteria described in Ref. [95], and reside within the region $|\eta| < 2.47$. Additionally, the baseline-electron tracks must pass within $|z_0 \sin\theta| =$ 0.5 mm of the primary vertex, defined as the vertex with the largest sum of track p_{T}^2, where z_0 is the longitudinal impact parameter with respect to the primary vertex. Signal electrons are required to satisfy the 'medium likelihood' criteria of Ref. [95] and to have $p_{\mathrm{T}} > 25$ GeV. The transverse-plane distance of closest approach of the signal electron to the beamline, divided by the corresponding uncertainty, must satisfy $|d_0/\sigma_{d_0}| < 5$. These electrons must also be isolated from other objects in the event according to a p_{T}-dependent isolation requirement based on calorimeter ($\mathrm{E}_{\mathrm{T}}^{\mathrm{cone20}}/p_{\mathrm{T}} < 0.06$) and tracking information ($p_{\mathrm{T}}^{\mathrm{varcone20}}/p_{\mathrm{T}} < 0.06$). In RJR search regions with more than two leptons (only used for validation regions (VRs) and control regions (CRs)), the electron p_{T} requirement is lowered to 20 GeV for the third and

Table 2 Simulated background event samples used in this analysis with the corresponding matrix element and parton shower generators, cross-section order in perturbative QCD (pQCD) used to normalize the event yield, underlying-event tune and PDF set. V represents either a W or Z boson

Physics process	Generator	Parton shower	Cross-section order in pQCD	Tune	PDF set
$t\bar{t}$ [49]	POWHEG BOX v2 [45–47]	PYTHIA 8.230 [48]	NNLO+NNLL [50–54]	A14 [55]	NNPDF2.3LO [56]
Wt [49]	POWHEG BOX v2	PYTHIA 8.230	NNLO+NNLL [57–60]	A14	NNPDF3.0NLO [61]
VV [62]	SHERPA 2.2.2 [44]	SHERPA 2.2.2	NLO [63,64]	SHERPA default	NNPDF3.0NNLO
$Z/\gamma^*(\rightarrow \ell\ell)$ +jets [65]	SHERPA 2.2.1	SHERPA 2.2.1	NNLO [66,67]	SHERPA default	NNPDF3.0NNLO
Higgs ($t\bar{t}H$)	POWHEG BOX v2	PYTHIA 8.230	NLO [68]	A14	NPDF2.3LO
Higgs (VBF, Vh)	POWHEG BOX v2	PYTHIA 8.212	NNLO [68]	AZNLO [69]	CTEQ6L1 [70]
Higgs (ggF)	POWHEG BOX v2	PYTHIA 8.212	NNNLO [68]	AZNLO	CTEQ6L1
ttt, $tttt$, $t\bar{t}+WW$	MG5_aMC@NLO [71]	PYTHIA 8.186 [72]	NLO [73], [71]	A14	NNPDF2.3LO
$t\bar{t}+V$ [74,75]	MG5_aMC@NLO	PYTHIA 8.210	NLO [71,76,77]	A14	NNPDF2.3LO
VVV [62]	SHERPA 2.2.2	SHERPA 2.2.2	NLO [44]	SHERPA default	NNPDF3.0NNLO

fourth electrons. Measured in $Z \to ee$ events, the 'medium' electron identification efficiency increases from 75% at a p_{T} of 20 GeV to 91% at 100 GeV. The isolation requirement is approximately 70% efficient for 'medium likelihood' electrons at a p_{T} of 20 GeV, rising to above 98% at 60 GeV and beyond [95].

Baseline muons are reconstructed from either inner-detector tracks matched to muon track segments in the muon spectrometer or combined tracks formed in the inner detector and muon spectrometer. They are required to satisfy the 'medium' selection criteria described in Ref. [96], $p_{\mathrm{T}} > 3$ GeV, and $|\eta| < 2.7$. For consistency with the previous analysis, the RJR search limits the muon acceptance to $|\eta| < 2.4$. Similarly to electrons, the muon must pass within $|z_0 \sin\theta| = 0.5$ mm of the primary vertex. Signal muons are required to be isolated with $\mathrm{E}_{\mathrm{T}}^{\mathrm{topocone20}}/p_{\mathrm{T}} < 0.15$ and $p_{\mathrm{T}}^{\mathrm{varcone30}}/p_{\mathrm{T}} < 0.04$, and they must have $|d_0/\sigma_{d_0}| < 3$, $|\eta| < 2.6$, and $p_{\mathrm{T}} > 25$ GeV. In RJR search regions with more than two leptons (only used for VRs and CRs), the muon p_{T} requirement is lowered to 20 GeV for the third and fourth muon. Measured in $Z \to \mu\mu$ events, the 'medium' muon identification efficiency exceeds 98% in regions with muon spectrometer coverage [96]. The isolation requirement efficiency increases from approximately 85% at a p_{T} of 20 GeV to more than 99% at 60 GeV and above. Proximity to a jet, which can occur in the Strong search, lowers the muon isolation efficiency by up to 10%.

Jets are reconstructed from topological clusters of energy [97] in the calorimeter using the anti-k_t algorithm [98,99] with a radius parameter of 0.4 by making use of utilities within the `FastJet` package [100]. The reconstructed jets are then calibrated to parton level by the application of a jet energy scale (JES) derived from 13 TeV data and simulation [101]. A residual correction applied to jets in data is based on studies of the p_{T} balance between jets and well-calibrated objects in the MC simulation and data. Baseline jets are defined as jet candidates that have $p_{\mathrm{T}} > 20$ GeV and reside within the region $|\eta| < 2.8$. Additional track-based criteria designed to select jets from the hard scatter and reject those originating from pile-up are applied to jets with $p_{\mathrm{T}} < 120$ GeV and $|\eta| < 2.5$. These are imposed by using the 'medium' working point of the jet vertex tagger (JVT) described in Refs. [102,103]. For jets with $p_{\mathrm{T}} < 50$ GeV in the region $|\eta| > 2.5$, outside of the inner-detector acceptance, the tighter working point of forward JVT, fJVT < 0.4 as defined in Ref. [104], uses shape and topological information to suppress jets originating from pile-up. Signal jets are further required to have $p_{\mathrm{T}} > 30$ GeV. To be consistent with the previous analysis, the RJR search limits the jet acceptance to $|\eta| < 2.4$. Finally, events containing a baseline jet that does not pass jet quality requirements are vetoed in order to remove events impacted by detector noise and non-collision backgrounds [105,106].

The MV2C10 boosted decision tree algorithm [107] identifies jets containing b-hadrons by using quantities such as the impact parameters of associated tracks and the positions of any good reconstructed secondary vertices. A selection that provides 77% efficiency for tagging jets from b-quarks in simulated $t\bar{t}$ events is used. These tagged jets are called b-jets. The corresponding rejection factors against jets originating from c-quarks and light quarks in the same sample for this selection are 5 and 110 respectively [107,108].

Photon candidates, used only in the computation of $\vec{p}_{\mathrm{T}}^{\,\mathrm{miss}}$, are reconstructed using energy clusters in the electromagnetic calorimeter without matching inner-detector tracks, or with tracks consistent with having originated from a photon conversion vertex. Photons are required to satisfy the 'tight' selection criteria described in Ref. [95], have $p_{\mathrm{T}} > 25$ GeV, and reside within the region $|\eta| < 2.37$, excluding the transition region ($1.37 < |\eta| < 1.52$) between the barrel and endcaps of the electromagnetic calorimeter.

To avoid the duplication of analysis objects and resolve ambiguities, an overlap removal procedure is applied to baseline jets and signal leptons in the following order. Electron candidates that share an inner-detector track with a baseline muon are rejected to remove electrons originating from photons radiated from muons. Any baseline jet within $\Delta R = 0.2$ of a baseline electron is removed. Any electron that lies within $\Delta R = \min(0.04 + (10\,\mathrm{GeV})/p_{\mathrm{T}}, 0.4)$ of a baseline jet is removed in order to suppress electrons from heavy-flavour decays. If a baseline muon either resides within $\Delta R = 0.2$ of, or has a track associated with, a remaining baseline jet, that jet is removed. Muons are removed in favour of baseline jets with the same p_{T}-dependent ΔR requirement as electrons. For the purpose of computing $\vec{p}_{\mathrm{T}}^{\,\mathrm{miss}}$, photon candidates sharing their calorimeter cluster with an electron are removed.

The $\vec{p}_{\mathrm{T}}^{\,\mathrm{miss}}$ is defined as the negative vector sum of the transverse momenta of all baseline electrons, muons, jets, and photons [109]. Low-momentum contributions from particle tracks originating from the primary vertex that are not associated with reconstructed analysis objects are also included in the calculation of $\vec{p}_{\mathrm{T}}^{\,\mathrm{miss}}$.

All MC samples have corrections applied to take into account small differences between data and MC simulation in the identification, reconstruction and trigger efficiencies. The p_{T} values of leptons in MC samples are smeared to match the momentum resolution in data.

6 Event selection

The searches are carried out in SRs designed to be sensitive to heavy new particles inspired by SUSY. Auxiliary mea-

surements are performed in CRs, which are orthogonal to their associated SRs, designed to be enriched in a particular background process and have low contamination from signal processes. To validate the background estimation in the SRs, VRs are defined to be similar, but orthogonal, to the SRs and CRs. The VRs typically have signal contaminations of less than 10% near the exclusion limits, but in a few regions can be larger, close to 20%.

All three searches share some common event requirements. Events entering the SRs must have exactly two OS SF signal leptons (electrons or muons) with $p_{\mathrm{T}} > 25$ GeV, without any additional baseline leptons. This requirement rejects events with a third, low-momentum lepton, such as from WZ production. This also means that for signal models which may result in more than two leptons, those decay modes are suppressed in favour of hadronic decays of bosons or additional neutrinos in the final state. The majority of the search regions require events to have at least two jets with $p_{\mathrm{T}} > 30$ GeV. Analysis objects are ordered by decreasing p_{T} for further selections. Sections 6.1 and 6.2 describe variables used to construct the regions in the searches. The RJR, EWK, and Strong search-specific selections are described in Sects. 6.3, 6.4, and 6.5 respectively. The regions defined in the searches, in the same order, have a suffix -RJR, -EWK, or -STR. Except in the case of the RJR search, which replicates the selection of the previous search, the event selections are optimized for the different final states depending on the type of sparticles and sparticle masses in the targeted models.

6.1 Additional event selection variables

Signal models with large hadronic activity are targeted by placing additional requirements on the quantity H_{T}, defined as the scalar sum of the p_{T} values of all signal jets. For the purpose of rejecting $t\bar{t}$ background events, the m_{T2} [110,111] variable is used, defined as an extension of the transverse mass m_{T} for the case of two missing particles:

$$m_{\mathrm{T}}^2\left(\vec{p}_{\mathrm{T},a}, \vec{p}_{\mathrm{T}}^{\,\mathrm{miss}}\right) = 2 \times \left(p_{\mathrm{T},a} \times E_{\mathrm{T}}^{\mathrm{miss}} - \vec{p}_{\mathrm{T}a} \cdot \vec{p}_{\mathrm{T}}^{\,\mathrm{miss}}\right), \quad (1)$$

$$m_{\mathrm{T2}}^2 = \min_{\vec{x}_{\mathrm{T},1}+\vec{x}_{\mathrm{T},2}=\vec{p}_{\mathrm{T}}^{\,\mathrm{miss}}} \left[\max\{m_{\mathrm{T}}^2\left(\vec{p}_{\mathrm{T}1}, \vec{x}_{\mathrm{T},1}\right), m_{\mathrm{T}}^2\left(\vec{p}_{\mathrm{T}2}, \vec{x}_{\mathrm{T},2}\right)\}\right], \quad (2)$$

where $\vec{p}_{\mathrm{T},a}$ is the transverse-momentum vector of the highest-p_{T} ($a = 1$) or second-highest-p_{T} ($a = 2$) lepton, and $\vec{x}_{\mathrm{T,b}}$ ($b = 1, 2$) are two vectors representing the possible momenta of the invisible particles that minimize the m_{T2} in the event. The masses of the invisible particles are set to zero in the calculation. The m_{T2} variable tends to have an endpoint near the mass of the parent particle, e.g. the W boson mass for $t\bar{t}$ events when considering the leptons and $E_{\mathrm{T}}^{\mathrm{miss}}$. Thus it can be used to separate signal models with larger mass-splittings from typical $t\bar{t}$ events.

The $E_{\mathrm{T}}^{\mathrm{miss}}$ significance $\mathcal{S}(E_{\mathrm{T}}^{\mathrm{miss}})$ quantifies how consistent the $E_{\mathrm{T}}^{\mathrm{miss}}$ is with mismeasurements of objects in events without any genuine source of $E_{\mathrm{T}}^{\mathrm{miss}}$. It is used to select events where it is more likely that invisible particles are contributing to the $E_{\mathrm{T}}^{\mathrm{miss}}$. The $E_{\mathrm{T}}^{\mathrm{miss}}$ significance is defined [112] as

$$\mathcal{S}^2 = \frac{|E_{\mathrm{T}}^{\mathrm{miss}}|^2}{\sigma_{\mathrm{L}}^2(1-\rho_{\mathrm{LT}}^2)},$$

where σ_{L}^2 is the total variance in the longitudinal direction along $\vec{p}_{\mathrm{T}}^{\,\mathrm{miss}}$, with the resolutions of all of the objects taken into account, and ρ_{LT} is the correlation between the longitudinal and transverse resolutions of the objects.

6.2 Recursive-jigsaw reconstruction

The RJR technique [16] is a method for decomposing measured properties event by event to provide a basis of kinematic variables. This is achieved by approximating the rest frames of intermediate particle states in each event. This reconstructed view of the event gives rise to a natural basis of kinematic observables, calculated by evaluating the momentum and energy of different objects in these rest frames. Backgrounds are reduced by testing whether each event exhibits the anticipated properties of the imposed decay tree under investigation while only applying minimal selection criteria to visible-object momenta and missing momenta. The RJR technique is described in detail in Refs. [16,113,114], and has been used in previous ATLAS searches [115–117].

Electrons, muons, jets, and $\vec{p}_{\mathrm{T}}^{\,\mathrm{miss}}$ are used as input to the RJR algorithm. A decay tree for the $2\ell+2j$ final state in this search, shown in Fig. 2b, is constructed following the canonical process shown in Fig. 2a. These decay trees are motivated by the pair production of sparticles in R-parity-conserving models. Each event is evaluated as if two sparticles (labelled PP) were produced, assigned to two hemispheres ($\mathrm{P_a}$ and $\mathrm{P_b}$), and subsequently decay into the particles observed in the detector, with V denoting the visible objects and I the invisible objects. The benchmark signal models probed in this search give rise to signal events with at least two weakly interacting particles associated with two systems of invisible particles (shown in green). Both of the leptons must be assigned to either V_a or V_b, not split across both. The jets must also be assigned to either of the two visible frames.

After partitioning the visible objects, the remaining unmeasured quantities related to the invisible particles (masses, longitudinal momenta, and contribution to $\vec{p}_{\mathrm{T}}^{\,\mathrm{miss}}$) are associated with the two collections of invisible particles $\mathrm{I_{a/b}}$. The RJR algorithm determines values for the unmeasured particles' four-momenta, while requiring the masses of the invisible particles to be positive. In cases with multiple solutions, the solution with the smallest invariant mass of

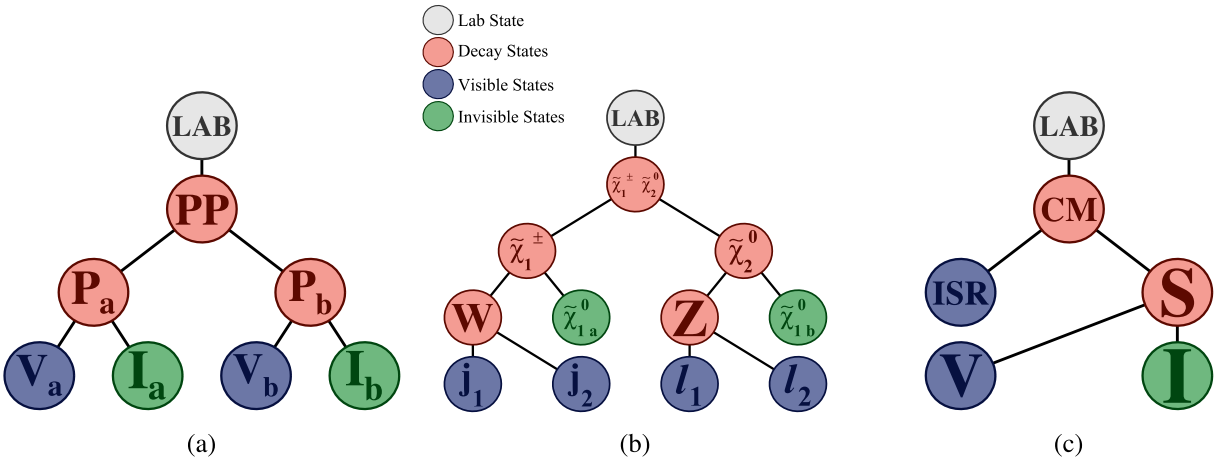

Fig. 2 **a** The standard decay tree applied to pair-produced (PP) sparticles (parent objects), $P_{a,b}$, decaying to visible states $V_{a,b}$ and invisible states $I_{a,b}$. **b** Decay tree for the C1N2 model with decays to the $2\ell+2$-jets final state. **c** The decay tree for compressed scenarios with an initial-state radiation jet (ISR). The signal sparticle system S recoils against the jet-radiation system ISR. *CM* centre-of-mass frame

the visible system is chosen [16]. Once all measured and unmeasured momenta are defined, a set of variables can be constructed, such as multi-object invariant masses and angles between objects. The primary energy-scale-sensitive observables used in the search presented here are a suite of variables denoted by H. As shown in Eq. (3), the H variables are constructed using different combinations of object momenta, including contributions from the invisible particles' four-momenta, and are not necessarily evaluated in the lab frame, nor only in the transverse plane. The H variables are labelled with a superscript F and two subscripts n and m:

$$H^{\mathrm{F}}_{n,m} = \sum_{i=1}^{n} |\vec{p}^{\,\mathrm{F}}_{\mathrm{vis},\,i}| + \sum_{j=1}^{m} |\vec{p}^{\,\mathrm{F}}_{\mathrm{inv},\,j}|. \tag{3}$$

The F represents the rest frame in which the momenta are evaluated. In this analysis, this may be the lab frame, the proxy for the sparticle–sparticle frame PP, or the proxy for the rest frame of an individual sparticle, P. The subscripts n and m represent the number of visible and invisible momentum vectors considered, respectively. For events with fewer than n visible objects, the sum only runs over the available momenta. Only the leading $n - n_\ell$ jets are considered, where n_ℓ is the number of reconstructed leptons in the event. An additional subscript 'T' denotes a transverse version of the variable, where the transverse plane is defined in a frame F as follows: the Lorentz transformation relating F to the lab frame is decomposed into a boost along the beam axis, followed by a subsequent transverse boost. The transverse plane is defined to be perpendicular to the longitudinal boost. In this analysis, it is the plane transverse to the beamline.

The following variables are used in the definition of the SRs. The value of n depends on the number of visible objects; for the $2\ell+2$-jets final state, $n = 4$.

- $H^{\mathrm{PP}}_{4,1}$ is a scale variable as described above that behaves similarly to the effective mass, m_{eff} (defined as the scalar sum of the transverse momenta of the visible objects and $E^{\mathrm{miss}}_{\mathrm{T}}$), used in previous ATLAS SUSY searches.
- $H^{\mathrm{PP}}_{1,1}/H^{\mathrm{PP}}_{4,1}$ provides additional information when testing the balance between the two scale variables. This provides excellent discrimination against unbalanced events where the large scale is dominated by a particular object's p_{T} or by large $E^{\mathrm{miss}}_{\mathrm{T}}$. It behaves similarly to $E^{\mathrm{miss}}_{\mathrm{T}}/m_{\mathrm{eff}}$ and is used to reduce the Z/γ^*+jets background in cases where one high-p_{T} jet dominates.
- $p^{\mathrm{lab}}_{\mathrm{T\,PP}}/(p^{\mathrm{lab}}_{\mathrm{T\,PP}} + H^{\mathrm{PP}}_{\mathrm{T}\,4,1})$ compares the magnitude of the vector sum of the transverse momenta of all objects assigned to the PP system in the lab frame ($p^{\mathrm{lab}}_{\mathrm{T\,PP}}$) with the overall transverse scale variable considered. This quantity tests for a significant boost in the transverse direction. For signal events this quantity peaks sharply towards zero while for background processes the distribution is broader. It is a test of how much a given process resembles the imposed PP system in the decay tree.
- $\min(H^{\mathrm{P_a}}_{1,1}, H^{\mathrm{P_b}}_{1,1})/\min(H^{\mathrm{P_a}}_{2,1}, H^{\mathrm{P_b}}_{2,1})$ compares the scale due to one visible object and $E^{\mathrm{miss}}_{\mathrm{T}}$ ($H^{\mathrm{P_a}}_{1,1}$ and $H^{\mathrm{P_b}}_{1,1}$ in their respective production frames) with the scale due to two visible objects ($H^{\mathrm{P_a}}_{2,1}$ and $H^{\mathrm{P_b}}_{2,1}$). The numerator and denominator are each defined by finding the smaller of the values of these quantities. This variable tests against a single object taking a large portion of the hemisphere momentum. It is particularly useful in discriminating against Z/γ^*+jets events.
- $\Delta\phi^{\mathrm{P}}_{\mathrm{V}}$ is the azimuthal opening angle between the visible system V in frame P and the direction of the boost from the PP frame to the P frame. Standard Model backgrounds from diboson, top and Z/γ^*+jets processes

peak towards zero and π due to their topologies not obeying the imposed decay tree while signal events tend to have a flat distribution in this variable.

For selections involving three charged leptons, the W boson transverse mass, m_{T}^{W}, is used. It is derived as in Eq. (2) from $\vec{p}_{\mathrm{T}}^{\,\mathrm{miss}}$ and the transverse momentum of the charged lepton not associated with the Z boson. The three-lepton regions are only used for CRs and VRs.

For sparticle spectra with smaller mass-splittings and lower intrinsic $E_{\mathrm{T}}^{\mathrm{miss}}$, it can be useful to define a decay tree with a partially resolved sparticle system recoiling against a high-p_{T} initial-state radiation (ISR) jet, instead of the fully resolved decay tree described above. This is shown Fig. 2c. This tree is simpler and attempts to identify visible (V) and invisible (I) systems that are the result of an intermediate state corresponding to the system of sparticles and their decay products (S). Since the $E_{\mathrm{T}}^{\mathrm{miss}}$ is used to identify which jets come from ISR, a transverse view of the reconstructed event is used which ignores the longitudinal momentum of the jets and leptons, as described in Ref. [113]. The reference frames appearing in the decay tree shown in Fig. 2c, such as the centre-of-mass (CM) frame of the whole interaction, are approximations in this transverse projection. The variables which are derived from this process leverage the relationship between the ISR and the total S system:

- $p_{\mathrm{T\,ISR}}^{\mathrm{CM}}$ is the magnitude of the vector-summed transverse momenta of all jets assigned to the ISR system.
- $p_{\mathrm{T\,I}}^{\mathrm{CM}}$ is the magnitude of the vector-summed transverse momenta of the invisible system, which behaves similarly to $E_{\mathrm{T}}^{\mathrm{miss}}$.
- $p_{\mathrm{T}}^{\mathrm{CM}}$ is the magnitude of the vector-summed transverse momenta of the CM system.
- $R_{\mathrm{ISR}} \equiv \vec{p}_{\mathrm{I}}^{\,\mathrm{CM}} \cdot \hat{p}_{\mathrm{T\,S}}^{\mathrm{CM}} / p_{\mathrm{T\,S}}^{\mathrm{CM}}$ serves as an estimate of $m_{\tilde{\chi}_1^0}/m_{\tilde{\chi}_2^0/\tilde{\chi}_1^\pm}$. This corresponds to the fraction of the momentum of the S system that is carried by its invisible system I, with momentum $\vec{p}_{\mathrm{I}}^{\,\mathrm{CM}}$ in the CM frame. As $p_{\mathrm{T\,S}}^{\mathrm{CM}}$ grows it becomes increasingly hard for backgrounds to possess a large value in this ratio – a feature exhibited by compressed signals [113].
- $N_{\mathrm{jet}}^{\mathrm{S}}$ is the number of jets assigned to the signal system S.
- $N_{\mathrm{jet}}^{\mathrm{ISR}}$ is the number of jets assigned to the ISR system.
- $\Delta\phi_{\mathrm{ISR,I}}^{\mathrm{CM}}$ is the azimuthal opening angle between the ISR system and the invisible system in the CM frame.
- m_{T}^{Z} is the transverse mass of the dilepton pair assigned to the signal system.
- m_{T}^{J} is the transverse mass of the jet system assigned to the signal system.

6.3 Recursive-jigsaw reconstruction search selections

The RJR search is a follow-up to the 36.1 fb^{-1} search [17] which observed 1.4σ and 2.0σ excesses in regions named SR2ℓ-Low-RJR and SR2ℓ-ISR-RJR respectively. Thus the selection is kept the same and not optimized for the full Run 2 dataset. These SRs were designed to target C1N2 models with $\tilde{\chi}_1^\pm$–$\tilde{\chi}_1^0$ mass-splittings of approximately 100 GeV. The selections begin with the common selections defined in Sect. 6, and include requirements on the lepton multiplicity (n_{leptons}), the jet multiplicity (n_{jets}), the b-tagged jet multiplicity ($n_{b\text{-tag}}$), the transverse momenta of the leading ($p_{\mathrm{T}}^{\ell_1}$, $p_{\mathrm{T}}^{j_1}$) and subleading ($p_{\mathrm{T}}^{\ell_2}$, $p_{\mathrm{T}}^{j_2}$) leptons and jets, as well as the invariant masses of the dilepton $m_{\ell\ell}$ and dijet m_{jj} systems. The selections used to define SR2ℓ-Low-RJR, and the CRs and VRs associated with it, are summarized in Tables 3 and 4. Selections which enforce orthogonality between the CRs and VRs are in boldface. CRs are defined to extract data-driven normalization factors for the main background processes: diboson and $t\bar{t}+Wt$. Details of the background estimation are described in Sect. 7.1.

Most of the regions are defined to have exactly two OS SF leptons with transverse momentum greater than 25 GeV, and a dilepton invariant mass consistent with originating from a Z boson. The diboson CR (CR2ℓ-VV-RJR) is an exception and requires three or four leptons, which ensures orthogonality to the SRs while also enriching the sample with diboson events. The OS SF dilepton pair with an invariant mass closest to the Z boson mass is chosen as the Z boson candidate. For the purpose of RJR calculations, the third and fourth leptons are treated as invisible objects contributing to $\vec{p}_{\mathrm{T}}^{\,\mathrm{miss}}$. An additional requirement on m_{T}^{W} is applied, which ensures orthogonality to the 3ℓ searches using the 36.1 fb^{-1} dataset. Both the top CR (CR2ℓ-Top-RJR) and VR (VR2ℓ-Top-RJR) require a b-tagged jet. Inverting the $m_{\ell\ell}$ requirement makes the VR orthogonal to the CR. The SRs require m_{jj} to be consistent with a W boson, whereas VR2ℓ-VV-RJR selects events outside the W boson mass window. The min $\Delta\phi(\boldsymbol{j}_{1,2}, \vec{p}_{\mathrm{T}}^{\,\mathrm{miss}})$ variable corresponds to the azimuthal angle between the jets and $\vec{p}_{\mathrm{T}}^{\,\mathrm{miss}}$ and is applied to suppress Z/γ^*+jets contributions to SR2ℓ-Low-RJR. VR2ℓ-VV is the only region with an $H_{1,1}^{\mathrm{PP}}$ requirement, and it suppresses the Z/γ^*+jets contribution.

SR2ℓ-ISR-RJR requires three or four jets, which makes it orthogonal to SR2ℓ-Low-RJR. All CRs and VRs for SR2ℓ-ISR-RJR require at least one jet to be assigned to the ISR system (N_J^{ISR}), and at least two to the signal system (N_J^{S}). The assignment of the jets is determined by the configuration that minimizes the mass of both S and ISR systems. Both CR2ℓ-ISR-VV-RJR and VR2ℓ-ISR-VV-RJR require three or four leptons. To increase the number of events in VR2ℓ-ISR-VV-RJR, the transverse momentum requirement for jets is relaxed to 20 GeV, compared to 30 GeV in other regions. The ISR regions are further defined by a series of requirements based on the variables from the ISR decay tree, described in Sect. 6.2. These requirements are listed in Tables 5 and 6. Selections that enforce orthogonality to the

SR are in boldface. SR2ℓ-ISR-RJR requires a highly energetic ISR jet system which recoils against the signal system in the CM frame. In VR2ℓ-ISR-VV-RJR the m_{T}^{Z} requirement is inverted in order to be orthogonal to CR2ℓ-ISR-VV-RJR. The top CR (CR2ℓ-ISR-Top-RJR) and VR (VR2ℓ-ISR-Top-RJR) both require a b-tagged jet and have broader m_{T}^{Z} and m_{T}^{J} requirements. These regions are orthogonal due to the inversion of the $p_{\mathrm{T}}^{\mathrm{CM}}$ requirement.

6.4 Electroweak search selections

The EWK search uses 13 orthogonal SRs designed to cover different regions of the C1N2 and GMSB models' parameter spaces. In addition to the use of new kinematic variables, the strategy from the 36 fb^{-1} search [22] is extended by optimizing binned SRs to maximize the model-dependent search sensitivity. The SRs labelled -OffShell, -Low, -Int, and -High target increasing NLSP–LSP mass-splittings. The SR labelled -$\ell\ell bb$ targets the GMSB model with either a Higgs or Z boson decaying into two b-quarks. The selections defining each region in the search are summarized in Tables 7, 8 and 9, along with the control and validation regions used for the estimation and validation of the SM backgrounds. The acceptance times efficiency for several example signal models are listed in Table 10.

Lepton pair and jet pair mass windows are used to select events with a ZW, Zh, or ZZ topology. In all regions, except for the OffShell regions, the dilepton invariant mass is required to be on the Z boson mass peak, and the mass of the jet system is required to be consistent with a hadronically decaying boson. Most regions require the jet system mass to be around the W or Z boson mass, $60 < m_X < 110$ GeV, where m_X refers to the dijet system for all regions except for SR-1J-High-EWK, where it is the single-jet mass. The $\ell\ell bb$ region expands this window to $60 < m_{bb} < 150$ GeV in order to additionally account for Higgs boson decays in the GMSB model.

When performing model-dependent fits, SR-High-EWK uses a two-dimensional binning in $\mathcal{S}(E_{\mathrm{T}}^{\mathrm{miss}})$ with boundaries $(18, 21, \infty)$ and ΔR_{jj} with boundaries $[0, 0.8, 1.6)$, labelled as ΔR_X in Tables 7 and 8. The variable ΔR_X is sensitive to signal events where the leptons or jets are expected to be closer together due to the boost of the decay system, which is increased by the large mass splittings targeted by these regions. SR-Int-EWK and SR-Low-EWK are binned only in $\mathcal{S}(E_{\mathrm{T}}^{\mathrm{miss}})$, with boundaries (12, 15, 18) and (6, 9, 12) respectively. SR-OffShell-EWK is split into ranges of 12–40 and 40–71 GeV in $m_{\ell\ell}$. The SR binning was optimized by checking the performance of a few variables, e.g. binning in jet p_{T} did not perform as well as ΔR_{jj}, and binning the main discriminant, $\mathcal{S}(E_{\mathrm{T}}^{\mathrm{miss}})$, so that at least one background event is expected in each bin. All remaining SRs are treated as single bins. For all of the SRs, VRs are defined using the jet system mass sidebands or by inverting criteria for kinematic variables defining the SRs. The criteria ensuring orthogonality to the corresponding SRs are highlighted in boldface in Tables 7, 8 and 9. CRs are defined in order to extract data-driven normalization factors for the main background processes: diboson, $t\bar{t}$, Z/γ^*+jets, and low-mass off-shell Z/γ^*+jets. These are discussed further in Sect. 7.2.

6.5 Strong search selections

The SRs targeting production of gluinos and squarks start with the common selection described at the beginning of Sect. 6. The four overlapping SRs designed for a kinematic endpoint, or 'edge' feature, are binned in the dilepton invariant mass, $m_{\ell\ell}$. They are named SRC-STR, SRLow-STR, SRMed-STR, and SRHigh-STR in order of sensitivity to gluino–$\tilde{\chi}_1^0$ mass splittings from those that are compressed, or small, to those that are large. SRs designed for an excess of events near the Z boson mass, 'on-Z', are a single bin in the window $81 < m_{\ell\ell} < 101$ GeV. They share the same naming as the edge SRs, with the addition of a 'Z' in the name. The selection used for each region in the analysis is summarized in Table 11. The bin boundaries in $m_{\ell\ell}$ used for interpretations were chosen such that there is a finer division in the mass region targeted by each SR, while keeping enough events per bin for the background estimates and a bin around the Z mass where possible. The boundaries in units of GeV are as follows:

- SRC-STR: 12, 31, 46, 61, 71, 81, 101, 201;
- SRLow-STR: 12, 41, 61, 81, 101, 141, 201, 301, 501;
- SRMed-STR: 12, 81, 101, 201, 301, 601;
- SRHigh-STR: 12, 101, 301, 1001.

The acceptance times efficiency for the simulated simplified models in the various regions depends on the model and region. SRHigh-STR has an acceptance times efficiency of 10% for the gluino-slepton model with $m_{\tilde{g}} = 2000$ GeV and $m_{\tilde{\chi}_1^0} = 300$ GeV. SRC-STR has an acceptance times efficiency of 0.02% for the gluino-$Z^{(*)}$ model with $m_{\tilde{g}} = 800$ GeV and $m_{\tilde{\chi}_1^0} = 700$ GeV. This is very small due to the compressed mass-splittings between sparticles, resulting in low-momentum decay products, and the Z boson branching fraction to leptons. SRZMed-STR has an acceptance times efficiency of 1% for the squark-$Z^{(*)}$ model with $m_{\tilde{q}} = 1200$ GeV and $m_{\tilde{\chi}_1^0} = 700$ GeV.

As described before, all of the SRs require exactly two OS SF signal leptons with $p_{\mathrm{T}} > 25$ GeV, without any additional baseline leptons. This also applies to the Strong search CRs and VRs, except for VR3L-STR, which requires exactly three signal leptons. All signal models studied are expected to have several quarks in the final state, so events are further required

Table 3 Preselection criteria for the standard-decay-tree 2ℓ SR (SR2ℓ-Low-RJR) and the associated CRs and VRs. Selections which enforce orthogonality between the CRs and VRs are in boldface

Region	n_{leptons}	n_{jets}	$n_{b\text{-tag}}$	$p_{\text{T}}^{\ell_1,\ell_2}$ [GeV]	$p_{\text{T}}^{j_1,j_2}$ [GeV]	$m_{\ell\ell}$ [GeV]	m_{jj} [GeV]	m_{T}^{W} [GeV]
CR2ℓ-VV-RJR	**$\in$ [3, 4]**	≥ 2	$= 0$	> 25	> 30	$\in (80, 100)$	> 20	$\in (70, 100)$ if $n_{\text{leptons}} = 3$
CR2ℓ-Top-RJR	$= 2$	≥ 2	**$= 1$**	> 25	> 30	**$\in (20, 80)$**	$\in (40, 250)$	–
						or > 100		–
VR2ℓ-VV-RJR	$= 2$	≥ 2	$= 0$	> 25	> 30	$\in (80, 100)$	**$\in (40, 70)$**	–
							or $\in (90, 500)$	–
VR2ℓ-Top-RJR	$= 2$	≥ 2	**$= 1$**	> 25	> 30	$\in (80, 100)$	$\in (40, 250)$	–
SR2ℓ-Low-RJR	$= 2$	$= 2$	$= 0$	> 25	> 30	$\in (80, 100)$	$\in (70, 90)$	–

Table 4 Selection criteria for the standard-decay-tree 2ℓ SR (SR2ℓ-Low-RJR) and the associated CRs and VRs

Region	$H_{4,1}^{\text{PP}}$ [GeV]	$H_{1,1}^{\text{PP}}$ [GeV]	$\frac{p_{\text{T PP}}^{\text{lab}}}{p_{\text{T PP}}^{\text{lab}} + H_{\text{T 4,1}}^{\text{PP}}}$	$\frac{\min(H_{1,1}^{\text{Pa}}, H_{1,1}^{\text{Pb}})}{\min(H_{2,1}^{\text{Pa}}, H_{2,1}^{\text{Pb}})}$	$\frac{H_{1,1}^{\text{PP}}}{H_{4,1}^{\text{PP}}}$	$\Delta\phi_{\text{V}}^{\text{P}}$	$\min \Delta\phi(\boldsymbol{j}_{1,2}, \vec{p}_{\text{T}}^{\text{miss}})$
CR2ℓ-VV-RJR	> 200	–	< 0.05	> 0.2	–	$\in (0.3, 2.8)$	–
CR2ℓ-Top-RJR	> 400	–	< 0.05	> 0.5	–	$\in (0.3, 2.8)$	–
VR2ℓ-VV-RJR	> 400	> 250	< 0.05	$\in (0.4, 0.8)$	–	$\in (0.3, 2.8)$	–
VR2ℓ-Top-RJR	> 400	–	< 0.05	> 0.5	–	$\in (0.3, 2.8)$	–
SR2ℓ-Low-RJR	> 400	–	< 0.05	–	$\in (0.35, 0.60)$	–	> 2.4

Table 5 Preselection criteria for the ISR-decay-tree 2ℓ SR (SR2ℓ-ISR-RJR) and the associated CRs and VRs. Selections which enforce orthogonality between the CRs and VRs are in boldface

Region	n_{leptons}	$N_{\text{jet}}^{\text{ISR}}$	$N_{\text{jet}}^{\text{S}}$	n_{jets}	$n_{b\text{-tag}}$	$p_{\text{T}}^{\ell_1,\ell_2}$ [GeV]	$p_{\text{T}}^{j_1,j_2}$ [GeV]
CR2ℓ-ISR-VV-RJR	**$\in$ [3, 4]**	≥ 1	≥ 2	> 2	$= 0$	> 25	> 30
CR2ℓ-ISR-Top-RJR	$= 2$	≥ 1	$= 2$	$\in [3, 4]$	**$= 1$**	> 25	> 30
VR2ℓ-ISR-VV-RJR	**$\in$ [3, 4]**	≥ 1	≥ 2	≥ 3	$= 0$	> 25	> 20
VR2ℓ-ISR-Top-RJR	$= 2$	≥ 1	$= 2$	$\in [3, 4]$	**$= 1$**	> 25	> 30
SR2ℓ-ISR-RJR	$= 2$	≥ 1	$= 2$	$\in [3, 4]$	$= 0$	> 25	> 30

Table 6 Selection criteria for the ISR-decay-tree 2ℓ SR (SR2ℓ-ISR-RJR) and the associated CRs and VRs. Selections which enforce orthogonality between the CRs and VRs are in boldface

Region	m_{T}^{Z} [GeV]	m_{T}^{J} [GeV]	$\Delta\phi_{\text{ISR,I}}^{\text{CM}}$	R_{ISR}	$p_{\text{T ISR}}^{\text{CM}}$ [GeV]	$p_{\text{T I}}^{\text{CM}}$ [GeV]	p_{T}^{CM} [GeV]
CR2ℓ-ISR-VV-RJR	$\in (80, 100)$	> 20	> 2.0	$\in (0.0, 0.5)$	> 50	> 50	< 30
CR2ℓ-ISR-Top-RJR	$\in (50, 200)$	$\in (50, 200)$	> 2.8	$\in (0.4, 0.75)$	> 180	> 100	< 20
VR2ℓ-ISR-VV-RJR	**$\in (20, 80)$**	> 20	> 2.0	$\in (0.0, 1.0)$	> 70	> 70	< 30
	or > 100						
VR2ℓ-ISR-Top-RJR	$\in (50, 200)$	$\in (50, 200)$	> 2.8	$\in (0.4, 0.75)$	> 180	> 100	**> 20**
SR2ℓ-ISR-RJR	$\in (80, 100)$	$\in (50, 110)$	> 2.8	$\in (0.4, 0.75)$	> 180	> 100	< 20

Table 7 Overview of the High and Intermediate signal, control, and validations regions of the electroweak search. The main requirements that distinguish the control and validation regions from the signal regions are highlighted in boldface. The bracketed requirements denote the binning used in model-dependent fits, as described in the text

Region	n_{jets}	$n_{\text{jets}}^{b\text{-tag}}$	$\mathcal{S}(E_{\text{T}}^{\text{miss}})$	$m_{\ell\ell}$ [GeV]	m_X [GeV]	m_{T2} [GeV]	ΔR_X	$p_{\text{T}}^{j_1}$ [GeV]
SR-High-EWK	≥ 2	≤ 1	$(18, 21, \infty)$	71–111	$60 < m_{jj} < 110$	> 80	$\Delta R_{jj} \in (0, 0.8, 1.6)$	–
VR-High-Sideband-EWK	≥ 2	≤ 1	> 18	71–111	$\mathbf{20 < m_{jj} < 60 \cup m_{jj} > 110}$	> 80	$\Delta R_{jj} < 1.6$	–
VR-High-R-EWK	≥ 2	≤ 1	> 18	71–111	$\mathbf{m_{jj} > 20}$	> 80	$\mathbf{\Delta R_{jj} > 1.6}$	–
SR-1J-High-EWK	1	≤ 1	> 12	71–111	$60 < m_{j_1} < 110$	> 80	–	–
VR-1J-High-Sideband-EWK	1	≤ 1	> 12	71–111	$\mathbf{20 < m_{j_1} < 60 \cup m_{j_1} > 110}$	> 80	–	–
SR-$\ell\ell bb$-EWK	≥ 2	≥ 2	> 18	71–111	$60 < m_{bb} < 150$	> 80	–	–
VR-$\ell\ell bb$-EWK	≥ 2	≥ 2	**12–18**	71–111	$60 < m_{bb} < 150$	> 80	–	–
SR-Int-EWK	≥ 2	0	(12, 15, 18)	81–101	$60 < m_{jj} < 110$	> 80	–	> 60
VR-Int-EWK	≥ 2	0	12–18	81–101	$60 < m_{jj} < 110$	> 80	–	$\mathbf{< 60}$
CR-VZ-EWK	≥ 2	0	12–18	81–101	$\mathbf{20 < m_{jj} < 60 \cup m_{jj} > 110}$	> 80	–	–
CR-tt-EWK	≥ 2	≥ 1	**9–12**	81–101	$\mathbf{m_{jj} > 20}$	> 80	–	> 60

Table 8 Overview of the Low signal, control, and validations regions of the electroweak search. The main requirements that distinguish the control and validation regions from the signal regions are highlighted in boldface. The bracketed requirements denote the binning used in model-dependent fits, as described in the text

Region	n_{jets}	$n_{\text{jets}}^{b\text{-tag}}$	$\mathcal{S}(E_{\text{T}}^{\text{miss}})$	$m_{\ell\ell}$ [GeV]	m_X [GeV]	m_{T2} [GeV]	ΔR_X	$\Delta\phi(p_{\text{T}}^{\ell\ell}, \vec{p}_{\text{T}}^{\text{miss}})$
SR-Low-EWK	2	0	(6, 9, 12)	81–101	$60 < m_{jj} < 110$	> 80	$\Delta R_{\ell\ell} < 1$	–
VR-Low-EWK	2	0	6–12	81–101	$60 < m_{jj} < 110$	> 80	$\mathbf{1 < \Delta R_{\ell\ell} < 1.4}$	–
SR-Low-2-EWK	2	0	6–9	81–101	$60 < m_{jj} < 110$	< 80	$\Delta R_{\ell\ell} < 1.6$	< 0.6
VR-Low-2-EWK	2	0	6–9	81–101	$\mathbf{20 < m_{jj} < 60 \cup m_{jj} > 110}$	< 80	$\Delta R_{\ell\ell} < 1.6$	< 0.6
CR-Z-EWK	2	0	6–9	81–101	$\mathbf{20 < m_{jj} < 60 \cup m_{jj} > 110}$	$\mathbf{> 80}$	–	–

Table 9 Overview of the OffShell signal, control, and validations regions of the electroweak search. The main requirements that distinguish the control and validation regions from the signal regions are highlighted in boldface. The bracketed requirements denote the binning used in model-dependent fits, as described in the text

Region	n_{jets}	$n_{\text{jets}}^{b\text{-tag}}$	$\mathcal{S}(E_{\text{T}}^{\text{miss}})$	$m_{\ell\ell}$ [GeV]	m_{T2} [GeV]	$p_{\text{T}}^{j_1}$ [GeV]	$\Delta\phi(p_{\text{T}}^{j_1}, \vec{p}_{\text{T}}^{\text{miss}})$
SR-OffShell-EWK	≥ 2	0	> 9	(12, 40, 71)	> 100	> 100	> 2
VR-OffShell-EWK	≥ 2	0	> 9	12–71	**80–100**	> 100	> 2
CR-DY-EWK	≥ 2	0	**6–9**	12–71	> 100	–	–

to have at least two jets with $p_{\text{T}} > 30$ GeV. Since the SR selection requires exactly two leptons, it is likely that events passing the selection from models with Z bosons contain both a leptonically and hadronically decaying Z boson. Thus the on-Z SRs require at least four jets with $p_{\text{T}} > 30$ GeV to take this into account. All regions require $m_{\ell\ell} > 12$ GeV in order to reduce contributions from low-mass resonances. Several variables, such as $E_{\text{T}}^{\text{miss}}$ and H_{T}, are used to isolate SUSY-like events from the background. Most regions require the angular separation in ϕ between the $\vec{p}_{\text{T}}^{\text{miss}}$ and the two leading jets, $\Delta\phi(\boldsymbol{j}_{1,2}, \vec{p}_{\text{T}}^{\text{miss}})$, to be greater than 0.4 to remove events with $E_{\text{T}}^{\text{miss}}$ arising from jet mismeasurements. CRs for Z/γ^*+jets are defined, identified with a '-Z', by inverting this requirement, adding an $m_{\ell\ell}$ window of 81–101 GeV, and otherwise keeping the selections the same. CRs for flavour-symmetric (FS) processes, such as $t\bar{t}$ and WW, are defined (labelled with '-FS') by requiring the leptons to be different-flavour (DF). VRs are defined for each edge SR, below their $E_{\text{T}}^{\text{miss}}$ requirement, by $150 < E_{\text{T}}^{\text{miss}} < 250$ GeV. Additional VRs targeting WZ and FNP leptons are defined by requiring three leptons and same-charge (SS) leptons respectively; the

Table 10 Acceptance times efficiency in the summed EWK signal regions for example C1N2 and GMSB signal models

	C1N2	
$m_{\tilde{\chi}_1^\pm/\tilde{\chi}_2^0}$ [GeV]	$m_{\tilde{\chi}_1^0}$ [GeV]	$A \times \epsilon$ [%]
100	60	0.0003
150	70	0.0007
250	100	0.042
400	200	0.21
650	250	0.64
	GMSB	
$m_{\tilde{\chi}_1^0}$ [GeV]	$B(\tilde{\chi}_1^0 \to h\tilde{G})$ [%]	$A \times \epsilon$ [%]
200	50	0.02
500	80	0.21
700	0	1.6

$E_{\mathrm{T}}^{\mathrm{miss}}$ requirement in these regions is lowered in order to increase the number of events.

The requirements chosen for each SR are based on an optimization performed with a few test points with different mass-splittings between the $\tilde{g}$ or $\tilde{q}$ and the $\tilde{\chi}_1^0$ from each model. One of the main changes with larger mass-splittings is the increase in jet activity. The requirement on H_{T} varies from > 250 GeV in the more compressed regions to > 800 GeV in the regions targeting large splittings. The lower bound on the dilepton system's momentum, $p_{\mathrm{T}}^{\ell\ell} > 40$ GeV, was imposed to allow use of the γ + jets process to estimate the Z/γ^* + jets background, but this method was not used due to poor modelling. After all of the other requirements this removes less than one expected event from each SR. The more compressed signal models tend to have small values of $p_{\mathrm{T}}^{\ell\ell}$, so an upper bound is imposed to reduce the Z/γ^* + jets contribution. The requirement is relaxed for SRs targeting larger mass-splittings. The $E_{\mathrm{T}}^{\mathrm{miss}}$ requirement removes a large portion of the SM backgrounds and is set to > 250 GeV for the C and Low regions and > 300 GeV for the Med and High regions. Requirements on $\mathcal{S}(E_{\mathrm{T}}^{\mathrm{miss}})$ and m_{T2} are used to reduce the contribution from $t\bar{t}$ in the signal regions.

7 Background estimation

This section describes the methods used to estimate the contributions from SM processes to each of the search regions. An overview of how the various processes are estimated in each search is shown in Table 12. Several processes are estimated using data-driven methods in order to estimate both the yield and distribution from data. Depending on the search and SR, some processes are estimated using orthogonal CRs to normalize the yield to data while taking the shape from MC simulation. The choice of background estimation method depends on the dominant backgrounds, expected yields, and whether the shape of the background is important. For the RJR search, the background estimation methods are repeated from the 36 fb^{-1} analysis. The use of b-tagging in the EWK search requirements allows for a $t\bar{t}$ CR with inverted b-jet requirements. While the Strong search is inclusive in b-jets and modelling the shape of the $m_{\ell\ell}$ spectrum is important, thus a method that also estimates the shape of the backgrounds from data is used. Finally, processes with smaller expected yields such as triboson production (VVV), Higgs production, and rare top processes ('Other Top') such as $t\bar{t}+V$ production are estimated directly from MC simulation. The common estimate of FNP leptons is described, and then methods specific to each search are described in Sects. 7.1–7.3.

All three searches estimate events with fake, misidentified and non-prompt leptons using the matrix method [118]. This method inverts a system of equations relating the number of observed baseline and signal leptons to the estimated number of real and FNP leptons via measured real- and FNP-lepton efficiencies. These events come mostly from semileptonic $t\bar{t}$, $W \to \ell\nu$, and single top (s- and t-channel) decays, which enter the dilepton channel when one hadron, photon, or non-prompt lepton from a heavy-flavour decay is misidentified as a signal lepton. In most SRs, the contribution from this background is less than 5%. However, in a few regions it is up to 20% of the background yield.

A control sample is constructed for each region in the searches with the same selection but removing the requirement of two signal leptons, requiring only two baseline leptons instead. The number of leptons that pass or fail the stricter signal lepton requirements is counted. A system of equations is constructed with the measured efficiencies for real and FNP leptons to pass these requirements and then inverted to solve for the number of FNP leptons passing the signal lepton requirement. In the case of a single-lepton selection, the number of FNP-lepton events in a given region would be estimated according to:

$$N_{\mathrm{pass}}^{\mathrm{FNP}} = \frac{N_{\mathrm{fail}} - (1/\epsilon^{\mathrm{real}} - 1) \times N_{\mathrm{pass}}}{1/\epsilon^{\mathrm{FNP}} - 1/\epsilon^{\mathrm{real}}},$$

where ϵ^{real} is the efficiency for a real, prompt lepton to pass the signal lepton requirements, and ϵ^{FNP} is the same for FNP leptons. The real-lepton efficiency is obtained from MC simulation which has been corrected to match the efficiency found in data and uses the MC simulation particle-level information to select prompt leptons. The FNP-lepton efficiency is measured using a tag-and-probe method. It is measured separately for misidentified leptons originating from light-flavour jets, heavy-flavour jets, and from the conversion of photons to electrons. The heavy-flavour and photon-conversion efficiencies are measured with data in regions with a b-jet or

Table 11 Overview of all of the signal, control, and validation regions of the Strong search. The flavour of the lepton pair is denoted by 'SF' for same-flavour and 'DF' for different-flavour. All regions require exactly two opposite-charge signal leptons with $p_{\mathrm{T}} > 25$ GeV, with the exception of VR3L which requires exactly three signal leptons (3 L). The main requirements that distinguish the control and validation regions from the signal regions are highlighted in boldface. The validation regions have an equivalent set of CRs with the lepton flavour and $\Delta\phi(\boldsymbol{j}_{1,2}, \vec{p}_{\mathrm{T}}^{\,\mathrm{miss}})$ flipped, but are omitted here for brevity

Region	n_{jets}	H_{T} [GeV]	$E_{\mathrm{T}}^{\mathrm{miss}}$ [GeV]	m_{T2} [GeV]	$\mathcal{S}(E_{\mathrm{T}}^{\mathrm{miss}})$	$p_{\mathrm{T}}^{\ell\ell}$ [GeV]	$\Delta\phi(\boldsymbol{j}_{1,2}, \vec{p}_{\mathrm{T}}^{\,\mathrm{miss}})$	SF/DF	$m_{\ell\ell}$ [GeV]
Signal regions									
SRC-STR	≥ 2	> 250	> 250	> 90	> 10	40–100	> 0.4	SF	> 12
SRLow-STR	≥ 2	> 250	> 250	> 100	–	40–500	> 0.4	SF	> 12
↪SRZLow-STR	≥ 4	> 250	> 250	> 100	–	40–500	> 0.4	SF	81–101
SRMed-STR	≥ 2	> 500	> 300	> 75	–	40–800	> 0.4	SF	> 12
↪SRZMed-STR	≥ 4	> 500	> 300	> 75	–	40–800	> 0.4	SF	81–101
SRHigh-STR	≥ 2	> 800	> 300	> 75	–	> 40	> 0.4	SF	> 12
↪SRZHigh-STR	≥ 4	> 800	> 300	> 75	–	> 40	> 0.4	SF	81–101
Control regions									
CRC-FS-STR	≥ 2	> 250	> 250	> 90	> 10	40–100	> 0.4	**DF**	> 12
CRLow-FS-STR	≥ 2	> 250	> 250	> 100	–	40–500	> 0.4	**DF**	> 12
↪CRZLow-FS-STR	≥ 4	> 250	> 250	> 100	–	40–500	> 0.4	**DF**	**61–121**
CRMed-FS-STR	≥ 2	> 500	> 300	> 75	–	40–800	> 0.4	**DF**	> 12
↪CRZMed-FS-STR	≥ 4	> 500	> 300	> 75	–	40–800	> 0.4	**DF**	**61–121**
CRHigh-FS-STR	≥ 2	> 800	> 300	> 75	–	> 40	> 0.4	**DF**	> 12
↪CRZHigh-FS-STR	≥ 4	> 800	> 300	> 75	–	> 40	> 0.4	**DF**	**61–121**
CRC-Z-STR	≥ 2	> 250	> 250	> 90	> 10	40–100	**< 0.4**	SF	**81–101**
CRLow-Z-STR	≥ 2	> 250	> 250	> 100	–	40–500	**< 0.4**	SF	**81–101**
↪CRZLow-Z-STR	≥ 4	> 250	> 250	> 100	–	40–500	**< 0.4**	SF	81–101
CRMed-Z-STR	≥ 2	> 500	> 300	> 75	–	40–800	**< 0.4**	SF	**81–101**
↪CRZMed-Z-STR	≥ 4	> 500	> 300	> 75	–	40–800	**< 0.4**	SF	81–101
CRHigh-Z-STR	≥ 2	> 800	> 300	> 75	–	> 40	**< 0.4**	SF	**81–101**
↪CRZHigh-Z-STR	≥ 4	> 800	> 300	> 75	–	> 40	**< 0.4**	SF	81–101
Validation regions									
VRC-STR	≥ 2	> 250	**150–250**	> 90	> 10	40–100	> 0.4	SF	> 12
VRLow-STR	≥ 2	> 250	**150–250**	> 100	–	40–500	> 0.4	SF	> 12
VRMed-STR	≥ 2	> 500	**150–250**	> 75	–	40–800	> 0.4	SF	> 12
VRHigh-STR	≥ 2	> 800	**150–250**	> 75	–	> 40	> 0.4	SF	> 12
VR3L-STR	≥ 2	> 250	**> 200**	> 100	–	> 40	> 0.4	**3 L**	> 12

Table 12 Breakdown of background estimation methods for the three searches. 'MC' processes are estimated directly from a Monte Carlo (MC) simulated sample, 'CR' processes are MC samples normalized to data in a control region (CR), and 'DD' processes are estimated via a data-driven method where both the shape and normalization are obtained from data. Entries with multiple categories depend on the specific region or process, e.g. $t\bar{t}$ and Wt

Process	Z/γ^*+jets and Drell–Yan	Top	Diboson	FNP	VVV	Other Top	Higgs
RJR	DD	CR	CR	DD	MC	MC	MC
EWK	CR	MC/CR	CR	DD	MC	MC	MC
Strong	CR	DD	MC/DD	DD	MC	MC	MC

$\mu\mu e$ events on the Z boson mass peak respectively. The light-flavour efficiency is measured in SS events with MC simulation since it is difficult to construct a region pure in FNP leptons from light-flavour jets. The three sources are combined according to their expected relative contributions to the search regions, measured using MC simulation with selections similar to those for each search.

7.1 Recursive-jigsaw reconstruction search backgrounds

In the RJR search, the diboson and top backgrounds are normalized in CRs, the Z/γ^*+jets background is estimated using the so-called ABCD method, the FNP-lepton background is estimated with the data-driven approach previously described, and the remaining backgrounds are estimated via MC simulation.

The ABCD method requires two SR selections that are uncorrelated with respect to the Z/γ^*+jets background. These selections are used to construct three CRs: A, B, and D (region C is the SR), which are adjacent to the SR. Table 13 lists the requirements on these variables and their adjacency to the SRs for both cases. As the selections are uncorrelated, there is a linear relation between the regions, $N_{\mathrm{SR}} \approx N_{\mathrm{D}} \cdot N_{\mathrm{A}}/N_{\mathrm{B}}$, where N is the fitted Z/γ^*+jets estimate in each region. This provides a background estimate in each of the SRs.

For SR2ℓ-Low-RJR, the CRs are defined with m_{jj} and $H^{\mathrm{PP}}_{1,1}/H^{\mathrm{PP}}_{4,1}$, and for SR2$\ell$-ISR-RJR, m^{J}_{T} and $p^{\mathrm{CM}}_{\mathrm{T\,I}}$ are used to define the CRs. For $\mathrm{A_{Low}}$, $\mathrm{B_{Low}}$, and $\mathrm{D_{Low}}$, the Z/γ^*+jets purities are 77%, 98%, and 96% respectively. For $\mathrm{A_{ISR}}$, $\mathrm{B_{ISR}}$, $\mathrm{D_{ISR}}$, the Z/γ^*+jets purities are 36%, 85%, and 91% respectively. The ABCD regions are included in the simultaneous fits. A cross-check Z/γ^*+jets estimate obtained by fitting the sidebands in m_{jj}, i.e. outside of the W boson mass window, produces a compatible yield, but the ABCD method results in a lower overall uncertainty.

The top and diboson backgrounds are normalized to data in the CRs defined in Sect. 6.3 with a separate simultaneous fit to each corresponding SR. The $t\bar{t}$ and Wt processes share the same normalization factors of 1.03 ± 0.08 and 0.96 ± 0.19 in SR2ℓ-Low-RJR and SR2ℓ-ISR-RJR respectively. The normalization factors derived for the diboson backgrounds are 1.09 ± 0.10 and 0.96 ± 0.13 in the same regions. The yields in these CRs, along with the corresponding VRs, are listed in Tables 14 and 15 for the Low and ISR regions respectively. Distributions in the Low and ISR top and diboson VRs are shown in Fig. 3. The yields and distributions for Z/γ^*+jets in the tables and figure are from MC simulation because the ABCD method is only constructed for the SRs. The expected and observed distributions agree well in the VRs.

7.2 Electroweak search backgrounds

The dominant backgrounds in the EWK SRs are WZ, ZZ, and $t\bar{t}$ production. Additionally, Z/γ^*+jets is an important background for the Low and OffShell regions. Data-driven normalization factors for these backgrounds are extracted using a simultaneous likelihood fit to data in the SRs and CRs that are designed to be enriched in each background. CR-tt-EWK targets $t\bar{t}$ production and requires at least one b-jet and intermediate $\mathcal{S}(E^{\mathrm{miss}}_{\mathrm{T}}) \in [9, 12]$ to ensure orthogonality to the SRs; unlike the RJR search, the resulting normalization factor is not applied to Wt, which is instead normalized to the theoretical cross-section. CR-VZ-EWK targets WZ/ZZ production and uses the sideband of the SR-Int-EWK m_{jj} distribution, relaxing the $p^{j_1}_{\mathrm{T}}$ requirement. A common diboson normalization factor is applied to the SRs. To account for different kinematics, two separate normalization factors are defined for Z/γ^*+jets. CR-Z-EWK targets on-shell Z+jets production ($m_{\ell\ell} > 71$ GeV, which is the lowest edge of the Z mass window) while CR-DY-EWK targets low-mass Z/γ^*+jets production ($12 < m_{\ell\ell} < 71$ GeV). The resulting Z+jets normalization factor is applied everywhere, except for the OffShell regions, where the low-mass Z/γ^*+jets normalization factor is applied. The definitions of the CRs are provided in Tables 7, 8 and 9. The resulting normalization factors are 0.93 ± 0.09, 0.84 ± 0.08, 1.21 ± 0.14, and 0.86 ± 0.25 for $t\bar{t}$, diboson, Z+jets, and Z/γ^*+jets respectively.

To validate the normalization and modelling of the SM predictions, eight VRs are defined. For the High SRs, two VRs use the sideband of the m_{j_1} or m_{jj} distribution, while VR-High-R-EWK provides additional validation of the diboson background modelling inside the m_{jj} mass window by inverting the ΔR_{jj} requirement. VR-$\ell\ell bb$-EWK validates the top background in a $\mathcal{S}(E^{\mathrm{miss}}_{\mathrm{T}})$ window of 12–18 below the SR-$\ell\ell bb$-EWK threshold. Distributions of $\mathcal{S}(E^{\mathrm{miss}}_{\mathrm{T}})$ in the High and $\ell\ell bb$ VRs, with the normalizations from the simultaneous fit applied, are shown in Fig. 4. Good agreement between the data and the background prediction is observed.

VR-Int-EWK has the same requirements as SR-Int-EWK but with the requirement on $p^{j_1}_{\mathrm{T}}$ inverted and is dominated by the diboson processes. For the Low SRs, two VRs are defined. VR-Low-EWK requires a larger value of $\Delta R_{\ell\ell}$ than SR-Int-EWK, and VR-Low-2-EWK inverts the m_{jj} window. For the OffShell regions, VR-OffShell-EWK maintains orthogonality by using an m_{T2} window below that in the SR. Distributions of $\mathcal{S}(E^{\mathrm{miss}}_{\mathrm{T}})$ in the Int, Low, and OffShell VRs are shown in Fig. 5 with the normalization from the simultaneous fit applied. Good agreement is observed in all VRs.

Table 13 The selection criteria for the regions used in the ABCD Z/γ^*+jets background estimate for the RJR search. The left three columns coincide with the Standard Region, and the right three columns with the ISR Region

Standard Region	m_{jj} [GeV]	$H_{1,1}^{\mathrm{PP}}/H_{4,1}^{\mathrm{PP}}$	ISR Region	m_{T}^{J} [GeV]	$p_{\mathrm{T}1}^{\mathrm{CM}}$ [GeV]
SR2ℓ-Low-RJR	$\in (70, 90)$	$\in (0.35, 0.60)$	SR2ℓ-ISR-RJR	$\in (50, 110)$	> 100
$\mathrm{A_{Low}}$	$\in (20, 70)$	$\in (0.35, 0.60)$	$\mathrm{A_{ISR}}$	$\in (0, 50)$ or > 100	> 100
$\mathrm{B_{Low}}$	$\in (20, 70)$	$\in (0.20, 0.35)$	$\mathrm{B_{ISR}}$	$\in (0, 50)$ or > 100	< 100
$\mathrm{D_{Low}}$	$\in (70, 90)$	$\in (0.20, 0.35)$	$\mathrm{D_{ISR}}$	$\in (50, 110)$	< 100

Table 14 Breakdown of expected and observed yields in the diboson (VV) and top CRs and VRs for the standard-decay-tree regions associated with SR2ℓ-Low-RJR after a simultaneous fit to the control regions. The yields for Z/γ^*+jets are from MC simulation. The uncertainties include both the statistical and systematic sources

	CR2ℓ-VV-RJR	VR2ℓ-VV-RJR	CR2ℓ-Top-RJR	VR2ℓ-Top-RJR
Observed events	216	232	1759	368
Total exp. bkg. events	216 ± 16	285 ± 78	1760 ± 40	389 ± 51
Diboson events	195 ± 17	180 ± 40	19.3 ± 3.2	20.2 ± 3.5
Top events	–	47 ± 8	1700 ± 40	269 ± 16
Z/γ^*+jets events	–	58 ± 56	13 ± 12	91 ± 45
Other events	21 ± 4	3.8 ± 3.1	23 ± 11	8.5 ± 1.3

Table 15 Breakdown of expected an observed yields in the diboson (VV) and top CRs and VRs for the ISR-decay-tree regions associated with SR2ℓ-ISR-RJR after a simultaneous fit to the control regions. The yields for Z/γ^*+jets are from MC simulation. The uncertainties include both the statistical and systematic sources

	CR2ℓ-ISR-VV-RJR	VR2ℓ-ISR-VV-RJR	CR2ℓ-ISR-Top-RJR	VR2ℓ-ISR-Top-RJR
Observed events	149	50	289	306
Total exp. bkg. events	149 ± 14	63 ± 9	289 ± 19	350 ± 60
Diboson events	125 ± 17	28 ± 5	3.0 ± 0.6	4.5 ± 1.0
Top events	–	–	254 ± 18	330 ± 60
Z/γ^*+jets events	–	–	18 ± 15	10 ± 4
Other events	24 ± 9	35 ± 10	14.0 ± 2.6	8.7 ± 2.3

7.3 Strong search backgrounds

For the Strong search, the Z/γ^*+jets background is normalized in CRs, the FS backgrounds are estimated from $e\mu$ data, the FNP-lepton background is estimated in a data-driven way as previously described, and the remaining backgrounds are fully estimated via MC simulation. FS processes include those with independent leptonic decays such that the expected number of $e\mu$ events is the same as the number $ee+\mu\mu$ events, e.g. $t\bar{t}$, WW, and $Z \to \tau\tau$. VRs are constructed with an $E_{\mathrm{T}}^{\mathrm{miss}}$ requirement, $150 < E_{\mathrm{T}}^{\mathrm{miss}} < 250$ GeV, below the SR requirement in order to validate the background estimation. VRs with SS instead of OS leptons and with three instead of two leptons are also constructed in order to validate the FNP-lepton and WZ/ZZ backgrounds respectively.

The Z/γ^*+jets background, with decays to ee or $\mu\mu$, mainly enter the SRs due to $E_{\mathrm{T}}^{\mathrm{miss}}$ from the mismeasurement of jets or from contributions by neutrinos in heavy-flavour decays. The requirement of $\Delta\phi(\boldsymbol{j}_{1,2}, \vec{p}_{\mathrm{T}}^{\mathrm{miss}}) > 0.4$ removes Z/γ^*+jets events where the $\vec{p}_{\mathrm{T}}^{\mathrm{miss}}$ is aligned with a jet, as is the case for mismeasured jets. A CR is constructed for each SR or VR by inverting this requirement, and roughly half of the yield in these CRs is from Z/γ^*+jets events. The normalization of the Z/γ^*+jets MC prediction is extracted with a simultaneous likelihood fit to the CR and respective SR or VR. The resulting factors are within one standard deviation of one for every region except SRC-STR, where the small MC simulation prediction is pulled up by approximately 1.5 standard deviations, and VRLow-STR, where the MC simulation prediction is pulled down by approximately 1.3 standard deviations.

The FS method makes use of a CR for each SF region, with the lepton flavour requirement changed to select $e\mu$ data events. Differences between the efficiencies to select events with electrons and events with muons are used to adjust the $e\mu$ data events to more accurately predict $ee+\mu\mu$ events. For the on-Z SRs, the $e\mu$ data yield is small. In order to decrease

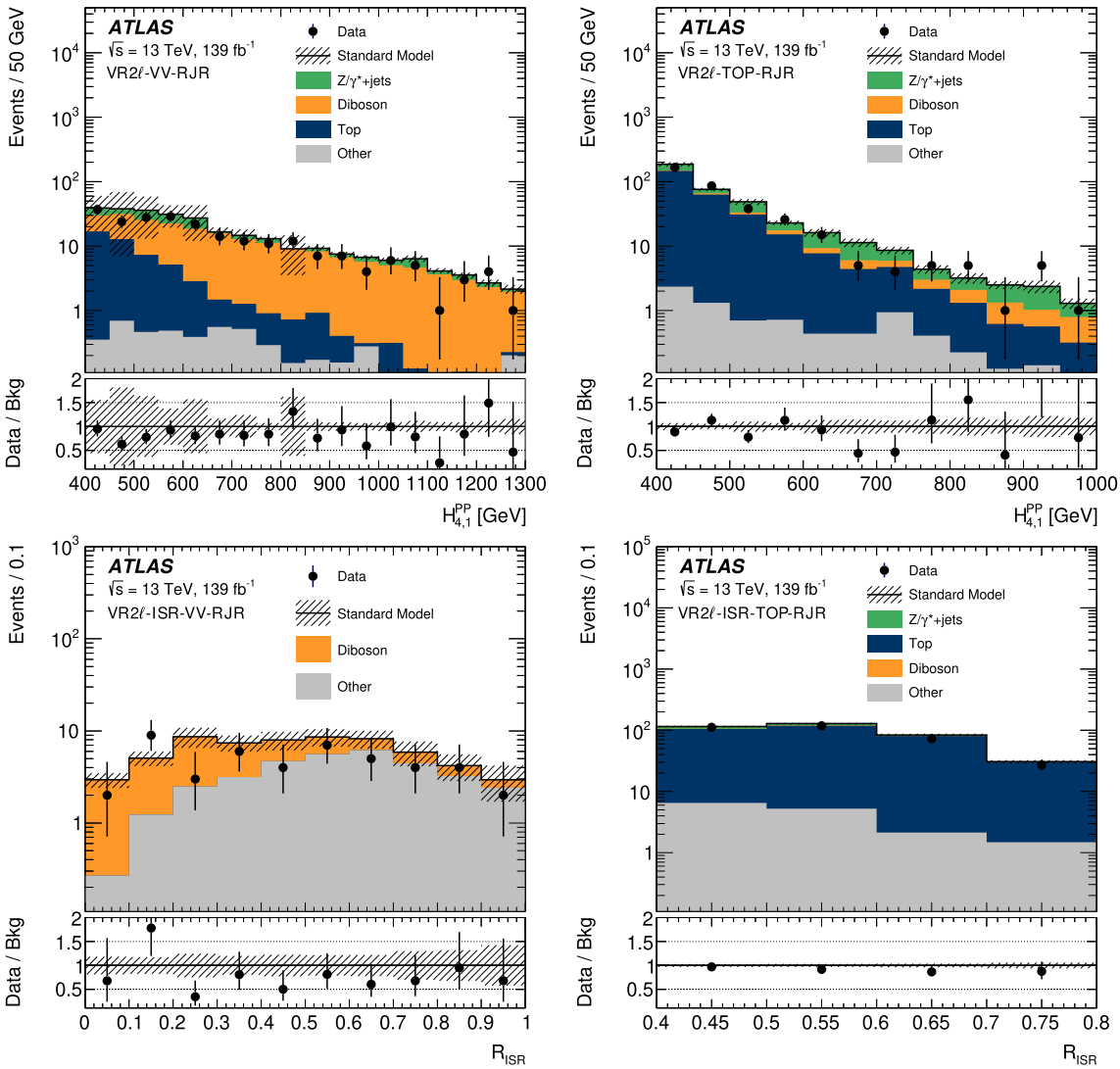

Fig. 3 Distributions of RJR variables in VR2ℓ-VV-RJR (top-left), VR2ℓ-Top-RJR (top-right), VR2ℓ-ISR-VV-RJR (bottom-left), and VR2ℓ-ISR-Top-RJR (bottom-right) from the RJR search. The background estimate models the data well in all regions after a simultaneous fit of the control regions. The standard and ISR regions are fit separately. The hatched band includes both the systematic and statistical uncertainties. The last bin contains the overflow

the statistical uncertainty of the FS prediction, the $m_{\ell\ell}$ window used to collect $e\mu$ events is widened to 61–121 GeV. The yield is then scaled down by the ratio of the yields in the narrower and wider $m_{\ell\ell}$ windows obtained from MC simulation. The estimated $ee+\mu\mu$ yield (N^{est}) is obtained as:

$$N^{\text{est}} = \frac{1}{2}\cdot\left[\sum_{i}^{N_{e\mu}^{\text{data}}}\left(k_e(p_{\text{T}}^{i,\mu},\eta^{i,\mu})+k_\mu(p_{\text{T}}^{i,e},\eta^{i,e})\right)\cdot\alpha(p_{\text{T}}^{i,\ell_1},\eta^{i,\ell_1})\right.$$
$$\left.-\sum_{i}^{N_{e\mu}^{\text{MC}}}\left(k_e(p_{\text{T}}^{i,\mu},\eta^{i,\mu})+k_\mu(p_{\text{T}}^{i,e},\eta^{i,e})\right)\cdot\alpha(p_{\text{T}}^{i,\ell_1},\eta^{i,\ell_1})\right], \quad (4)$$

where $N_{e\mu}^{\text{data}}$ is the number of data events observed in a given CR. Events from non-FS processes, e.g. WZ/ZZ, are subtracted from the $e\mu$ data events using MC simulation. This is the second term in Eq. (4), where $N_{e\mu}^{\text{MC}}$ is the number of events from non-FS processes in MC simulation in the CR. The factor $\alpha(p_{\text{T}}^{i},\eta^{i})$ accounts for the different trigger efficiencies for $ee/\mu\mu$ and $e\mu$ events, and $k_e(p_{\text{T}}^{i},\eta^{i})$ and $k_\mu(p_{\text{T}}^{i},\eta^{i})$ are the electron and muon selection efficiency factors for the kinematics of the lepton being replaced in event i. For example, if an event with a muon and electron is used to predict a $\mu\mu$ event, the kinematics of the electron are used to evaluate k_μ. The trigger and selection efficiency correction factors are derived from data events in an inclusive region with two

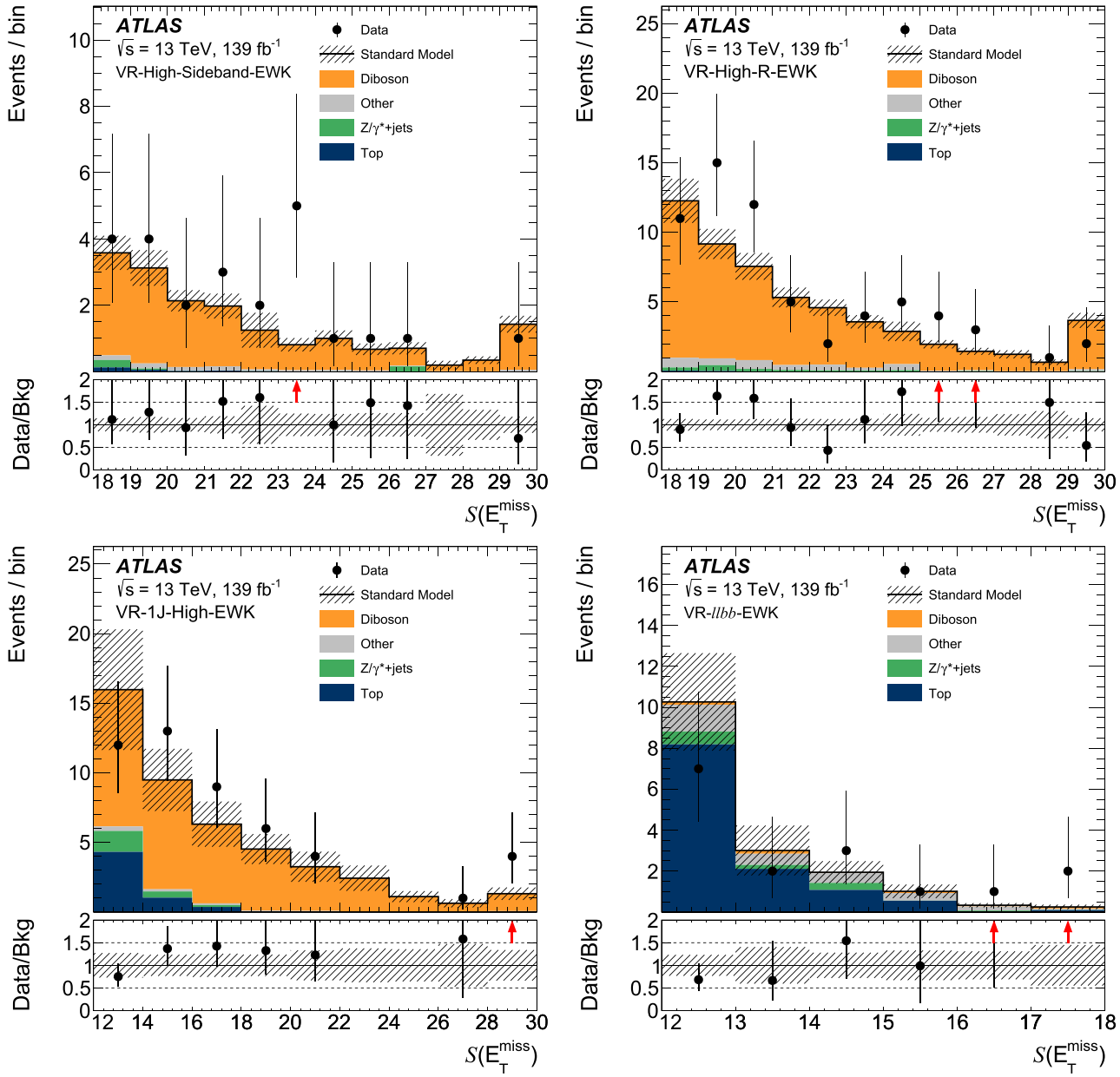

Fig. 4 Distributions of $\mathcal{S}(E_{\mathrm{T}}^{\mathrm{miss}})$ in VR-High-Sideband-EWK (top-left), VR-High-R-EWK (top-right), VR-1J-High-EWK (bottom-left), and VR-$\ell\ell bb$-EWK (bottom-right) from the EWK search after a simultaneous fit of the control regions. The hatched band includes both the systematic and statistical uncertainties. The last bin includes the overflow

signal leptons and at least two signal jets, according to:

$$k_e(p_{\mathrm{T}},\eta) = \sqrt{\frac{N_{ee}^{\mathrm{meas}}(p_{\mathrm{T}},\eta)}{N_{\mu\mu}^{\mathrm{meas}}(p_{\mathrm{T}},\eta)}},$$

$$k_\mu(p_{\mathrm{T}},\eta) = \sqrt{\frac{N_{\mu\mu}^{\mathrm{meas}}(p_{\mathrm{T}},\eta)}{N_{ee}^{\mathrm{meas}}(p_{\mathrm{T}},\eta)}},$$

$$\alpha(p_{\mathrm{T}},\eta) = \frac{\sqrt{\epsilon_{ee}^{\mathrm{trig}}(p_{\mathrm{T}}^{\ell_1},\eta^{\ell_1}) \times \epsilon_{\mu\mu}^{\mathrm{trig}}(p_{\mathrm{T}}^{\ell_1},\eta^{\ell_1})}}{\epsilon_{e\mu}^{\mathrm{trig}}(p_{\mathrm{T}}^{\ell_1},\eta^{\ell_1})},$$

where $\epsilon_{ee/\mu\mu/e\mu}^{\mathrm{trig}}$ is the trigger efficiency as a function of the leading-lepton (ℓ_1) kinematics and N_{ee}^{meas} ($N_{\mu\mu}^{\mathrm{meas}}$) is the number of ee ($\mu\mu$) data events in the inclusive region mentioned above. The factors $k_e(p_{\mathrm{T}},\eta)$ and $k_\mu(p_{\mathrm{T}},\eta)$ are calculated separately for leading and subleading leptons. The correction factors are typically within 20% of unity, except in the region $|\eta| < 0.1$, where they deviate by up to 40% from unity because of a lack of coverage by the muon spectrometer.

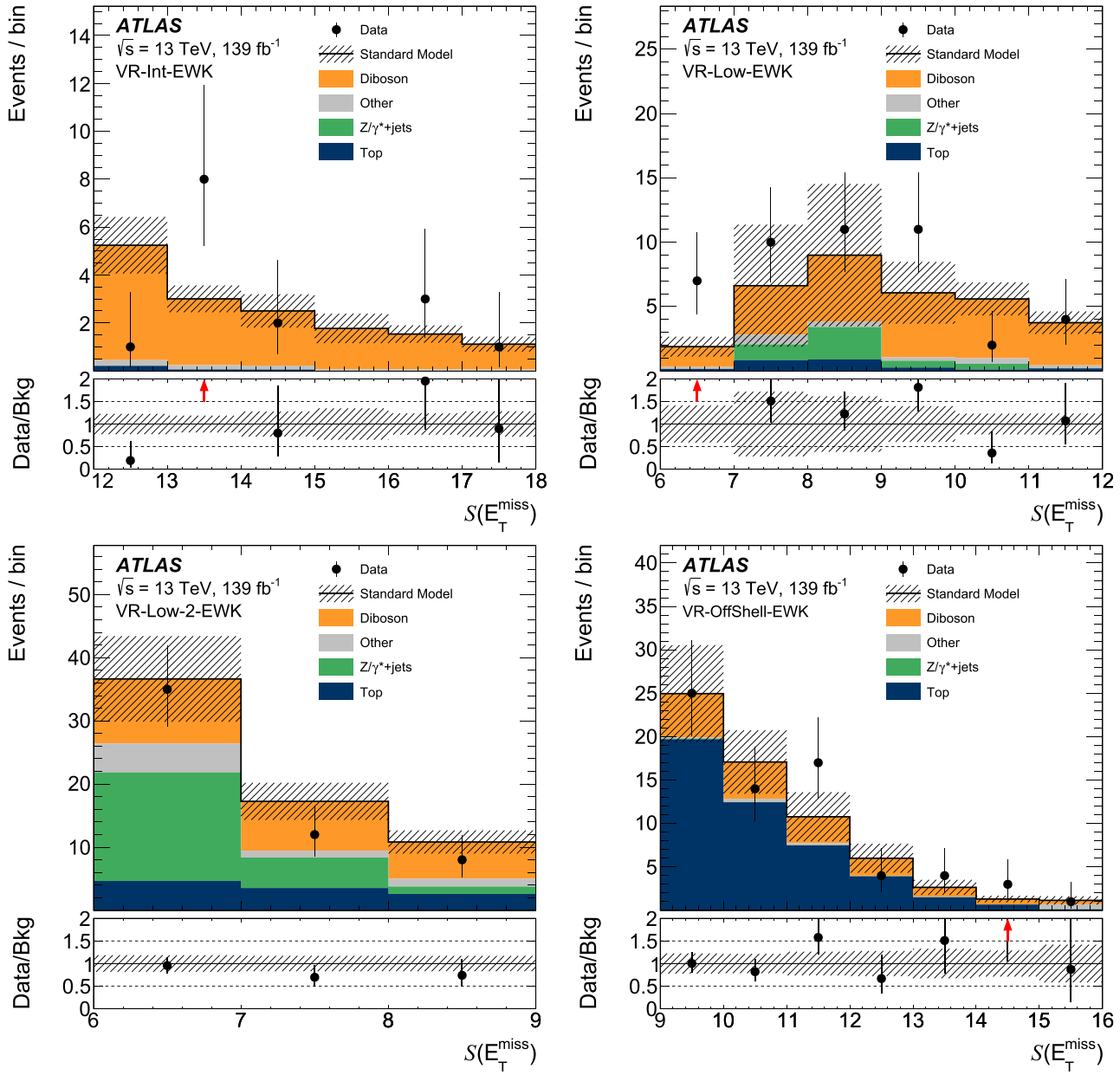

Fig. 5 Distributions of $\mathcal{S}(E_{\mathrm{T}}^{\mathrm{miss}})$ in VR-Int-EWK (top-left), VR-Low-EWK (top-right), VR-Low-2-EWK (bottom-left), and VR-OffShell-EWK (bottom-right) from the EWK search after a simultaneous fit of the control regions. The hatched band includes both the systematic and statistical uncertainties. The last bin includes the overflow

Comparisons of the $m_{\ell\ell}$ distribution between the background estimate and data in the VRs corresponding to the four edge SRs are shown in Fig. 6. Good agreement is observed in each of the regions. Since the on-Z SRs require at least four jets, their equivalent VRs correspond to the high-n_{jets} regions in the distribution of the number of jets for each VR shown in Fig. 7. Good agreement is seen in each VR. In order to validate the MC simulation of WZ/ZZ production, a three-lepton VR is constructed by selecting events with three signal leptons and applying requirements similar to those in the SRs, as shown near the bottom of Table 11. Figure 8 shows the $m_{\ell\ell}$ distribution in this VR3L-STR with a 13% theory uncertainty assigned to the WZ/ZZ background. Good agreement within the statistical uncertainty is observed.

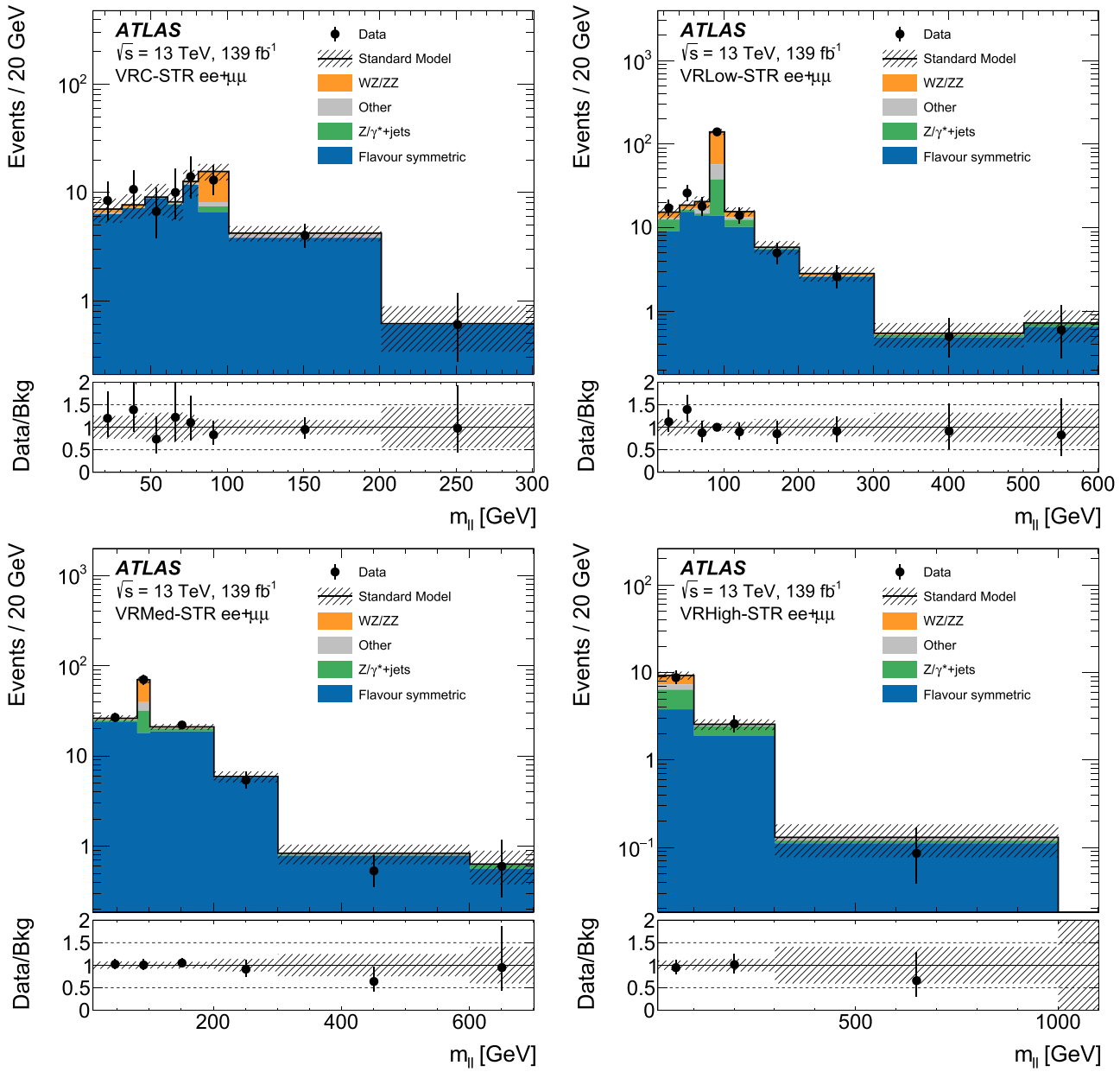

Fig. 6 Observed and expected dilepton mass distributions in VRC-STR (top-left), VRLow-STR (top-right), VRMed-STR (bottom-left), and VRHigh-STR (bottom-right). Each validation region is fit separately with the corresponding control region. All statistical and systematic uncertainties are included in the hatched band. The entries are normalized to the bin width, and the last bin is the overflow

8 Systematic uncertainties

Theoretical and experimental uncertainties are taken into account for the signal and background models. For processes that are not normalized to data, a 1.7% uncertainty is assigned to the integrated luminosity [40,41]. The estimated efficiencies from MC simulation to trigger on, reconstruct, and measure the objects required for this analysis are all subject to uncertainties to account for differences between data and simulation. For the jet energy scale, uncertainties due to the jet flavour composition, pile-up, and the jet and event kinematics [103] are considered. The jet energy resolution (JER) is also subject to additional uncertainties to account for differences between data and simulation [101]. Uncertainties in the lepton energy scales, resolutions, identification efficiencies, isolation efficiencies, reconstruction efficiencies, and trigger efficiencies are also considered. The uncertainties associated with the objects used to compute

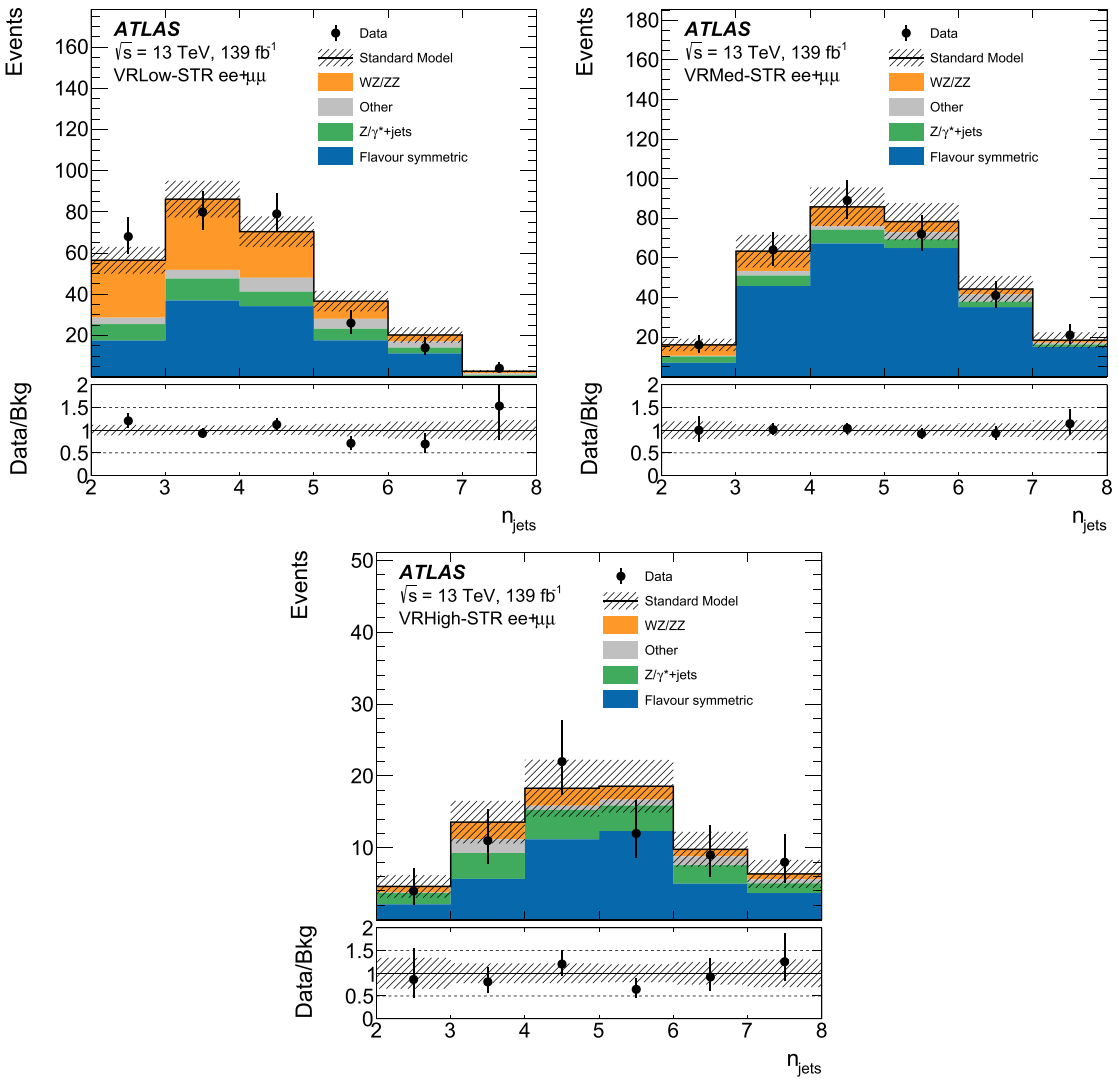

Fig. 7 Observed and expected jet multiplicity in VRLow-STR (top-left), VRMed-STR (top-right), and VRHigh-STR (bottom) after a fit performed on the $m_{\ell\ell}$ distribution and corresponding control region. All statistical and systematic uncertainties are included in the hatched band. The last bin contains the overflow

the $\vec{p}_{\mathrm{T}}^{\,\mathrm{miss}}$ are propagated through the computation, and additional uncertainties in the scale and resolution of the contribution from low-momentum tracks not associated with the primary objects are also included [119]. These experimental uncertainties are correlated between regions and processes, including signal models. The largest experimental uncertainties are related to the measurement of jets and typically result in an uncertainty in the total background of a few percent, but reach 10–20% in a couple of search regions. All of the uncertainties quoted below are for the expected yield of the process in analysis regions.

Uncertainties in the predicted cross-sections and modelling of background processes predicted via MC simulation are considered. If the background process is normalized to data, the total cross-section uncertainty is not applied, but instead an uncertainty for the extrapolation from the CR to the SR is evaluated. For background processes making large contributions to regions in the searches, acceptance uncertainties due to various choices, such as the PDF set and QCD scales, are applied. For small-background processes, these are ignored and only the total cross-section uncertainty is applied. In a few cases, negligibly small uncertainties are ignored in order to simplify the statistical evaluation of the level of data-to-background agreement. As an example, uncertainties due to the assumed value of the strong coupling, α_{s}, are ignored as they are found to be negligible. These uncertainties from theoretical predictions are correlated between regions for a given process, but uncorrelated between processes.

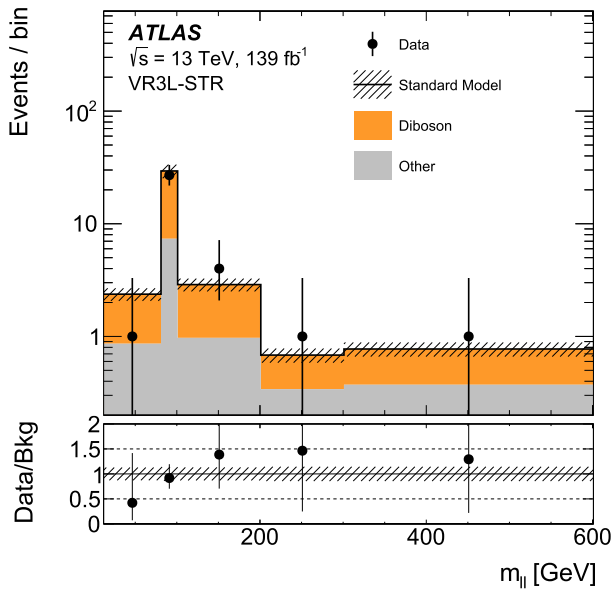

Fig. 8 Observed and expected dilepton mass distributions in VR3L-STR without a fit to the data. The 'Other' category includes the negligible contributions from $t\bar{t}$ and Z/γ^*+jets processes. The hatched band contains the statistical uncertainty and the theoretical systematic uncertainties of the WZ/ZZ prediction, which are the dominant sources of uncertainty in VR3L-STR. No fit is performed. The last bin contains the overflow

For the RJR and EWK searches, uncertainties in the $t\bar{t}$ ME are evaluated by a comparison of the default POWHEG generator and MG5_AMC@NLO. The effects of uncertainties in the PS are evaluated by comparing the default PYTHIA 8 showering with HERWIG 7 showering [120]. Uncertainties due to the amount of initial- and final-state radiation are evaluated by varying the relevant parameters in the generator. The effects of uncertainties in the QCD renormalization and factorization scales are evaluated by representing these scale uncertainties by three nuisance parameters in the fit: two nuisance parameters to independently vary each scale upwards and downwards by a factor of two, and one nuisance parameters for a correlated variation of both. Finally, uncertainties due to the choice of PDF are evaluated following the recommendations of Ref. [121]. The largest $t\bar{t}$ uncertainties in the RJR search regions SR2ℓ-Low-RJR and SR2ℓ-ISR-RJR are due to the uncertainty in the PS, 20% and 30% respectively. The uncertainty due to the amount of initial-state radiation is also large, 20% in SR2ℓ-ISR-RJR. The largest $t\bar{t}$ uncertainties in the EWK SRs tend to be from the ME comparison and range from 20% to 60%. The PS and radiation uncertainties are of similar size.

For the diboson processes, uncertainties from the choice of PDF set and QCD scales are evaluated in the same way as for $t\bar{t}$. Additional uncertainties are evaluated by varying the resummation scale upwards and downwards by a factor of two and by varying the merging scale between 15 and 30 GeV. Finally, an alternative PS recoil scheme in SHERPA is evaluated, and the difference from the nominal sample is taken as the one standard deviation variation. For the Strong search, where the diboson processes are not normalized to data, a 6% uncertainty [62] is applied to the total cross-section. The uncertainty due to the choice of various scales is generally the largest one for the diboson backgrounds and varies from 10 to 30% depending on the region.

For the EWK and Strong searches, the Z/γ^*+jets processes are also subject to the same uncertainties from the choice of PDF, QCD scales, resummation scale, and merging scale as the diboson processes. An additional uncertainty from the ME calculation and is evaluated by comparing the nominal SHERPA sample with an alternative MG5_AMC@NLO sample. Uncertainties in the Z/γ^*+jets background in the EWK search regions range from 10 to 20% from the choice of scale and up to 60% from the ME comparison in regions with at least one predicted Z/γ^*+jets event. The largest uncertainty in the Z/γ^*+jets background in the Strong search regions is typically from the ME comparison, and ranges from 20% to 60% in regions with at least one predicted Z/γ^*+jets event.

In the SR-$\ell\ell bb$ region of the EWK search a large fraction of the background events are from $t\bar{t}+Z$. For $t\bar{t}+Z$ in the EWK search regions, uncertainties from the ME and PS are evaluated by comparisons with a SHERPA sample and a MG5_AMC@NLO+HERWIG 7 sample respectively. The same renormalization scale, factorization scale, and PDF uncertainties described above are also evaluated. The largest uncertainty is from the ME comparison and ranges from 10% to 50%, depending on the region. In addition, a 6% uncertainty on the Wt background is applied.

Uncertainties in the cross-sections of smaller backgrounds estimated directly from MC simulation are applied as follows. A conservative uncertainty of 10% is applied to the entire Higgs boson sample, based on the $t\bar{t}H$ cross-section uncertainty in Ref. [68]. The Other Top sample is predominantly $t\bar{t}+V$, so a cross-section uncertainty of 13%, also from Ref. [68], is applied to this background category. An uncertainty of 32% is applied to the VVV background, based on comparisons between SHERPA and VBFNLO [62].

For data-driven background estimates, uncertainties in the prediction are derived from the limited number of events used in the prediction and by varying the assumptions used. In cases where CRs are used to normalize the yield of a process, theoretical uncertainties are evaluated, as described above, for the acceptance of the CR relative to the SR.

Uncertainties in the matrix-method estimate of the FNP leptons arise from the size of the samples used and the composition of the FNP-lepton sources, and the total uncertainty of the estimate is obtained by combining uncertainties from several sources. The statistical uncertainties arise from the limited number of events in regions used to derive the var-

ious efficiencies and are propagated to the final estimate. The variations of the lepton efficiency corrections are propagated to the light-flavour efficiencies because MC simulation is used in the derivation. For heavy-flavour efficiencies, an uncertainty in the prompt-lepton contamination from MC simulation is taken into account. Finally, an uncertainty in the estimated proportions of light-flavour jets, heavy-flavour jets, and photon conversions contributing to the processes producing FNP leptons is included. This is computed by varying the composition, using MC simulation, of the regions with selections similar to various analysis regions used to construct the weights. In cases where the number of events in a region is not sufficient to predict the FNP lepton contribution with the matrix method, the central value and uncertainty are taken from the larger of two computations. The first computation is the mean of the weights in the matrix method with the root mean square of these weights as the uncertainty. This would be the average prediction if there were one event for the matrix method. The second computation is the FNP-lepton yield predicted by MC simulation with a 100% uncertainty. These extra computations of the FNP-lepton background are only used in the EWK search, where the search regions have small yields.

For the flavour-symmetric background estimate in the Strong search regions, the uncertainties due to a limited number of events in the DF regions and the regions used to derive the correction factors are propagated to the final estimate. An additional uncertainty of 10% is applied to the estimate, based on closure tests. The closure tests were performed on both data and MC events in the region used to derive the weights, with $E_{\mathrm{T}}^{\mathrm{miss}}$ restricted to be between 100 and 200 GeV, and on MC events in the SRs. Finally, for the on-Z regions where the $m_{\ell\ell}$ window used to collect DF events is expanded, an additional uncertainty is applied to account for the limited number of events in the MC simulation used to evaluate this extrapolation.

Uncertainties are applied to the estimate of Z/γ^*+jets with the ABCD method in the RJR search to account for the limited number of events in the regions used to extract the estimate and the theoretical and experimental uncertainties, discussed above, in the non-Z/γ^*+jets MC simulation backgrounds. The correlations between the ABCD variables are found to be very small and the related systematic uncertainties are treated as negligible.

For signal models with the production of squarks or gluinos, the nominal cross-section and its uncertainty due to scale variations and the choice of PDF are determined as described in Ref. [84]. For signal models containing the direct production of electroweakinos, the cross-section and its uncertainty are taken from Ref. [82]. The uncertainties in the acceptance of signal model events, from scale variations and the PS tuning and radiation, are estimated and summed in quadrature.

The most important uncertainties in the total background estimate across the various searches are related to the theoretical prediction of the largest backgrounds (e.g. diboson and $t\bar{t}$ production), experimental uncertainties related to jets, and the number of simulated MC events for the estimation of SM processes. The most important uncertainties in the RJR search SRs (SR2ℓ-Low-RJR / SR2ℓ-ISR-RJR), relative to the total expected background, are from the normalization of Z/γ^*+jets via the ABCD background estimate (19%/28%), the size of the simulated samples (7%), and the matching scale for the diboson processes (5%/6%). The largest jet-related experimental uncertainty is a component of the JER (1%) in SR2ℓ-Low-RJR, and the b-jet tagging efficiency (2%) in SR2ℓ-ISR-RJR. The sizes of the uncertainties in the total background, grouped into categories after fits to the SRs, are summarized in Fig. 9a.

The most important uncertainties in the EWK search SRs depend on the region. The largest uncertainties in the total background in the SR-High-EWK regions arise from the size of the simulated samples (4–23%), the prediction of the fake and non-prompt leptons (3–17%), and in SR-1J-High-EWK the uncertainty in the jet mass measurement (37%). The largest jet-related experimental uncertainties in regions that do not use the jet mass are 2–3%. In SR-Int_a-EWK, the dominant uncertainty is from the amount of final-state radiation in the simulation of $t\bar{t}$ production (16%). In SR-Int_b-EWK, the dominant uncertainty is related to the JER, with several components in the 4–6% range. In the SR-Low-EWK regions, the largest uncertainties are from the size of the simulated samples (6–35%), the JER (6–18%), and the choice of generator for the Z/γ^*+jets ME (13–23%). In the SR-OffShell-EWK and SR-$\ell\ell bb$-EWK regions, the largest uncertainties arise from the size of the simulated samples (7–12%), the choice of generator for the Z/γ^*+jets ME (4–10%), and the JER (4–11%). Additionally, in SR-$\ell\ell bb$-EWK, the uncertainties from the $t\bar{t}$ PS and ME calculation are 12% for each. The sizes of the uncertainties in the total background, grouped into categories after a fit to the regions, are summarized in Fig. 9b.

The most important uncertainties in the Strong search SRs are those from the various scales used in the simulation of diboson production and the PS recoil scheme, typically 3–6% in the edge SRs and up to 18% in the on-Z SRs; the non-closure of the flavour-symmetric background estimate (2–6%) in the edge SRs; the ME generator for Z/γ^*+jets, up to 7% in SRZ-High-STR; and the size of the simulated samples (2–11%). The largest jet-related experimental uncertainties are 1–5% from uncertainties in the parton origin, or flavour, of the jet, depending on the region. The sizes of the uncertainties in the total background, grouped into categories after fits to the SRs, are summarized in Fig. 9c.

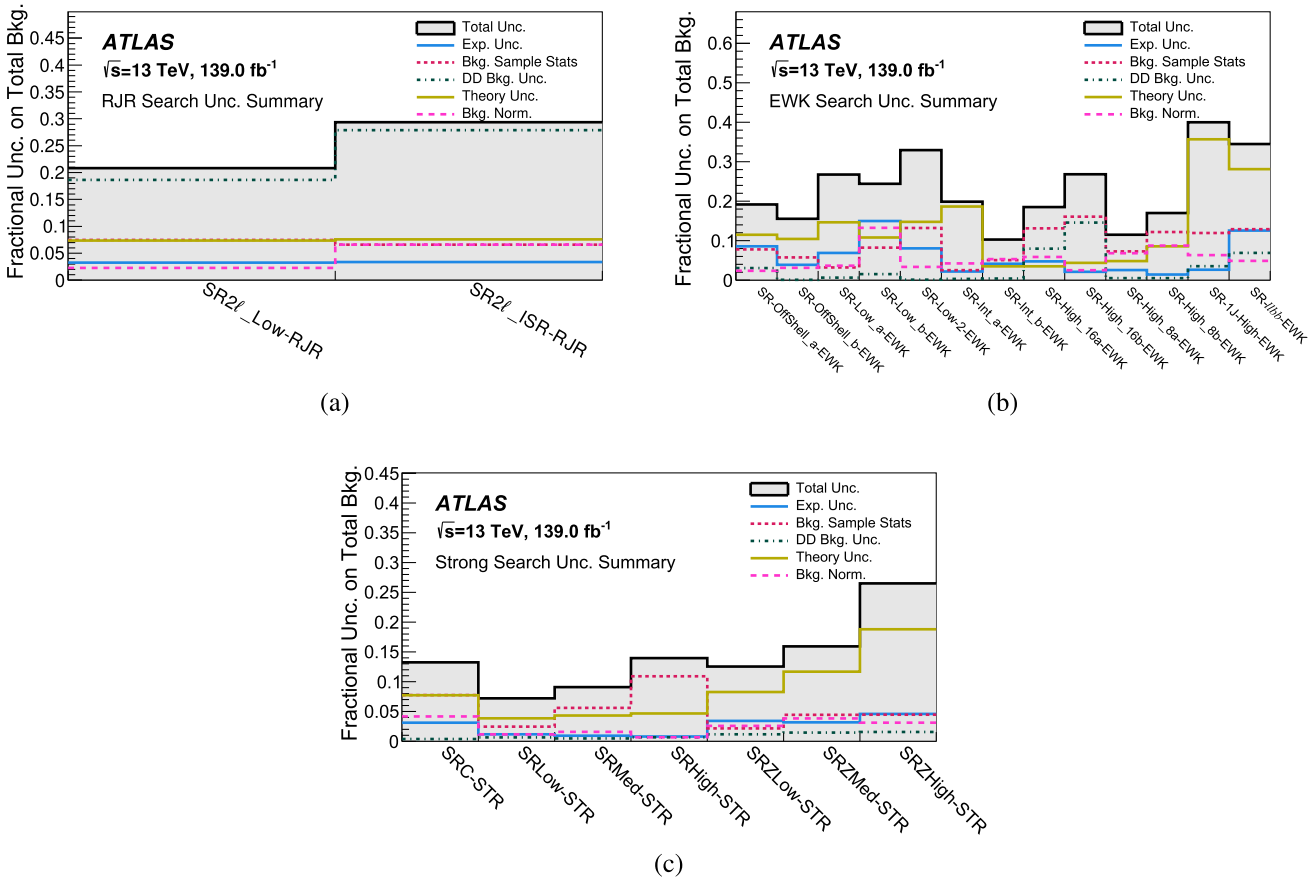

Fig. 9 Breakdown of the uncertainties in each of the (**a**) RJR, (**b**) EWK, and (**c**) strong searches into categories. The total fractional uncertainty of the background is shown as a shaded histogram. The experimental uncertainties include those from object reconstruction and identification efficiencies, object resolutions and scales, pile-up distribution, and trigger efficiencies. The background sample statistical uncertainty includes the uncertainty in the number of Monte Carlo and data-driven background events. The data-driven background uncertainty includes additional uncertainties, e.g. the uncertainty in the FNP-lepton estimate. The theory uncertainty includes any theory uncertainties in background estimates. The background normalization category includes the uncertainty associated with the normalization factors derived from CRs

9 Results

The data are compared with SM predictions using the profile likelihood method [24]. The HistFitter framework [122], built on RooFit, RooStats, HistFactory, and ROOT [123–126], is used to produce the presented statistical results. Model-independent upper limits on the number of events (S^{95}) at 95% CL that could be attributed to BSM processes are evaluated using the CL_s prescription [127]. Yields are reported after a fit to the background-only model, i.e. the zero signal-strength model. Compatibility tests are reported for the observed data and the background-only hypothesis ($p(s = 0)$) and for the observed data and the hypothesis with the signal strength at the 95% CL limit (CL_b).

9.1 Recursive-jigsaw reconstruction search results

A breakdown of the observed and expected yields in the RJR search SRs is shown in Table 16. The background yields result from a simultaneous profile likelihood fit of the CRs, excluding the SRs themselves. The fits for SR2ℓ-Low-RJR and SR2ℓ-ISR-RJR are performed separately and are not combined. The background estimate agrees with the observed data in both cases. Figure 10 summarizes the event yields in the CRs, VRs, and SRs of the RJR search. The asymptotic approximation [24] is used to set model-independent upper limits on the number of events, or cross-section, which could arise from BSM processes in the two SRs. These are presented in Table 17. The asymptotic approximation was validated against pseudo-experiments.

Table 16 Breakdown of expected and observed yields in the two recursive-jigsaw reconstruction signal regions after a simultaneous fit of the CRs. The two sets of regions are fit separately. The uncertainties include both the statistical and systematic sources

	SR2ℓ-Low-RJR	SR2ℓ-ISR-RJR
Observed events	39	30
Total expected background events	42 ± 9	31 ± 9
Diboson events	10.6 ± 3.4	8.9 ± 2.5
Top events	3.5 ± 1.7	8.2 ± 2.3
Z/γ^*+jets events	27 ± 8	12 ± 9
Other events	$0.3^{+0.5}_{-0.3}$	0.11 ± 0.04

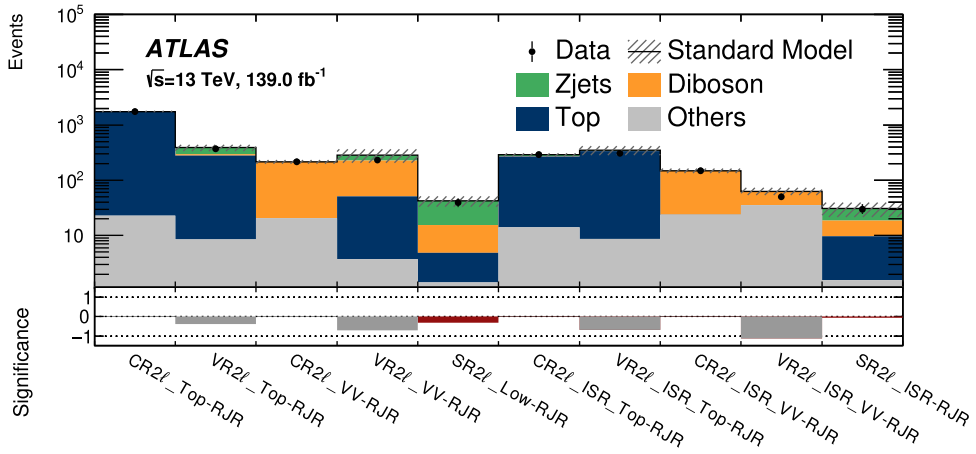

Fig. 10 The observed and expected yields in the control regions, validation regions, and signal regions of the RJR search after a simultaneous fit of the background-only model to control regions. The standard regions are shown to the left, and the ISR regions are shown to the right. These two sets of regions are fit separately. The hatched band includes the statistical and systematic uncertainties of the background prediction in each region. The significance of the difference between the observed data and the expected yield in each region is shown in the lower panel using the profile likelihood method of Ref. [128]; the colours black, grey, and red separate the CRs, VRs, and SRs, respectively. For the cases where the expected yield is larger than the data, a negative significance is shown. The relevant backgrounds are normalized to data in the CR by the fit and the significances are therefore zero

Table 17 Model-independent upper limits on the observed visible cross-section in the two recursive-jigsaw reconstruction signal regions, derived using the asymptotic approximation. Left to right: background-only model post-fit total expected background, with the combined statistical and systematic uncertainties; observed data; 95% CL upper limits on the visible cross-section ($\langle A\epsilon\sigma\rangle^{95}_{\text{obs}}$) and on the number of signal events (S^{95}_{obs}). The sixth column (S^{95}_{exp}) shows the expected 95% CL upper limit on the number of signal events, given the expected number (and $\pm 1\sigma$ excursions of the expectation) of background events. The last two columns indicate the confidence level of the background-only hypothesis (CL_b) and discovery p-value with the corresponding Gaussian significance ($Z(s=0)$). CL_b provides a measure of compatibility of the observed data with the signal strength hypothesis at the 95% CL limit relative to fluctuations of the background, and $p(s=0)$ provides a measure of compatibility of the observed data with the background-only hypothesis relative to fluctuations of the background. The p-value is capped at 0.5

Signal Region	Total Bkg.	Data	$\langle A\epsilon\sigma\rangle^{95}_{\text{obs}}$ [fb]	S^{95}_{obs}	S^{95}_{exp}	CL_b	$p(s=0)$ (Z)
SR2ℓ-Low-RJR	42 ± 9	39	0.13	17.9	$20.0^{+7.0}_{-5.4}$	0.40	0.50 (0.00)
SR2ℓ-ISR-RJR	31 ± 9	30	0.13	18.2	$18.2^{+7.8}_{-2.6}$	0.50	0.50 (0.00)

9.2 Electroweak search results

The yields in the High, $\ell\ell bb$, Int, Low, and OffShell SRs of the EWK search are listed in Tables 18 and 19. Each SR in the tables is split by the binning described in Sect. 6.4. For SR-High-EWK the 8 or 16 suffix denotes the ΔR_{jj} ranges of 0–0.8 and 0.8–1.6 respectively. Similarly, the a and b suffixes denote the $\mathcal{S}(E_{\text{T}}^{\text{miss}})$ ranges of 18–21 and > 21 respectively. For SR-Int-EWK and SR-Low-EWK, the a and b suffixes denote the lower and upper ranges of $\mathcal{S}(E_{\text{T}}^{\text{miss}})$ in the binning $(12, 15, 18)$ and $(6, 9, 12)$ respectively. For SR-OffShell-EWK, the a and b suffixes denote the lower and upper $m_{\ell\ell}$ ranges of 12–40 and 40–70 GeV. The results are extracted after a simultaneous profile likelihood fit to the four CRs and

Table 18 Breakdown of expected and observed yields in the electroweak search High and $\ell\ell bb$ signal regions after a simultaneous fit to the signal regions and control regions. All statistical and systematic uncertainties are included

	SR-High_16a-EWK	SR-High_8a-EWK	SR-1J-High-EWK	SR-$\ell\ell bb$-EWK
Observed events	4	0	1	0
Total exp. bkg. events	3.9 ± 0.7	2.00 ± 0.23	0.85 ± 0.34	0.58 ± 0.20
Diboson events	3.2 ± 0.6	1.86 ± 0.22	0.80 ± 0.31	0.13 ± 0.03
Top events	$0.00^{+0.01}_{-0.00}$	0.0 ± 0.0	$0.03^{+0.04}_{-0.03}$	$0.05^{+0.08}_{-0.05}$
Z/γ^*+jets events	0.0 ± 0.0	0.0 ± 0.0	0.0 ± 0.0	0.0 ± 0.0
Other events	0.7 ± 0.4	0.15 ± 0.07	$0.02^{+0.04}_{-0.02}$	0.39 ± 0.16
	SR-High_16b-EWK	SR-High_8b-EWK		
Observed events	3	0		
Total exp. bkg. events	3.4 ± 0.9	2.00 ± 0.33		
Diboson events	2.5 ± 0.6	1.94 ± 0.33		
Top events	0.0 ± 0.0	0.0 ± 0.0		
Z/γ^*+jets events	0.0 ± 0.0	0.0 ± 0.0		
Other events	0.9 ± 0.7	0.06 ± 0.04		

Table 19 Breakdown of expected and observed yields in the electroweak search Int, Low, and OffShell signal regions after a simultaneous fit to the signal regions and control regions. All statistical and systematic uncertainties are included

	SR-Int_a-EWK	SR-Low_a-EWK	SR-Low-2-EWK	SR-OffShell_a-EWK
Observed events	24	10	8	6
Total exp. bkg. events	22.8 ± 3.5	12.8 ± 3.4	9 ± 4	9.2 ± 1.7
Diboson events	16.5 ± 1.7	7.3 ± 1.3	4.0 ± 2.1	4.9 ± 1.3
Top events	4 ± 4	$0.06^{+0.14}_{-0.06}$	$1.0^{+1.2}_{-1.0}$	1.4 ± 0.7
Z/γ^*+jets events	2.1 ± 0.7	3.7 ± 3.3	4 ± 4	1.2 ± 1.2
Other events	0.44 ± 0.13	1.7 ± 0.4	0.58 ± 0.3	1.6 ± 0.4
	SR-Int_b-EWK	SR-Low_b-EWK		SR-OffShell_b-EWK
Observed events	14	8		15
Total exp. bkg. events	10.1 ± 1.0	10.5 ± 2.5		12.5 ± 1.9
Diboson events	9.2 ± 1.0	8.6 ± 1.2		6.1 ± 1.5
Top events	0.22 ± 0.13	0.0 ± 0.0		2.8 ± 1.4
Z/γ^*+jets events	0.51 ± 0.31	$1.3^{+2.2}_{-1.3}$		3.1 ± 1.4
Other events	0.19 ± 0.08	0.70 ± 0.11		0.54 ± 0.24

all of the SRs. SR-High-EWK regions have small deficits in the observed data compared to the expected background yield. No systematic trends are observed in the VRs around these regions, VR-High-Sideband-EWK and VR-High-R-EWK. Figure 11 shows distributions in five regions, plotting the variable used for the binning denoted by a and b above. Example signal distributions are overlaid from models near the edge of sensitivity for this search. Figure 12 summarizes all of the CRs, VRs, and SRs of the EWK search.

In order to perform model-independent tests, the five SR categories are merged into single discovery region (DR) bins. DR-High-EWK is SR-High_8-EWK merged over its $\mathcal{S}(E_{\mathrm{T}}^{\mathrm{miss}})$ bins, and DR-Low-EWK is SR-Low-EWK merged over its $\mathcal{S}(E_{\mathrm{T}}^{\mathrm{miss}})$ bins. DR-High-EWK has the largest deficit of data compared to the expected background, resulting in a local significance of -2.8σ. The resulting upper limits, based on pseudo-experiments, on the number of possible BSM events in each region are summarized in Table 20.

9.3 Strong search results

The integrated data yields in the edge and on-Z regions are compared to the expected background yields in Tables 21 and 22 respectively. The $m_{\ell\ell}$ distributions in the four edge regions are shown in Fig. 13. The yields and distributions are shown after a profile likelihood fit to the SR and its respective CR. The SM expectations agree well with the observed data.

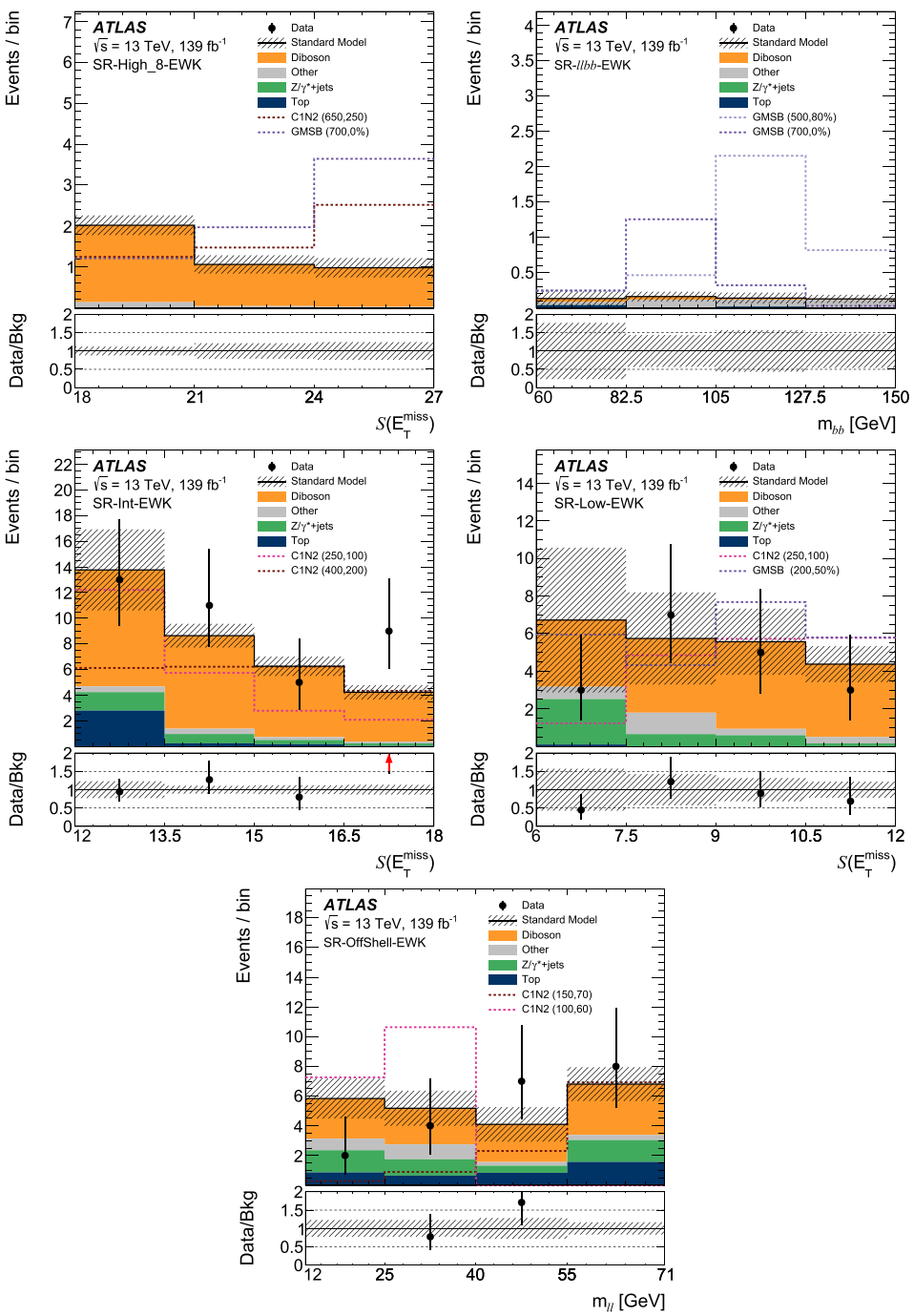

Fig. 11 Observed and expected distributions in five EWK search regions after a simultaneous fit to the signal regions and control regions. In the top row, left-to-right, are $\mathcal{S}(E_{\mathrm{T}}^{\mathrm{miss}})$ in SR-High_8-EWK and m_{bb} in SR-$\ell\ell bb$-EWK. In the middle row, left-to-right, are $\mathcal{S}(E_{\mathrm{T}}^{\mathrm{miss}})$ in SR-Int-EWK and $\mathcal{S}(E_{\mathrm{T}}^{\mathrm{miss}})$ in SR-Low-EWK. In the bottom row is $m_{\ell\ell}$ in SR-OffShell-EWK. Overlaid are example C1N2 and GMSB signal models, where the numbers in the brackets indicate the masses, in GeV, of the $\tilde{\chi}_1^{\pm}$ and $\tilde{\chi}_2^0$ or the mass of the $\tilde{\chi}_1^0$ and branching ratio to the Higgs boson respectively. All statistical and systematic uncertainties are included in the hatched bands. The last bin includes the overflow

Figure 14 summarizes the observed and expected yields in all of the CRs, VRs, and SRs in the Strong search.

Since the signal models may produce a kinematic edge anywhere along the $m_{\ell\ell}$ distribution, below the Z boson mass for those with a Z boson in the decay, several $m_{\ell\ell}$ windows are used to search for an excess of data events above the expectation. Twelve windows covering various $m_{\ell\ell}$ ranges in the edge SRs are considered, along with the three single-bin on-Z SRs. Results in each of these windows are summarized in Table 23. The data are generally consistent with the background to one standard deviation. The high $m_{\ell\ell}$ bins of SRLow-STR have a slightly higher local deviation above the expectation. The table also includes model-independent limits on the number of possible BSM events, as described at the beginning of this section, evaluated with pseudo-experiments.

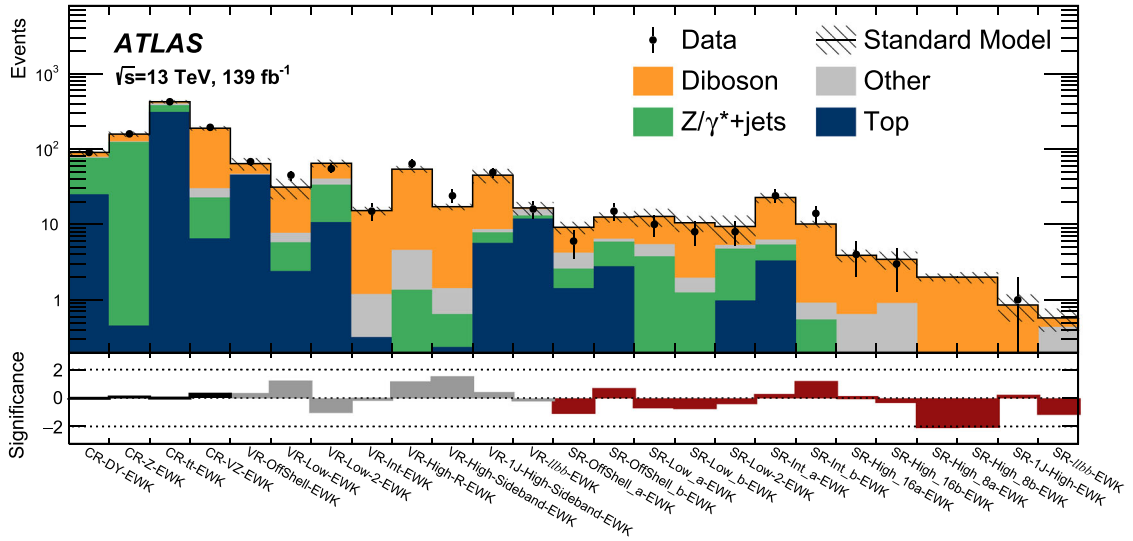

Fig. 12 The observed and expected yields in the control regions (left), validation regions (middle), and signal regions (right) of the EWK search after a simultaneous fit to the signal regions and control regions. The hatched band includes the statistical and systematic uncertainties of the background prediction in each region. The significance of the difference between the observed data and the expected yield in each region is shown in the lower panel using the profile likelihood method of Ref. [128]; the colours black, grey, and red separate the CRs, VRs, and SRs, respectively. For the cases where the expected yield is larger than the data, a negative significance is shown

Table 20 Model-independent upper limits on the observed visible cross-section in the five electroweak search discovery regions, derived using pseudo-experiments. Left to right: background-only model post-fit total expected background, with the combined statistical and systematic uncertainties; observed data; 95% CL upper limits on the visible cross-section ($\langle A\epsilon\sigma\rangle^{95}_{\text{obs}}$) and on the number of signal events (S^{95}_{obs}). The sixth column (S^{95}_{exp}) shows the expected 95% CL upper limit on the number of signal events, given the expected number (and $\pm 1\sigma$ excursions of the expectation) of background events. The last two columns indicate the confidence level of the background-only hypothesis (CL_b) and discovery p-value with the corresponding Gaussian significance ($Z(s=0)$). CL_b provides a measure of compatibility of the observed data with the signal strength hypothesis at the 95% CL limit relative to fluctuations of the background, and $p(s=0)$ measures compatibility of the observed data with the background-only hypothesis relative to fluctuations of the background. The p-value is capped at 0.5

Signal Region	Total Bkg.	Data	$\langle A\epsilon\sigma\rangle^{95}_{\text{obs}}$ [fb]	S^{95}_{obs}	S^{95}_{exp}	CL_b	$p(s=0)$ (Z)
DR-OffShell-EWK	22.1 ± 2.7	21	0.10	14.3	$12.3^{+4.7}_{-3.1}$	0.68	0.50 (0.0)
DR-Low-EWK	22 ± 4	18	0.08	10.8	$15.3^{+5.7}_{-4.0}$	0.09	0.50 (0.0)
DR-Int-EWK	35 ± 4	38	0.15	20.9	$17.5^{+5.9}_{-3.9}$	0.73	0.23 (0.8)
DR-High-EWK	3.9 ± 0.5	0	0.02	3.0	$5.6^{+2.2}_{-1.5}$	0.00	0.50 (0.0)
DR-$\ell\ell bb$-EWK	0.51 ± 0.20	0	0.02	3.0	$3.0^{+1.3}_{-0.0}$	0.19	0.50 (0.0)

Table 21 Breakdown of expected and observed yields in the four edge signal regions, integrated over the $m_{\ell\ell}$ distribution after a separate simultaneous fit to each signal region and control region pair. The uncertainties include both the statistical and systematic sources

	SRC-STR	SRLow-STR	SRMed-STR	SRHigh-STR
Observed events	38	118	65	19
Total expected background events	35 ± 4	116 ± 8	68 ± 6	24.1 ± 3.4
WZ/ZZ events	15.8 ± 3.4	76 ± 8	25 ± 4	6.1 ± 1.6
Flavour-symmetric events	15.3 ± 2.4	23.9 ± 2.8	35 ± 4	14.5 ± 2.3
Z/γ^*+jets events	$1.8^{+3.0}_{-1.8}$	4.8 ± 2.7	2.9 ± 1.7	1.7 ± 1.3
Other events	1.6 ± 0.4	11.2 ± 2.4	4.3 ± 1.1	1.8 ± 0.5

Table 22 Breakdown of expected and observed yields in the three on-Z signal regions after a separate simultaneous fit to each signal region and control region pair. The uncertainties include both the statistical and systematic sources

	SRZLow-STR	SRZMed-STR	SRZHigh-STR
Observed events	35	15	3
Total expected background events	33 ± 4	15.2 ± 2.4	4.5 ± 1.2
WZ/ZZ events	24 ± 4	10.0 ± 2.5	3.2 ± 1.2
Flavour-symmetric events	1.5 ± 0.7	2.3 ± 0.4	0.32 ± 0.07
Z/γ^*+jets events	1.7 ± 1.3	0.9 ± 0.5	$0.3^{+0.4}_{-0.3}$
Other events	5.1 ± 1.1	2.0 ± 0.5	0.72 ± 0.14

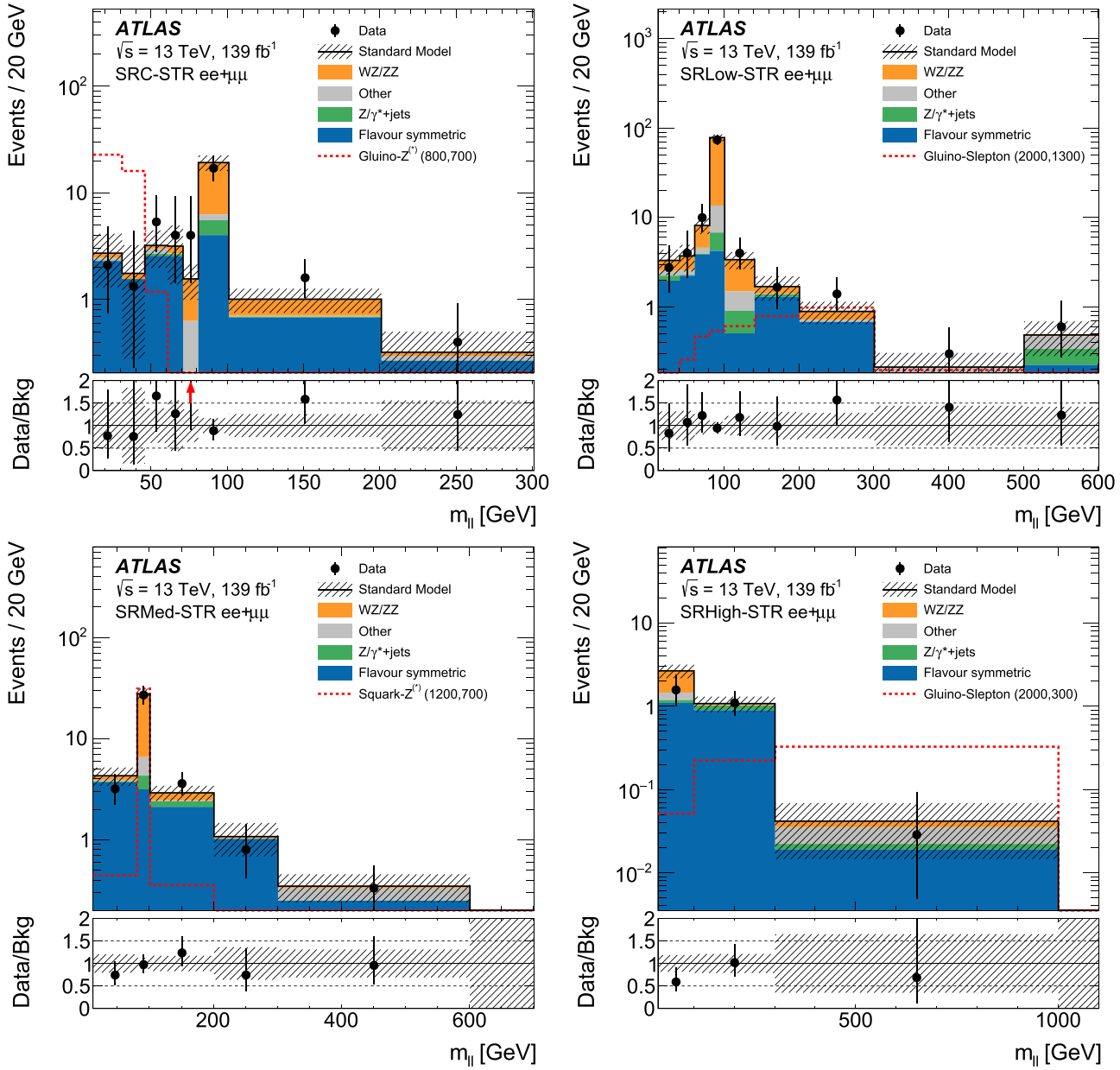

Fig. 13 Observed and expected dilepton mass distributions in SRC-STR (top-left), SRLow-STR (top-right), SRMed-STR (bottom-left), and SRHigh-STR (bottom-right), with the binning used for interpretations after a separate simultaneous fit to each signal region and control region pair. The red dashed lines are example signal models overlaid on the figure. All statistical and systematic uncertainties are included in the hatched bands. The last bins are the overflow

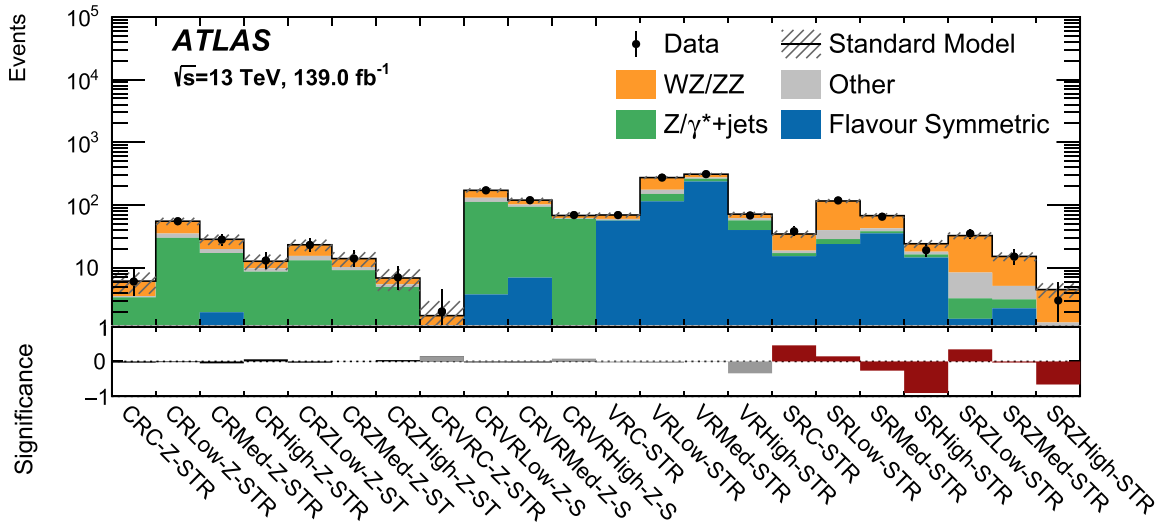

Fig. 14 The observed and expected yields in the control regions (left), validation regions (middle), and signal regions (right) of the Strong search after a separate simultaneous fit to each signal region and control region pair. The hatched band includes the statistical and systematic uncertainties of the background prediction in each region. The significance of the difference between the observed data and the expected yield in each region is shown in the lower panel using the profile likelihood method of Ref. [128]; the colours black, grey, and red separate the CRs, VRs, and SRs, respectively. For the cases where the expected yield is larger than the data, a negative significance is shown. The absence of significant yield differences in the control regions is by construction

10 Interpretation

This section contains the model-dependent interpretations of the EWK and Strong searches. The RJR search does not interpret any signal models as it is a model-independent follow-up to a previously observed excess. The exclusion contours are presented on a two-dimensional plane of sparticle masses, or in the case of the GMSB model the branching ratio to the $\tilde{\chi}_1^0$ to a Higgs boson and gravitino and the mass of the $\tilde{\chi}_1^0$. They are evaluated at 95% CL using the CL_s method. The dashed lines represent the expected exclusion contour given the background estimates and is surrounded by a yellow-shaded region identifying the $\pm 1\sigma$ variation of the median expected limit. The red solid line denotes the observed exclusion contours. Uncertainties in the signal cross-sections are not directly included in this contour, but instead shown as red dashed lines denoting $\pm 1\sigma$ variations of the signal cross-section. Grey-shaded areas cover regions excluded by previous similar analyses.

10.1 Electroweak search interpretation

This section presents mass and branching fraction exclusion limits for the C1N2 and GMSB models described in Sect. 2. All of the SRs and CRs are fitted simultaneously in order to test each model.

The left panel of Fig. 15 shows the exclusion contours in the $m_{\tilde{\chi}_1^\pm,\tilde{\chi}_2^0}$–$m_{\tilde{\chi}_1^0}$ plane for the C1N2 model. Masses of the $\tilde{\chi}_2^0$ and $\tilde{\chi}_1^\pm$ up to 820 GeV (740 GeV expected) are excluded for $\tilde{\chi}_1^0$ masses up to 375 GeV. In the region where the Z boson decay is off-shell at $m_{\tilde{\chi}_2^0} = m_{\tilde{\chi}_1^\pm} = 100$ GeV, masses of the $\tilde{\chi}_1^0$ up to 100 GeV are excluded. The observed limit at high $\tilde{\chi}_2^0$ and $\tilde{\chi}_1^\pm$ masses is stronger than expected due to the data event deficits observed in SR-High-EWK.

The right panel of Fig. 15 shows the exclusion contours in the $m_{\tilde{\chi}_1^0}$–$B(\tilde{\chi}_1^0 \to h\tilde{G})$ plane. For a branching fraction entirely to Z bosons, masses of the $\tilde{\chi}_1^0$ up to 900 GeV (800 GeV expected) are excluded. Branching fractions up to 95% (85% expected) of the $\tilde{\chi}_1^0$ to Higgs bosons are excluded for $\tilde{\chi}_1^0$ masses around 450 GeV. Sensitivity to models with decays entirely through Higgs bosons is limited since the majority of Higgs boson decays do not produce a dilepton system with a mass around the Z boson mass. The observed limit at moderate to high $\tilde{\chi}_1^0$ mass is stronger than expected due to the deficits observed in SR-$\ell\ell bb$-EWK and SR-High-EWK.

10.2 Strong search interpretation

This section presents mass exclusion limits for the squark- and gluino-initiated SUSY models described in Sect. 2. These model-dependent exclusion limits are computed separately

Table 23 Expected and observed yields in 12 $m_{\ell\ell}$ windows of the edge signal regions and model-independent upper limits derived using pseudo-experiments. The $m_{\ell\ell}$ range is indicated in the leftmost column of the table, with units of GeV. Left to right: background-only model post-fit total expected background, with the combined statistical and systematic uncertainties; observed data; 95% CL upper limits on the visible cross-section ($\langle A\epsilon\sigma\rangle^{95}_{\text{obs}}$) and on the number of signal events (S^{95}_{obs}). The sixth column (S^{95}_{exp}) shows the expected 95% CL upper limit on the number of signal events, given the expected number (and $\pm 1\sigma$ excursions of the expectation) of background events. The last two columns indicate the confidence level of the background-only hypothesis (CL_b) and discovery p-value with the corresponding Gaussian significance ($Z(s=0)$). CL_b provides a measure of compatibility of the observed data with the signal strength hypothesis at the 95% CL limit relative to fluctuations of the background, and $p(s=0)$ measures compatibility of the observed data with the background-only hypothesis relative to fluctuations of the background. The p-value is capped at 0.5

Signal Region	Total Bkg.	Data	$\langle A\epsilon\sigma\rangle^{95}_{\text{obs}}$ [fb]	S^{95}_{obs}	S^{95}_{exp}	CL_b	$p(s=0)$ (Z)
SRC-STR							
12–31	2.6 ± 1.3	2	0.03	4.7	$5.7^{+2.1}_{-1.5}$	0.33	0.50 (0.0)
12–61	6.3 ± 1.9	7	0.06	8.4	$8.3^{+3.1}_{-2.3}$	0.51	0.50 (0.0)
31–81	6.8 ± 2.8	9	0.08	11.0	$8.0^{+3.2}_{-1.7}$	0.83	0.18 (0.9)
81–	25.4 ± 3.5	27	0.12	16.4	$15.3^{+5.0}_{-4.6}$	0.61	0.34 (0.4)
SRLow-STR							
12–81	16.8 ± 2.6	18	0.09	12.6	$11.6^{+4.5}_{-3.6}$	0.61	0.39 (0.3)
101–201	12.0 ± 2.3	13	0.08	11.2	$9.6^{+3.8}_{-2.5}$	0.67	0.30 (0.5)
101–301	16.5 ± 2.6	20	0.11	15.4	$11.4^{+4.1}_{-3.6}$	0.84	0.17 (1.0)
301–	4.6 ± 1.4	6	0.07	9.5	$6.6^{+2.8}_{-1.8}$	0.85	0.09 (1.3)
SRMed-STR							
12–101	42 ± 5	38	0.10	13.6	$18.8^{+7.2}_{-5.0}$	0.15	0.50 (0.0)
101–	26 ± 4	27	0.12	16.7	$15.8^{+6.2}_{-4.2}$	0.56	0.41 (0.2)
SRHigh-STR							
12–301	22.7 ± 3.2	18	0.06	8.9	$13.0^{+5.8}_{-3.0}$	0.11	0.50 (0.0)
301–	1.5 ± 1.0	1	0.03	3.7	$4.4^{+1.8}_{-1.0}$	0.32	0.50 (0.0)
On-Z							
SRZLow-STR	33 ± 4	35	0.15	20.5	$17.0^{+5.4}_{-4.5}$	0.76	0.25 (0.7)
SRZMed-STR	15.2 ± 2.4	15	0.08	10.7	$10.3^{+4.4}_{-2.8}$	0.53	0.50 (0.0)
SRZHigh-STR	4.5 ± 1.2	3	0.04	5.0	$6.4^{+2.5}_{-1.9}$	0.24	0.50 (0.0)

for each SR, and then combined according to which SR has the best expected sensitivity for a particular set of the model parameters. This can result in sharp contour features where the best expected sensitivity switches between SRs with different data-to-background ratios. A shape fit of the binned $m_{\ell\ell}$ distribution and the Z/γ^*+jets CR is performed for the four edge SRs, shown in Fig. 13. A fit to the single-bin SR and its Z/γ^*+jets CR is performed for three on-Z regions in Table 22.

The first plot in Fig. 16 shows the exclusion contours in the $m(\tilde{g})$–$m(\tilde{\chi}^0_1)$ plane for a simplified model where the gluino decays via sleptons. The limit is derived from only the four edge SRs. SRHigh-STR drives the limit for large splittings between the $\tilde{g}$ and $\tilde{\chi}^0_1$ masses. Moving up in $\tilde{\chi}^0_1$ mass, SRLow-STR takes over around $m(\tilde{g}) = 2.0$ TeV, $m(\tilde{\chi}^0_1) = 0.8$ TeV. In SRLow-STR, the $m_{\ell\ell}$ bins above a value of 200 GeV have a slight excess, as seen in Table 23, hence the weaker observed exclusion limit in this part of the combined contour. The largest excluded gluino mass is observed (expected) to be 2.25 (2.20) TeV.

The second plot in Fig. 16 shows the exclusion contours in the $m(\tilde{g})$–$m(\tilde{\chi}^0_1)$ plane for a simplified model where the gluino decays via a Z boson. The limit is derived using the four edge SRs and three on-Z SRs. The three kinks in the observed limit, from left to right, are the transition from SRLow-STR to SRZLow-STR, then to SRZMed-STR, and then to SRZHigh-STR. The largest excluded gluino mass is observed (expected) to be 1.95 (1.90) TeV.

The third plot in Fig. 16 shows the exclusion contours in the $m(\tilde{q})$–$m(\tilde{\chi}^0_1)$ plane for a simplified model where the squark decays via a Z boson. As above, all of the SRs are included. The three kinks in the observed limit, from left to right, are the same transitions as in the $m(\tilde{g})$–$m(\tilde{\chi}^0_1)$ contour. The largest excluded squark mass is observed (expected) to be 1.55 (1.50) TeV.

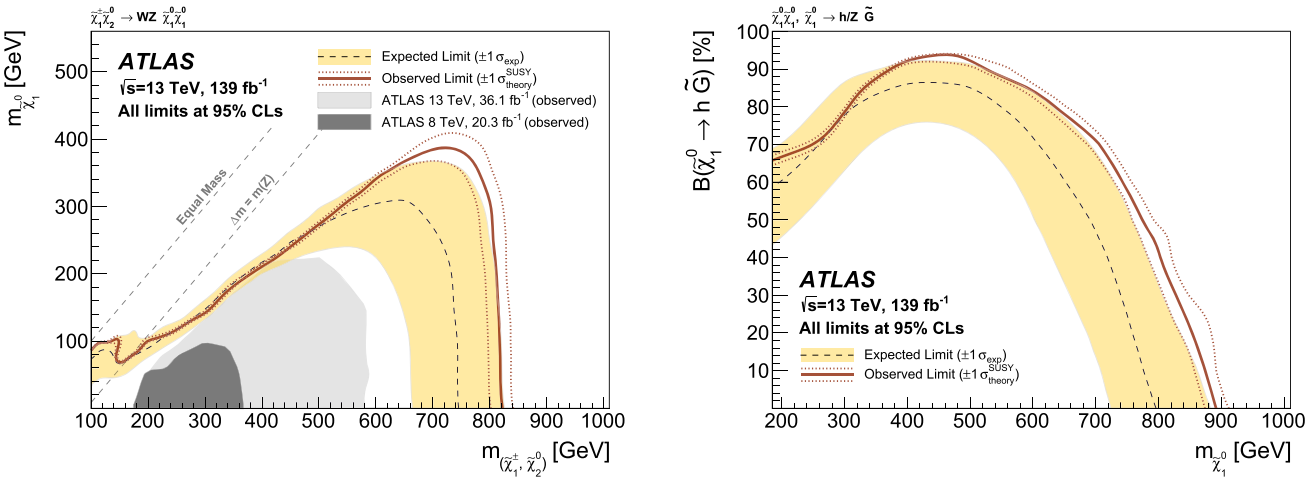

Fig. 15 Expected and observed exclusion contours from the EWK analysis for the C1N2 model (left) and GMSB model (right). The dashed line indicates the expected limits at 95% CL and the surrounding band shows the 1σ variation of the expected limit as a consequence of the uncertainties in the background prediction and experimental uncertainties of the signal ($\pm 1\sigma_{\text{exp}}$). The red dotted lines surrounding the observed limit contours indicate the variation resulting from changing the signal cross-section within its uncertainty ($\pm 1\sigma^{\text{SUSY}}_{\text{theory}}$). The grey-shaded areas indicate observed limits on these models from the two-lepton channels in Ref. [22] and Ref. [129]

11 Conclusion

This paper presents searches for new phenomena in final states with exactly two oppositely charged same-flavour leptons, jets, and missing transverse momentum using the 139 fb^{-1} Run 2 dataset of $\sqrt{s} = 13$ TeV proton–proton collision data collected by the ATLAS detector at the LHC. The analysis is split into three searches, probing both strong and electroweak production of sparticles. The data are found to be consistent with SM expectations in each, and strong limits are set on possible beyond-the-SM contributions to the signal regions. The RJR search does not see significant excesses above the background expectation. Thus the small excesses in the two-lepton channel of the 36 fb^{-1} dataset did not persist with more data. The EWK search and Strong search interpret the data with simplified models inspired by SUSY and set exclusion limits on these models, expanding the sensitivity reach compared to previous analyses. The EWK search targets electroweak production of chargino–neutralino pairs and a GMSB model with higgsino NLSPs. Limits up to 820 GeV and 900 GeV are set on the masses of the mass-degenerate chargino/neutralino and higgsino NLSP respectively. This is an improvement on the previous result by roughly 200 GeV in chargino/neutralino masses. The EWK search covers masses and branching ratios of the GMSB model that are between the limits from the ATLAS four-lepton and all-hadronic searches. The Strong search targets strong production of gluino- or squark-pairs decaying via a Z boson or the NLSP to lepton-pairs and jets. Limits up to 2250 GeV and 1550 GeV are set on the masses of the gluino and squarks respectively. Compared to the previous result, the limits on the gluino mass improved by 400 GeV and the limits on squark masses by 300 GeV. Improvements to both the Strong and EWK searches result from the increased size of the dataset and subsequent optimizations of analysis requirements.

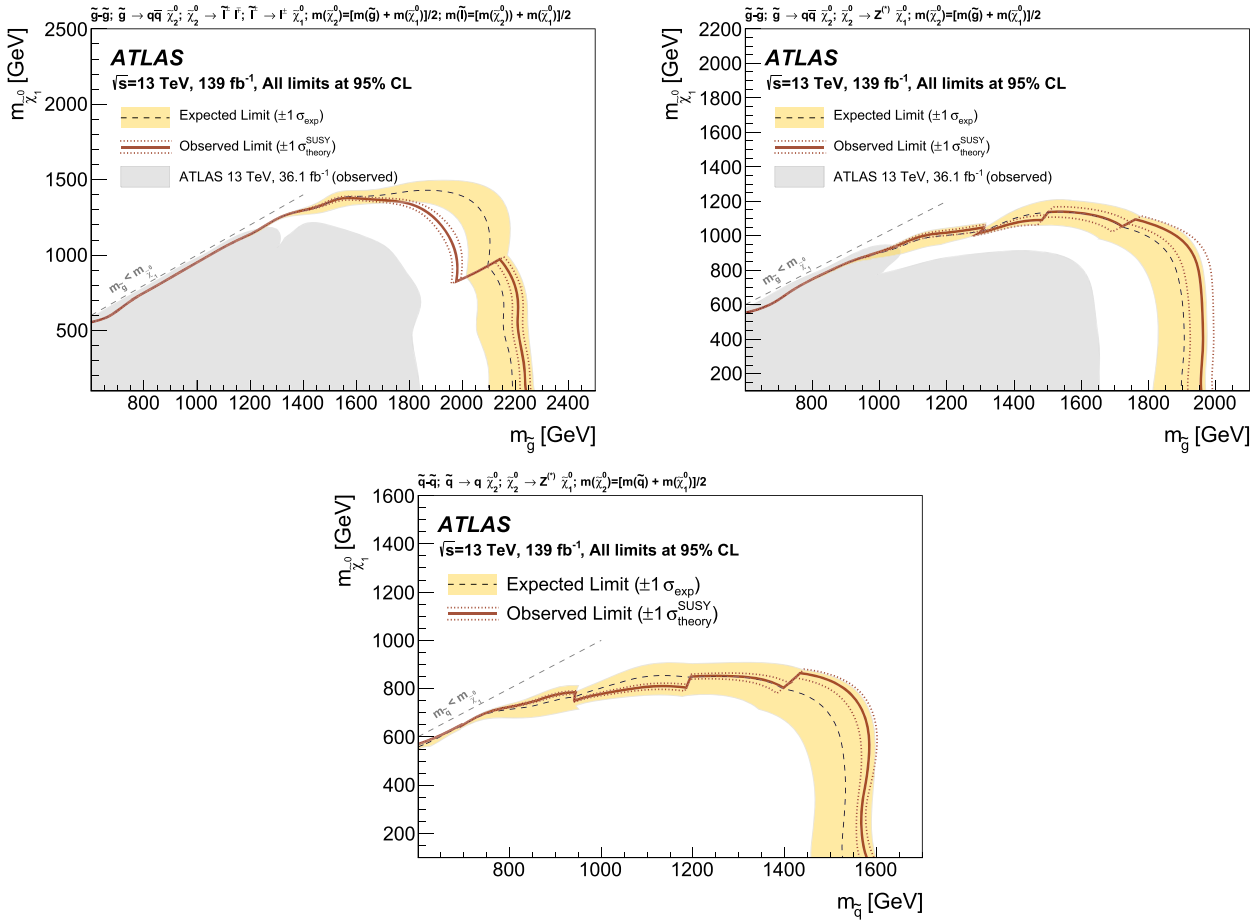

Fig. 16 Expected and observed exclusion contours derived from the combination of all of the Strong search SRs for the $\tilde{g}$–$\tilde{\ell}$ (top-left), $\tilde{g}$–Z (top-right), and $\tilde{q}$–Z (bottom) models. The dashed line indicates the expected limits at 95% CL and the surrounding band shows the 1σ variation of the expected limit as a consequence of the uncertainties in the background prediction and experimental uncertainties of the signal ($\pm 1\sigma_{\text{exp}}$). The red dotted lines surrounding the observed limit contours indicate the variation resulting from changing the signal cross-section within its uncertainty ($\pm 1\sigma^{\text{SUSY}}_{\text{theory}}$). The grey-shaded area indicates the observed limits on these models from Ref. [23]

Acknowledgements We thank CERN for the very successful operation of the LHC, as well as the support staff from our institutions without whom ATLAS could not be operated efficiently.
We acknowledge the support of ANPCyT, Argentina; YerPhI, Armenia; ARC, Australia; BMWFW and FWF, Austria; ANAS, Azerbaijan; CNPq and FAPESP, Brazil; NSERC, NRC and CFI, Canada; CERN; ANID, Chile; CAS, MOST and NSFC, China; Minciencias, Colombia; MEYS CR, Czech Republic; DNRF and DNSRC, Denmark; IN2P3-CNRS and CEA-DRF/IRFU, France; SRNSFG, Georgia; BMBF, HGF and MPG, Germany; GSRI, Greece; RGC and Hong Kong SAR, China; ISF and Benoziyo Center, Israel; INFN, Italy; MEXT and JSPS, Japan; CNRST, Morocco; NWO, Netherlands; RCN, Norway; MEiN, Poland; FCT, Portugal; MNE/IFA, Romania; MESTD, Serbia; MSSR, Slovakia; ARRS and MIZŠ, Slovenia; DSI/NRF, South Africa; MICINN, Spain; SRC and Wallenberg Foundation, Sweden; SERI, SNSF and Cantons of Bern and Geneva, Switzerland; MOST, Taiwan; TENMAK, Türkiye; STFC, United Kingdom; DOE and NSF, United States of America. In addition, individual groups and members have received support from BCKDF, CANARIE, Compute Canada and CRC, Canada; PRIMUS 21/SCI/017 and UNCE SCI/013, Czech Republic; COST, ERC, ERDF, Horizon 2020 and Marie Skłodowska-Curie Actions, European Union; Investissements d'Avenir Labex, Investissements d'Avenir Idex and ANR, France; DFG and AvH Foundation, Germany; Herakleitos, Thales and Aristeia programmes co-financed by EU-ESF and the Greek NSRF, Greece; BSF-NSF and MINERVA, Israel; Norwegian Financial Mechanism 2014-2021, Norway; NCN and NAWA, Poland; La Caixa Banking Foundation, CERCA Programme Generalitat de Catalunya and PROMETEO and GenT Programmes Generalitat Valenciana, Spain; Göran Gustafssons Stiftelse, Sweden; The Royal Society and Leverhulme Trust, United Kingdom. The crucial computing support from all WLCG partners is acknowledged gratefully, in particular from CERN, the ATLAS Tier-1 facilities at TRIUMF (Canada), NDGF (Denmark, Norway, Sweden), CC-IN2P3 (France), KIT/GridKA (Germany), INFN-CNAF (Italy), NL-T1 (Netherlands), PIC (Spain), ASGC (Taiwan), RAL (UK) and BNL (USA), the Tier-2 facilities worldwide and large non-WLCG resource providers. Major contributors of computing resources are listed in Ref. [130].

Data Availability Statement This manuscript has no associated data or the data will not be deposited. [Authors' comment: "All ATLAS scientific output is published in journals, and preliminary results are made available in Conference Notes. All are openly available, without restriction on use by external parties beyond copyright law and the standard conditions agreed by CERN. Data associated with journal publications

are also made available: tables and data from plots (e.g. cross section values, likelihood profiles, selection efficiencies, cross section limits, ...) are stored in appropriate repositories such as HEPDATA (http://hepdata.cedar.ac.uk/). ATLAS also strives to make additional material related to the paper available that allows a reinterpretation of the data in the context of new theoretical models. For example, an extended encapsulation of the analysis is often provided for measurements in the framework of RIVET (http://rivet.hepforge.org/)." This information is taken from the ATLAS Data Access Policy, which is a public document that can be downloaded from http://opendata.cern.ch/record/413 [opendata.cern.ch].]

Funded by SCOAP[3]. SCOAP[3] supports the goals of the International Year of Basic Sciences for Sustainable Development.

References

1. Y. Golfand, E. Likhtman, Extension of the algebra of Poincare group generators and violation of P invariance. JETP Lett. **13**, 323 (1971). [Pisma Zh. Eksp. Teor. Fiz. **13**, 452 (1971)]
2. D. Volkov, V. Akulov, Is the neutrino a goldstone particle? Phys. Lett. B **46**, 109 (1973). https://doi.org/10.1016/0370-2693(73)90490-5
3. J. Wess, B. Zumino, Supergauge transformations in four dimensions. Nucl. Phys. B **70**, 39 (1974). https://doi.org/10.1016/0550-3213(74)90355-1
4. J. Wess, B. Zumino, Supergauge invariant extension of quantum electrodynamics. Nucl. Phys. B **78**, 1 (1974). https://doi.org/10.1016/0550-3213(74)90112-6
5. S. Ferrara, B. Zumino, Supergauge invariant Yang–Mills theories. Nucl. Phys. B **79**, 413 (1974). https://doi.org/10.1016/0550-3213(74)90559-8
6. A. Salam, J. Strathdee, Super-symmetry and non-Abelian gauges. Phys. Lett. B **51**, 353 (1974). https://doi.org/10.1016/0370-2693(74)90226-3
7. H. Goldberg, Constraint on the photino mass from cosmology. Phys. Rev. Lett. 50, 1419 (1983). https://doi.org/10.1103/PhysRevLett.50.1419 (**Erratum: Phys. Rev. Lett. 103(2009), 099905**)
8. J. Ellis, J. Hagelin, D.V. Nanopoulos, K.A. Olive, M. Srednicki, Supersymmetric relics from the big bang. Nucl. Phys. B **238**, 453 (1984). https://doi.org/10.1016/0550-3213(84)90461-9
9. N. Sakai, Naturalness in supersymmetric GUTS. Z. Phys. C **11**, 153 (1981). https://doi.org/10.1007/BF01573998
10. S. Dimopoulos, S. Raby, F. Wilczek, Supersymmetry and the scale of unification. Phys. Rev. D **24**, 1681 (1981). https://doi.org/10.1103/PhysRevD.24.1681
11. L.E. Ibáñez, G.G. Ross, Low-energy predictions in supersymmetric grand unified theories. Phys. Lett. B **105**, 439 (1981). https://doi.org/10.1016/0370-2693(81)91200-4
12. S. Dimopoulos, H. Georgi, Softly broken supersymmetry and SU(5). Nucl. Phys. B **193**, 150 (1981). https://doi.org/10.1016/0550-3213(81)90522-8
13. G.R. Farrar, P. Fayet, Phenomenology of the production, decay, and detection of new hadronic states associated with supersymmetry. Phys. Lett. B **76**, 575 (1978). https://doi.org/10.1016/0370-2693(78)90858-4
14. ATLAS Collaboration, The ATLAS experiment at the CERN large hadron collider. JINST **3**, S08003 (2008). https://doi.org/10.1088/1748-0221/3/08/S08003
15. L. Evans, P. Bryant, L.H.C. Machine, JINST **3**, S08001 (2008). https://doi.org/10.1088/1748-0221/3/08/S08001
16. P. Jackson, C. Rogan, Recursive Jigsaw reconstruction: HEP event analysis in the presence of kinematic and combinatoric ambiguities. Phys. Rev. D **96**, 112007 (2017). https://doi.org/10.1103/PhysRevD.96.112007. arXiv:1705.10733 [hep-ph]
17. ATLAS Collaboration, Search for chargino–neutralino production using recursive jigsaw reconstruction in final states with two or three charged leptons in proton–proton collisions at $\sqrt{s}$= 13 TeV with the ATLAS detector. Phys. Rev. D **98**, 092012 (2018). https://doi.org/10.1103/PhysRevD.98.092012. arXiv:1806.02293 [hep-ex]
18. ATLAS Collaboration, Search for chargino–neutralino pair production in final states with three leptons and missing transverse momentum in $\sqrt{s}$= 13 TeV pp collisions with the ATLAS detector. Eur. Phys. J. C **81**, 1118 (2021). https://doi.org/10.1140/epjc/s10052-021-09749-7. arXiv:2106.01676 [hep-ex]
19. M. Dine, W. Fischler, A phenomenological model of particle physics based on supersymmetry. Phys. Lett. B **110**, 227 (1982). https://doi.org/10.1016/0370-2693(82)91241-2
20. L. Alvarez-Gaumé, M. Claudson, M.B. Wise, Low-energy supersymmetry. Nucl. Phys. B **207**, 96 (1982). https://doi.org/10.1016/0550-3213(82)90138-9
21. C.R. Nappi, B.A. Ovrut, Supersymmetric extension of the SU(3) x SU(2) x U(1) model. Phys. Lett. B **113**, 175 (1982). https://doi.org/10.1016/0370-2693(82)90418-X
22. ATLAS Collaboration, Search for electroweak production of supersymmetric particles in final states with two or three leptons at $\sqrt{s}$ = 13 TeV with the ATLAS detector. Eur. Phys. J. C **78**, 995 (2018). https://doi.org/10.1140/epjc/s10052-018-6423-7. arXiv:1803.02762 [hep-ex]
23. ATLAS Collaboration, Search for new phenomena using the invariant mass distribution of same-flavour opposite-sign dilepton pairs in events with missing transverse momentum in $\sqrt{s}$ = 13 TeV pp collisions with the ATLAS detector. Eur. Phys. J. C **78**, 625 (2018). https://doi.org/10.1140/epjc/s10052-018-6081-9. arXiv:1805.11381 [hep-ex]
24. G. Cowan, K. Cranmer, E. Gross, O. Vitells, Asymptotic formulae for likelihood-based tests of new physics. Eur. Phys. J. C **71**, 1554 (2011). https://doi.org/10.1140/epjc/s10052-011-1554-0. (Erratum: Eur. Phys. J. C 73 (2013) 2501). arXiv:1007.1727 [physics.data-an]
25. ATLAS Collaboration, Search for supersymmetry in events with four or more charged leptons in 139 fb^{-1} of $\sqrt{s}$ = 13 TeV pp collisions with the ATLAS detector. JHEP **07**, 167 (2021). https://doi.org/10.1007/JHEP07(2021)167. arXiv:2103.11684 [hep-ex]
26. ATLAS Collaboration, Search for charginos and neutralinos in final states with two boosted hadronically decaying bosons and missing transverse momentum in pp collisions at $\sqrt{s}$ = 13 TeV with the ATLAS detector. Phys. Rev. D **104**, 112010 (2021). https://doi.org/10.1103/PhysRevD.104.112010. arXiv:2108.07586 [hep-ex]
27. ATLAS Collaboration, Search for squarks and gluinos in final states with one isolated lepton, jets, and missing transverse momentum at $\sqrt{s}$ = 13 TeV with the ATLAS detector. Eur. Phys. J. C **81**, 600 (2021). https://doi.org/10.1140/epjc/

s10052-021-09344-w (Erratum: Eur. Phys. J. C 81 (2021) 956). arXiv:2101.01629 [hep-ex]
28. ATLAS Collaboration, Search for squarks and gluinos in final states with jets and missing transverse momentum using 139 fb^{-1} of $\sqrt{s}$ = 13 TeV pp collision data with the ATLAS detector. JHEP **02**, 143 (2021). https://doi.org/10.1007/JHEP02(2021)143. arXiv:2010.14293 [hep-ex]
29. CMS Collaboration, Search for supersymmetry in final states with two oppositely charged same-flavor leptons and missing transverse momentum in proton-proton collisions at $\sqrt{s}$ = 13 TeV. JHEP **04**, 123 (2021). https://doi.org/10.1007/JHEP04(2021)123. arXiv:2012.08600 [hep-ex]
30. CMS Collaboration, Search for electroweak production of charginos and neutralinos in proton–proton collisions at $\sqrt{s}$= 13 TeV (2021). arXiv:2106.14246 [hep-ex]
31. J. Alwall, M.-P. Le, M. Lisanti, J.G. Wacker, Searching for directly decaying gluinos at the Tevatron. Phys. Lett. B **666**, 34 (2008). https://doi.org/10.1016/j.physletb.2008.06.065. arXiv:0803.0019 [hep-ph]
32. J. Alwall, P. Schuster, N. Toro, Simplified models for a first characterization of new physics at the LHC. Phys. Rev. D **79**, 075020 (2009). https://doi.org/10.1103/PhysRevD.79.075020. arXiv:0810.3921 [hep-ph]
33. D. Alves et al., Simplified models for LHC new physics searches. J. Phys. G **39**, 105005 (2012). https://doi.org/10.1088/0954-3899/39/10/105005. arXiv:1105.2838 [hep-ph]
34. D. Alves, E. Izaguirre, J. Wacker, Where the sidewalk ends: jets and missing energy search strategies for the 7 TeV LHC. JHEP **10**, 012 (2011). https://doi.org/10.1007/JHEP10(2011)012. arXiv:1102.5338 [hep-ph]
35. F.E. Paige, Determining SUSY particle masses at LHC, eConf C960625 (1996) SUP114, arXiv:hep-ph/9609373
36. ATLAS Collaboration, ATLAS Insertable B-Layer: technical design report, ATLAS-TDR-19; CERN-LHCC-2010-013, 2010, https://cds.cern.ch/record/1291633, Addendum: ATLAS-TDR-19-ADD-1; CERN-LHCC-2012-009, 2012, https://cds.cern.ch/record/1451888
37. B. Abbott et al., Production and integration of the ATLAS Insertable B-Layer. JINST **13**, T05008 (2018). https://doi.org/10.1088/1748-0221/13/05/T05008. arXiv:1803.00844 [physics.ins-det]
38. ATLAS Collaboration, The ATLAS Collaboration Software and Firmware, ATL-SOFT-PUB-2021-001 (2021). https://cds.cern.ch/record/2767187
39. ATLAS Collaboration, ATLAS data quality operations and performance for 2015–2018 data-taking. JINST **15**, P04003 (2020). https://doi.org/10.1088/1748-0221/15/04/P04003. arXiv:1911.04632 [physics.ins-det]
40. ATLAS Collaboration, Luminosity determination in pp collisions at $\sqrt{s}$ = 13 TeV using the ATLAS detector at the LHC, ATLAS-CONF-2019-021 (2019). https://cds.cern.ch/record/2677054
41. G. Avoni et al., The new LUCID-2 detector for luminosity measurement and monitoring in ATLAS. JINST **13**, P07017 (2018). https://doi.org/10.1088/1748-0221/13/07/P07017
42. ATLAS Collaboration, Performance of the ATLAS muon triggers in Run 2. JINST **15**, P09015 (2020). https://doi.org/10.1088/1748-0221/15/09/p09015. arXiv:2004.13447 [hep-ex]
43. ATLAS Collaboration, Performance of electron and photon triggers in ATLAS during LHC Run 2. Eur. Phys. J. C **80**, 47 (2020). https://doi.org/10.1140/epjc/s10052-019-7500-2. arXiv:1909.00761 [hep-ex]
44. E. Bothmann et al., Event generation with Sherpa 2.2. SciPost Phys. **7**, 034 (2019). https://doi.org/10.21468/SciPostPhys.7.3.034. arXiv:1905.09127 [hep-ph]
45. P. Nason, A new method for combining NLO QCD with shower Monte Carlo algorithms. JHEP **11**, 040 (2004). https://doi.org/10.1088/1126-6708/2004/11/040. arXiv:hep-ph/0409146
46. S. Frixione, P. Nason, C. Oleari, Matching NLO QCD computations with parton shower simulations: the POWHEG method. JHEP **11**, 070 (2007). https://doi.org/10.1088/1126-6708/2007/11/070. arXiv:0709.2092 [hep-ph]
47. S. Alioli, P. Nason, C. Oleari, E. Re, A general framework for implementing NLO calculations in shower Monte Carlo programs: the POWHEG BOX. JHEP **06**, 043 (2010). https://doi.org/10.1007/JHEP06(2010)043. arXiv:1002.2581 [hep-ph]
48. T. Sjöstrand et al., An introduction to PYTHIA 8.2. Comput. Phys. Commun. **191**, 159 (2015). https://doi.org/10.1016/j.cpc.2015.01.024. arXiv:1410.3012 [hep-ph]
49. ATLAS Collaboration, Simulation of top-quark production for the ATLAS experiment at $\sqrt{s}$ = 13 TeV, ATL-PHYS-PUB-2016-004 (2016). https://cds.cern.ch/record/2120417
50. M. Czakon, P. Fiedler, A. Mitov, Total top-quark pair-production cross section at hadron colliders through $O(\alpha_S^4)$. Phys. Rev. Lett. **110**, 252004 (2013). https://doi.org/10.1103/PhysRevLett.110.252004. arXiv:1303.6254 [hep-ph]
51. M. Czakon, A. Mitov, Top++: a program for the calculation of the top-pair cross-section at hadron colliders. Comput. Phys. Commun. **185**, 2930 (2014). https://doi.org/10.1016/j.cpc.2014.06.021. arXiv:1112.5675 [hep-ph]
52. M. Cacciari, M. Czakon, M. Mangano, A. Mitov, P. Nason, Top-pair production at hadron colliders with next-to-next-to-leading logarithmic soft-gluon resummation. Phys. Lett. B **710**, 612 (2012). https://doi.org/10.1016/j.physletb.2012.03.013. arXiv:1111.5869 [hep-ph]
53. M. Czakon, A. Mitov, NNLO corrections to top-pair production at hadron colliders: the all-fermionic scattering channels. JHEP **12**, 054 (2012). https://doi.org/10.1007/JHEP12(2012)054. arXiv:1207.0236 [hep-ph]
54. M. Czakon, A. Mitov, NNLO corrections to top pair production at hadron colliders: the quark–gluon reaction. JHEP **01**, 080 (2013). https://doi.org/10.1007/JHEP01(2013)080. arXiv:1210.6832 [hep-ph]
55. ATLAS Collaboration, ATLAS Pythia 8 tunes to 7 TeV data, ATL-PHYS-PUB-2014-021 (2014). https://cds.cern.ch/record/1966419
56. R.D. Ball et al., Parton distributions with LHC data. Nucl. Phys. B **867**, 244 (2013). https://doi.org/10.1016/j.nuclphysb.2012.10.003. arXiv:1207.1303 [hep-ph]
57. N. Kidonakis, Two-loop soft anomalous dimensions for single top quark associated production with a W^- or H^-. Phys. Rev. D **82**, 054018 (2010). https://doi.org/10.1103/PhysRevD.82.054018. arXiv:1005.4451 [hep-ph]
58. N. Kidonakis, Next-to-next-to-leading logarithm resummation for s-channel single top quark production. Phys. Rev. D **81**, 054028 (2010). https://doi.org/10.1103/PhysRevD.81.054028. arXiv:1001.5034 [hep-ph]
59. N. Kidonakis, Next-to-next-to-leading-order collinear and soft gluon corrections for t-channel single top quark production. Phys. Rev. D **83**, 091503 (2011). https://doi.org/10.1103/PhysRevD.83.091503. arXiv:1103.2792 [hep-ph]
60. R. Frederix, E. Re, P. Torrielli, Single-top t-channel hadroproduction in the four-flavour scheme with POWHEG and aMC@NLO. JHEP **09**, 130 (2012). https://doi.org/10.1007/JHEP09(2012)130. arXiv:1207.5391 [hep-ph]
61. R.D. Ball et al., Parton distributions for the LHC run II. JHEP **04**, 040 (2015). https://doi.org/10.1007/JHEP04(2015)040. arXiv:1410.8849 [hep-ph]
62. ATLAS Collaboration, Multi-boson simulation for 13 TeV ATLAS analyses, ATL-PHYS-PUB-2016-002 (2016). https://cds.cern.ch/record/2119986

63. J.M. Campbell, R.K. Ellis, Update on vector boson pair production at hadron colliders. Phys. Rev. D **60**, 113006 (1999). https://doi.org/10.1103/PhysRevD.60.113006. arXiv:hep-ph/9905386
64. J.M. Campbell, R.K. Ellis, C. Williams, Vector boson pair production at the LHC. JHEP **07**, 018 (2011). https://doi.org/10.1007/JHEP07(2011)018. arXiv:1105.0020 [hep-ph]
65. ATLAS Collaboration, Monte Carlo Generators for the Production of a W or Z/γ^* Boson in Association with Jets at ATLAS in Run 2, ATL-PHYS-PUB-2016-003 (2016). https://cds.cern.ch/record/2120133
66. S. Catani, L. Cieri, G. Ferrera, D. de Florian, M. Grazzini, Vector boson production at hadron colliders: a fully exclusive QCD calculation at next-to-next-to-leading order. Phys. Rev. Lett. **103**, 082001 (2009). https://doi.org/10.1103/PhysRevLett.103.082001. arXiv:0903.2120 [hep-ph]
67. S. Catani, M. Grazzini, Next-to-next-to-leading-order subtraction formalism in hadron collisions and its application to Higgs-Boson production at the large hadron collider. Phys. Rev. Lett. **98**, 222002 (2007). https://doi.org/10.1103/PhysRevLett.98.222002. arXiv:hep-ph/0703012
68. D. de Florian et al., Handbook of LHC Higgs cross sections: 4. Deciphering the nature of the Higgs sector (2016). https://doi.org/10.23731/CYRM-2017-002. arXiv:1610.07922 [hep-ph]
69. ATLAS Collaboration, Measurement of the Z/γ^* boson transverse momentum distribution in pp collisions at $\sqrt{s}$ = 7 TeV with the ATLAS detector. JHEP **09**, 145 (2014). https://doi.org/10.1007/JHEP09(2014)145. arXiv:1406.3660 [hep-ex]
70. J. Pumplin et al., New generation of parton distributions with uncertainties from global QCD analysis. JHEP **07**, 012 (2002). https://doi.org/10.1088/1126-6708/2002/07/012. arXiv:hep-ph/0201195
71. J. Alwall et al., The automated computation of tree-level and next-to-leading order differential cross sections, and their matching to parton shower simulations. JHEP **07**, 079 (2014). https://doi.org/10.1007/JHEP07(2014)079. arXiv:1405.0301 [hep-ph]
72. P. Skands, S. Carrazza, J. Rojo, Tuning PYTHIA 8.1: the Monash 2013 Tune. Eur. Phys. J. C **74**, 3024 (2014). https://doi.org/10.1140/epjc/s10052-014-3024-y. arXiv:1404.5630 [hep-ph]
73. R. Frederix, D. Pagani, M. Zaro, Large NLO corrections in $t\bar{t}W^{\pm}$ and $t\bar{t}t\bar{t}$ hadroproduction from supposedly subleading EW contributions. JHEP **02**, 031 (2018). https://doi.org/10.1007/JHEP02(2018)031. arXiv:1711.02116 [hep-ph]
74. ATLAS Collaboration, Modelling of the $t\bar{t}H$ and $t\bar{t}V$ ($V = W, Z$) processes for $\sqrt{s}$ = 13 TeV ATLAS analyses, ATL-PHYS-PUB-2016-005 (2016). https://cds.cern.ch/record/2120826
75. M.V. Garzelli, A. Kardos, C.G. Papadopoulos, Z. Trocsanyi, $t\bar{t}W^{+-}$ and $t\bar{t}Z$ Hadroproduction at NLO accuracy in QCD with Parton Shower and Hadronization effects. JHEP **11**, 056 (2012). https://doi.org/10.1007/JHEP11(2012)056. arXiv:1208.2665 [hep-ph]
76. J.M. Campbell, R.K. Ellis, $t\bar{t}W^{+-}$ production and decay at NLO. JHEP **07**, 052 (2012). https://doi.org/10.1007/JHEP07(2012)052. arXiv:1204.5678 [hep-ph]
77. A. Lazopoulos, T. McElmurry, K. Melnikov, F. Petriello, Next-to-leading order QCD corrections to $t\bar{t}Z^{+-}$ production at the LHC. Phys. Lett. B **666**, 62 (2008). https://doi.org/10.1016/j.physletb.2008.06.073. arXiv:0804.2220 [hep-ph]
78. W. Beenakker et al., Production of charginos, neutralinos, and sleptons at hadron colliders. Phys. Rev. Lett. **83**, 3780. https://doi.org/10.1103/PhysRevLett.83.3780 **Erratum: Phys. Rev. Lett. 100, 029901 (2008) (1999)**. arXiv:hep-ph/9906298
79. J. Debove, B. Fuks, M. Klasen, Threshold resummation for gaugino pair production at hadron colliders. Nucl. Phys. B **842**, 51 (2011). https://doi.org/10.1016/j.nuclphysb.2010.08.016. arXiv:1005.2909 [hep-ph]
80. B. Fuks, M. Klasen, D.R. Lamprea, M. Rothering, Gaugino production in proton–proton collisions at a center-of-mass energy of 8 TeV. JHEP **10**, 081 (2012). https://doi.org/10.1007/JHEP10(2012)081. arXiv:1207.2159 [hep-ph]
81. B. Fuks, M. Klasen, D.R. Lamprea, M. Rothering, Precision predictions for electroweak superpartner production at hadron colliders with resummino. Eur. Phys. J. C **73**, 2480 (2013). https://doi.org/10.1140/epjc/s10052-013-2480-0. arXiv:1304.0790 [hep-ph]
82. J. Fiaschi, M. Klasen, Neutralino-chargino pair production at NLO+NLL with resummation-improved parton density functions for LHC Run II. Phys. Rev. D **98**, 055014 (2018). https://doi.org/10.1103/PhysRevD.98.055014. arXiv:1805.11322 [hep-ph]
83. C. Borschensky et al., Squark and gluino production cross sections in pp collisions at $\sqrt{s}$ = 13, 14, 33 and 100 TeV. Eur. Phys. J. C **74**, 3174 (2014). https://doi.org/10.1140/epjc/s10052-014-3174-y. arXiv:1407.5066 [hep-ph]
84. W. Beenakker, C. Borschensky, M. Krämer, A. Kulesza, E. Laenen, NNLL-fast: predictions for coloured supersymmetric particle production at the LHC with threshold and Coulomb resummation. JHEP **12**, 133 (2016). https://doi.org/10.1007/JHEP12(2016)133. arXiv:1607.07741 [hep-ph]
85. W. Beenakker et al., NNLL resummation for squark and gluino production at the LHC. JHEP **12**, 023 (2014). https://doi.org/10.1007/JHEP12(2014)023. arXiv:1404.3134 [hep-ph]
86. W. Beenakker et al., Towards NNLL resummation: hard matching coefficients for squark and gluino hadroproduction. JHEP **10**, 120 (2013). https://doi.org/10.1007/JHEP10(2013)120. arXiv:1304.6354 [hep-ph]
87. W. Beenakker et al., NNLL resummation for squark-antisquark pair production at the LHC. JHEP **01**, 076 (2012). https://doi.org/10.1007/JHEP01(2012)076. arXiv:1110.2446 [hep-ph]
88. W. Beenakker et al., Soft-gluon resummation for squark and gluino hadroproduction. JHEP **12**, 041 (2009). https://doi.org/10.1088/1126-6708/2009/12/041. arXiv:0909.4418 [hep-ph]
89. A. Kulesza, L. Motyka, Soft gluon resummation for the production of gluino-gluino and squark-antisquark pairs at the LHC. Phys. Rev. D **80**, 095004 (2009). https://doi.org/10.1103/PhysRevD.80.095004. arXiv:0905.4749 [hep-ph]
90. A. Kulesza, L. Motyka, Threshold resummation for squark-antisquark and gluino-pair production at the LHC. Phys. Rev. Lett. **102**, 111802 (2009). https://doi.org/10.1103/PhysRevLett.102.111802. arXiv:0807.2405 [hep-ph]
91. W. Beenakker, R. Höpker, M. Spira, P. Zerwas, Squark and gluino production at hadron colliders. Nucl. Phys. B **492**, 51 (1997). https://doi.org/10.1016/S0550-3213(97)00084-9. arXiv:hep-ph/9610490
92. J. Butterworth et al., PDF4LHC recommendations for LHC Run II. J. Phys. G **43**, 023001 (2016). https://doi.org/10.1088/0954-3899/43/2/023001. arXiv:1510.03865 [hep-ph]
93. ATLAS Collaboration, The ATLAS Simulation Infrastructure. Eur. Phys. J. C **70**, 823 (2010). https://doi.org/10.1140/epjc/s10052-010-1429-9. arXiv:1005.4568 [physics.ins-det]
94. GEANT4 Collaboration, S. Agostinelli et al., GEANT4: a simulation toolkit. Nucl. Instrum. Methods A **506**, 250 (2003). https://doi.org/10.1016/S0168-9002(03)01368-8
95. ATLAS Collaboration, Electron and photon performance measurements with the ATLAS detector using the 2015–2017 LHC proton–proton collision data. JINST **14**, P12006 (2019). https://doi.org/10.1088/1748-0221/14/12/P12006. arXiv:1908.00005 [hep-ex]
96. ATLAS Collaboration, Muon reconstruction and identification efficiency in ATLAS using the full Run 2 pp collision data set at $\sqrt{s}$ = 13 TeV. Eur. Phys. J. C **81**, 578 (2021). https://doi.org/10.1140/epjc/s10052-021-09233-2. arXiv:2012.00578 [hep-ex]

97. ATLAS Collaboration, Topological cell clustering in the ATLAS calorimeters and its performance in LHC Run 1. Eur. Phys. J. C **77**, 490 (2017). https://doi.org/10.1140/epjc/s10052-017-5004-5. arXiv:1603.02934 [hep-ex]
98. M. Cacciari, G.P. Salam, G. Soyez, The anti-k_t jet clustering algorithm. JHEP **04**, 063 (2008). https://doi.org/10.1088/1126-6708/2008/04/063. arXiv:0802.1189 [hep-ph]
99. M. Cacciari, G.P. Salam, Dispelling the N^3 myth for the k_t jet-finder. Phys. Lett. B **641**, 57 (2006). https://doi.org/10.1016/j.physletb.2006.08.037. arXiv:hep-ph/0512210
100. M. Cacciari, G.P. Salam, G. Soyez, FastJet user manual. Eur. Phys. J. C **72**, 1896 (2012). https://doi.org/10.1140/epjc/s10052-012-1896-2. arXiv:1111.6097 [hep-ph]
101. ATLAS Collaboration, Jet energy scale and resolution measured in proton–proton collisions at $\sqrt{s}$ = 13 TeV with the ATLAS detector. Eur. Phys. J. C **81**, 689 (2020), https://doi.org/10.1140/epjc/s10052-021-09402-3. arXiv:2007.02645 [hep-ex]
102. ATLAS Collaboration, Performance of pile-up mitigation techniques for jets in pp collisions at $\sqrt{s}$ = 8 TeV using the ATLAS detector. Eur. Phys. J. C **76**, 581 (2016). https://doi.org/10.1140/epjc/s10052-016-4395-z. arXiv:1510.03823 [hep-ex]
103. ATLAS Collaboration, Jet energy scale measurements and their systematic uncertainties in proton–proton collisions at $\sqrt{s}$ = 13 TeV with the ATLAS detector. Phys. Rev. D **96**, 072002 (2017). https://doi.org/10.1103/PhysRevD.96.072002. arXiv:1703.09665 [hep-ex]
104. ATLAS Collaboration, Identification and rejection of pile-up jets at high pseudorapidity with the ATLAS detector. Eur. Phys. J. C **77**, 580 (2017). https://doi.org/10.1140/epjc/s10052-017-5081-5. (Erratum: Eur. Phys. J. C 77 (2017), 712). arXiv:1705.02211 [hep-ex]
105. ATLAS Collaboration, Characterisation and mitigation of beam-induced backgrounds observed in the ATLAS detector during the, proton–proton run. JINST **8**(2013), P07004 (2011). https://doi.org/10.1088/1748-0221/8/07/P07004. arXiv:1303.0223 [hep-ex]
106. ATLAS Collaboration, Selection of jets produced in 13 TeV proton-proton collisions with the ATLAS detector, ATLAS-CONF-2015-029 (2015). https://cds.cern.ch/record/2037702
107. ATLAS Collaboration, ATLAS b-jet identification performance and efficiency measurement with $t\bar{t}$ events in pp collisions at $\sqrt{s}$ = 13 TeV. Eur. Phys. J. C **79**, 970 (2019). https://doi.org/10.1140/epjc/s10052-019-7450-8. arXiv:1907.05120 [hep-ex]
108. ATLAS Collaboration, Calibration of light-flavour ..-jet mistagging rates using ATLAS proton.proton collision data at $\sqrt{s}$ = 13 TeV, ATLAS-CONF-2018-006 (2018). https://cds.cern.ch/record/2314418
109. ATLAS Collaboration, Performance of missing transverse momentum reconstruction with the ATLAS detector using proton–proton collisions at $\sqrt{s}$ = 13 TeV. Eur. Phys. J. C **78**, 903 (2018). https://doi.org/10.1140/epjc/s10052-018-6288-9. arXiv:1802.08168 [hep-ex]
110. C.G. Lester, D.J. Summers, Measuring masses of semiinvisibly decaying particles pair produced at hadron colliders. Phys. Lett. B **463**, 99 (1999). https://doi.org/10.1016/S0370-2693(99)00945-4. arXiv:hep-ph/9906349
111. A. Barr, C. Lester, P. Stephens, A variable for measuring masses at hadron colliders when missing energy is expected; m_T^2: the truth behind the glamour. J. Phys. G **29**, 2343 (2003). https://doi.org/10.1088/0954-3899/29/10/304. arXiv:hep-ph/0304226
112. Object-based missing transverse momentum significance in the ATLAS detector, tech. rep. ATLAS-CONF-2018-038, CERN (2018). https://cds.cern.ch/record/2630948
113. P. Jackson, C. Rogan, M. Santoni, Sparticles in motion: analyzing compressed SUSY scenarios with a new method of event reconstruction. Phys. Rev. D **95**, 035031 (2017). https://doi.org/10.1103/physrevd.95.035031 (Issn: 2470-0029). arXiv:1607.08307 [hep-ph]
114. M. Santoni, Probing compressed mass spectra in electroweak supersymmetry with recursive Jigsaw reconstruction. JHEP **05**, 058 (2018). https://doi.org/10.1007/jhep05(2018)058 (**Issn: 1029-8479**). arXiv:1712.00877 [hep-ph]
115. ATLAS Collaboration, Search for a scalar partner of the top quark in the jets plus missing transverse momentum final state at $\sqrt{s}$ = 13 TeV with the ATLAS detector. JHEP **12**, 085 (2017). https://doi.org/10.1007/JHEP12(2017)085. arXiv:1709.04183 [hep-ex]
116. ATLAS Collaboration, Search for squarks and gluinos in final states with jets and missing transverse momentum using 36 fb^{-1} of $\sqrt{s}$ = 13 TeV pp collision data with the ATLAS detector. Phys. Rev. D **97**, 112001 (2018). https://doi.org/10.1103/PhysRevD.97.112001. arXiv:1712.02332 [hep-ex]
117. ATLAS Collaboration, Search for top-squark pair production in final states with one lepton, jets, and missing transverse momentum using 36 fb^{-1} of $\sqrt{s}$ = 13 TeV pp collision data with the ATLAS detector. JHEP **06**, 108 (2018). https://doi.org/10.1007/JHEP06(2018)108. arXiv:1711.11520 [hep-ex]
118. ATLAS Collaboration, Estimation of non-prompt and fake lepton backgrounds in final states with top quarks produced in proton–proton collisions at $\sqrt{s}$ = 8 TeV with the ATLAS Detector, ATLAS-CONF-2014-058 (2014).https://cds.cern.ch/record/1951336
119. ATLAS Collaboration, E^miss_T T performance in the ATLAS detector using 2015.2016 LHC pp collisions, ATLAS-CONF-2018-023 (2018). https://cds.cern.ch/record/2625233
120. J. Bellm et al., Herwig 7.0/Herwig++ 3.0 release note. Eur. Phys. J. C **76**, 196 (2016). https://doi.org/10.1140/epjc/s10052-016-4018-8. arXiv:1512.01178 [hep-ph]
121. J. Butterworth et al., PDF4LHC recommendations for LHC Run II. J. Phys. G **43**, 023001 (2016). https://doi.org/10.1088/0954-3899/43/2/023001. arXiv:1510.03865 [hep-ph]
122. M. Baak et al., HistFitter software framework for statistical data analysis. Eur. Phys. J. C **75**, 153 (2015). https://doi.org/10.1140/epjc/s10052-015-3327-7. arXiv:1410.1280 [hep-ex]
123. W. Verkerke, D. Kirkby, The RooFit toolkit for data modeling (2003). arXiv:physics/0306116
124. L. Moneta et al., The RooStats Project, PoS ACAT2010 (2010) 057, ed. by T. Speer et al., https://doi.org/10.22323/1.093.0057. arXiv:1009.1003 [physics.data-an]
125. K. Cranmer, G. Lewis, L. Moneta, A. Shibata, W. Verkerke, HistFactory: a tool for creating statistical models for use with RooFit and RooStats, tech. rep., New York U. (2012). https://cds.cern.ch/record/1456844
126. R. Brun, F. Rademakers, ROOT-An object oriented data analysis framework. Nucl. Instrum. Methods A **389**, 81 (1997). https://doi.org/10.1016/S0168-9002(97)00048-X. (**Issn: 0168-9002**)
127. A.L. Read, Presentation of search results: the CL_S technique. J. Phys. G **28**, 2693 (2002). https://doi.org/10.1088/0954-3899/28/10/313
128. R.D. Cousins, J.T. Linnemann, J. Tucker, Evaluation of three methods for calculating statistical significance when incorporating a systematic uncertainty into a test of the background-only hypothesis for a Poisson process. Nucl. Instrum. Methods A **595**, 480 (2008). https://doi.org/10.1016/j.nima.2008.07.086. arXiv:physics/0702156
129. ATLAS Collaboration, Search for direct production of charginos, neutralinos and sleptons in final states with two leptons and missing transverse momentum in pp collisions at $\sqrt{s}$ = 8 TeV with the ATLAS detector. JHEP **05**, 071 (2014). https://doi.org/10.1007/JHEP05(2014)071. arXiv:1403.5294 [hep-ex]
130. ATLAS Collaboration, ATLAS Computing Acknowledgements, ATL-SOFT-PUB-2021-003 (2021). https://cds.cern.ch/record/2776662

ATLAS Collaboration[*]

G. Aad[101], B. Abbott[119], D. C. Abbott[102], A. Abed Abud[36], K. Abeling[55], D. K. Abhayasinghe[94], S. H. Abidi[29], A. Aboulhorma[35e], H. Abramowicz[150], H. Abreu[149], Y. Abulaiti[116], A. C. Abusleme Hoffman[136a], B. S. Acharya[68a,68b,o], B. Achkar[55], L. Adam[99], C. Adam Bourdarios[4], L. Adamczyk[84a], L. Adamek[154], S. V. Addepalli[26], J. Adelman[114], A. Adiguzel[21c], S. Adorni[56], T. Adye[133], A. A. Affolder[135], Y. Afik[36], C. Agapopoulou[66], M. N. Agaras[13], J. Agarwala[72a,72b], A. Aggarwal[99], C. Agheorghiesei[27c], J. A. Aguilar-Saavedra[129f,129a,w], A. Ahmad[36], F. Ahmadov[38,u], W. S. Ahmed[103], X. Ai[48], G. Aielli[75a,75b], I. Aizenberg[167], M. Akbiyik[99], T. P. A. Åkesson[97], A. V. Akimov[37], K. Al Khoury[41], G. L. Alberghi[23b], J. Albert[163], P. Albicocco[53], M. J. Alconada Verzini[89], S. Alderweireldt[52], M. Aleksa[36], I. N. Aleksandrov[38], C. Alexa[27b], T. Alexopoulos[10], A. Alfonsi[113], F. Alfonsi[23b], M. Alhroob[119], B. Ali[131], S. Ali[147], M. Aliev[37], G. Alimonti[70a], C. Allaire[36], B. M. M. Allbrooke[145], P. P. Allport[20], A. Aloisio[71a,71b], F. Alonso[89], C. Alpigiani[137], E. Alunno Camelia[75a,75b], M. Alvarez Estevez[98], M. G. Alviggi[71a,71b], Y. Amaral Coutinho[81b], A. Ambler[103], L. Ambroz[125], C. Amelung[36], D. Amidei[105], S. P. Amor Dos Santos[129a], S. Amoroso[48], K. R. Amos[161], C. S. Amrouche[56], V. Ananiev[124], C. Anastopoulos[138], N. Andari[134], T. Andeen[11], J. K. Anders[19], S. Y. Andrean[47a,47b], A. Andreazza[70a,70b], S. Angelidakis[9], A. Angerami[41], A. V. Anisenkov[37], A. Annovi[73a], C. Antel[56], M. T. Anthony[138], E. Antipov[120], M. Antonelli[53], D. J. A. Antrim[17a], F. Anulli[74a], M. Aoki[82], J. A. Aparisi Pozo[161], M. A. Aparo[145], L. Aperio Bella[48], N. Aranzabal[36], V. Araujo Ferraz[81a], C. Arcangeletti[53], A. T. H. Arce[51], E. Arena[91], J-F. Arguin[107], S. Argyropoulos[54], J.-H. Arling[48], A. J. Armbruster[36], O. Arnaez[154], H. Arnold[113], Z. P. Arrubarrena Tame[108], G. Artoni[74a,74b], H. Asada[110], K. Asai[117], S. Asai[152], N. A. Asbah[61], E. M. Asimakopoulou[159], J. Assahsah[35d], K. Assamagan[29], R. Astalos[28a], R. J. Atkin[33a], M. Atkinson[160], N. B. Atlay[18], H. Atmani[62b], P. A. Atmasiddha[105], K. Augsten[131], S. Auricchio[71a,71b], V. A. Austrup[169], G. Avner[149], G. Avolio[36], M. K. Ayoub[14c], G. Azuelos[107,ab], D. Babal[28a], H. Bachacou[134], K. Bachas[151], A. Bachiu[34], F. Backman[47a,47b], A. Badea[61], P. Bagnaia[74a,74b], M. Bahmani[18], A. J. Bailey[161], V. R. Bailey[160], J. T. Baines[133], C. Bakalis[10], O. K. Baker[170], P. J. Bakker[113], E. Bakos[15], D. Bakshi Gupta[8], S. Balaji[146], R. Balasubramanian[113], E. M. Baldin[37], P. Balek[132], E. Ballabene[70a,70b], F. Balli[134], L. M. Baltes[63a], W. K. Balunas[32], J. Balz[99], E. Banas[85], M. Bandieramonte[128], A. Bandyopadhyay[24], S. Bansal[24], L. Barak[150], E. L. Barberio[104], D. Barberis[57a,57b], M. Barbero[101], G. Barbour[95], K. N. Barends[33a], T. Barillari[109], M-S. Barisits[36], J. Barkeloo[122], T. Barklow[142], R. M. Barnett[17a], P. Baron[121], A. Baroncelli[62a], G. Barone[29], A. J. Barr[125], L. Barranco Navarro[47a,47b], F. Barreiro[98], J. Barreiro Guimarães da Costa[14a], U. Barron[150], S. Barsov[37], F. Bartels[63a], R. Bartoldus[142], G. Bartolini[101], A. E. Barton[90], P. Bartos[28a], A. Basalaev[48], A. Basan[99], M. Baselga[48], I. Bashta[76a,76b], A. Bassalat[66,x], M. J. Basso[154], C. R. Basson[100], R. L. Bates[59], S. Batlamous[35e], J. R. Batley[32], B. Batool[140], M. Battaglia[135], M. Bauce[74a,74b], F. Bauer[134,*], P. Bauer[24], A. Bayirli[21a], J. B. Beacham[51], T. Beau[126], P. H. Beauchemin[157], F. Becherer[54], P. Bechtle[24], H. P. Beck[19,p], K. Becker[165], C. Becot[48], A. J. Beddall[21d], V. A. Bednyakov[38], C. P. Bee[144], L. J. Beemster[15], T. A. Beermann[36], M. Begalli[81b], M. Begel[29], A. Behera[144], J. K. Behr[48], C. Beirao Da Cruz E Silva[36], J. F. Beirer[55,36], F. Beisiegel[24], M. Belfkir[115b], G. Bella[150], L. Bellagamba[23b], A. Bellerive[34], P. Bellos[20], K. Beloborodov[37], K. Belotskiy[37], N. L. Belyaev[37], D. Benchekroun[35a], Y. Benhammou[150], D. P. Benjamin[29], M. Benoit[29], J. R. Bensinger[26], S. Bentvelsen[113], L. Beresford[36], M. Beretta[53], D. Berge[18], E. Bergeaas Kuutmann[159], N. Berger[4], B. Bergmann[131], L. J. Bergsten[26], J. Beringer[17a], S. Berlendis[7], G. Bernardi[5], C. Bernius[142], F. U. Bernlochner[24], T. Berry[94], P. Berta[132], A. Berthold[50], I. A. Bertram[90], O. Bessidskaia Bylund[169], S. Bethke[109], A. Betti[44], A. J. Bevan[93], S. Bhatta[144], D. S. Bhattacharya[164], P. Bhattarai[26], V. S. Bhopatkar[6], R. Bi[128], R. Bi[29], R. M. Bianchi[128], O. Biebel[108], R. Bielski[122], N. V. Biesuz[73a,73b], M. Biglietti[76a], T. R. V. Billoud[131], M. Bindi[55], A. Bingul[21b], C. Bini[74a,74b], S. Biondi[23a,23b], A. Biondini[91], C. J. Birch-sykes[100], G. A. Bird[20,133], M. Birman[167], T. Bisanz[36], D. Biswas[168,k], A. Bitadze[100], K. Bjørke[124], I. Bloch[48], C. Blocker[26], A. Blue[59], U. Blumenschein[93], J. Blumenthal[99], G. J. Bobbink[113], V. S. Bobrovnikov[37], M. Boehler[54], D. Bogavac[13], A. G. Bogdanchikov[37], C. Bohm[47a], V. Boisvert[94], P. Bokan[48], T. Bold[84a], M. Bomben[5], M. Bona[93], M. Boonekamp[134], C. D. Booth[94], A. G. Borbély[59], H. M. Borecka-Bielska[107], L. S. Borgna[95], G. Borissov[90], D. Bortoletto[125], D. Boscherini[23b], M. Bosman[13], J. D. Bossio Sola[36], K. Bouaouda[35a], J. Boudreau[128], E. V. Bouhova-Thacker[90], D. Boumediene[40], R. Bouquet[5], A. Boveia[118], J. Boyd[36], D. Boye[29], I. R. Boyko[38], J. Bracinik[20], N. Brahimi[62d,62c], G. Brandt[169], O. Brandt[32], F. Braren[48],

B. Brau[102], J. E. Brau[122], W. D. Breaden Madden[59], K. Brendlinger[48], R. Brener[167], L. Brenner[36], R. Brenner[159], S. Bressler[167], B. Brickwedde[99], D. Britton[59], D. Britzger[109], I. Brock[24], G. Brooijmans[41], W. K. Brooks[136f], E. Brost[29], P. A. Bruckman de Renstrom[85], B. Brüers[48], D. Bruncko[28b,*], A. Bruni[23b], G. Bruni[23b], M. Bruschi[23b], N. Bruscino[74a,74b], L. Bryngemark[142], T. Buanes[16], Q. Buat[137], P. Buchholz[140], A. G. Buckley[59], I. A. Budagov[38,*], M. K. Bugge[124], O. Bulekov[37], B. A. Bullard[61], S. Burdin[91], C. D. Burgard[48], A. M. Burger[120], B. Burghgrave[8], J. T. P. Burr[32], C. D. Burton[11], J. C. Burzynski[141], E. L. Busch[41], V. Büscher[99], P. J. Bussey[59], J. M. Butler[25], C. M. Buttar[59], J. M. Butterworth[95], W. Buttinger[133], C. J. Buxo Vazquez[106], A. R. Buzykaev[37], G. Cabras[23b], S. Cabrera Urbán[161], D. Caforio[58], H. Cai[128], Y. Cai[14a,14d], V. M. M. Cairo[142], O. Cakir[3a], N. Calace[36], P. Calafiura[17a], G. Calderini[126], P. Calfayan[67], G. Callea[59], L. P. Caloba[81b], D. Calvet[40], S. Calvet[40], T. P. Calvet[101], M. Calvetti[73a,73b], R. Camacho Toro[126], S. Camarda[36], D. Camarero Munoz[98], P. Camarri[75a,75b], M. T. Camerlingo[76a,76b], D. Cameron[124], C. Camincher[163], M. Campanelli[95], A. Camplani[42], V. Canale[71a,71b], A. Canesse[103], M. Cano Bret[79], J. Cantero[98], Y. Cao[160], F. Capocasa[26], M. Capua[43a,43b], A. Carbone[70a,70b], R. Cardarelli[75a], J. C. J. Cardenas[8], F. Cardillo[161], T. Carli[36], G. Carlino[71a], B. T. Carlson[128], E. M. Carlson[155a,163], L. Carminati[70a,70b], M. Carnesale[74a,74b], S. Caron[112], E. Carquin[136f], S. Carrá[48], G. Carratta[23a,23b], J. W. S. Carter[154], T. M. Carter[52], D. Casadei[33c], M. P. Casado[13,h], A. F. Casha[154], E. G. Castiglia[170], F. L. Castillo[63a], L. Castillo Garcia[13], V. Castillo Gimenez[161], N. F. Castro[129a,129e], A. Catinaccio[36], J. R. Catmore[124], V. Cavaliere[29], N. Cavalli[23a,23b], V. Cavasinni[73a,73b], E. Celebi[21a], F. Celli[125], M. S. Centonze[69a,69b], K. Cerny[121], A. S. Cerqueira[81a], A. Cerri[145], L. Cerrito[75a,75b], F. Cerutti[17a], A. Cervelli[23b], S. A. Cetin[21d], Z. Chadi[35a], D. Chakraborty[114], M. Chala[129f], J. Chan[168], W. S. Chan[113], W. Y. Chan[91], J. D. Chapman[32], B. Chargeishvili[148b], D. G. Charlton[20], T. P. Charman[93], M. Chatterjee[19], S. Chekanov[6], S. V. Chekulaev[155a], G. A. Chelkov[38,a], A. Chen[105], B. Chen[150], B. Chen[163], C. Chen[62a], H. Chen[14c], H. Chen[29], J. Chen[62c], J. Chen[26], S. Chen[127], S. J. Chen[14c], X. Chen[62c], X. Chen[14b,aa], Y. Chen[62a], C. L. Cheng[168], H. C. Cheng[64a], A. Cheplakov[38], E. Cheremushkina[48], E. Cherepanova[38], R. Cherkaoui El Moursli[35e], E. Cheu[7], K. Cheung[65], L. Chevalier[134], V. Chiarella[53], G. Chiarelli[73a], G. Chiodini[69a], A. S. Chisholm[20], A. Chitan[27b], Y. H. Chiu[163], M. V. Chizhov[38], K. Choi[11], A. R. Chomont[74a,74b], Y. Chou[102], E. Y. S. Chow[113], T. Chowdhury[33g], L. D. Christopher[33g], M. C. Chu[64a], X. Chu[14a,14d], J. Chudoba[130], J. J. Chwastowski[85], D. Cieri[109], K. M. Ciesla[85], V. Cindro[92], A. Ciocio[17a], F. Cirotto[71a,71b], Z. H. Citron[167,l], M. Citterio[70a], D. A. Ciubotaru[27b], B. M. Ciungu[154], A. Clark[56], P. J. Clark[52], J. M. Clavijo Columbie[48], S. E. Clawson[100], C. Clement[47a,47b], L. Clissa[23a,23b], Y. Coadou[101], M. Cobal[68a,68c], A. Coccaro[57b], R. F. Coelho Barrue[129a], R. Coelho Lopes De Sa[102], S. Coelli[70a], H. Cohen[150], A. E. C. Coimbra[36], B. Cole[41], J. Collot[60], P. Conde Muiño[129a,129g], S. H. Connell[33c], I. A. Connelly[59], E. I. Conroy[125], F. Conventi[71a,ac], H. G. Cooke[20], A. M. Cooper-Sarkar[125], F. Cormier[162], L. D. Corpe[36], M. Corradi[74a,74b], E. E. Corrigan[97], F. Corriveau[103,t], M. J. Costa[161], F. Costanza[4], D. Costanzo[138], B. M. Cote[118], G. Cowan[94], J. W. Cowley[32], K. Cranmer[116], S. Crépé-Renaudin[60], F. Crescioli[126], M. Cristinziani[140], M. Cristoforetti[77a,77b,c], V. Croft[157], G. Crosetti[43a,43b], A. Cueto[36], T. Cuhadar Donszelmann[158], H. Cui[14a,14d], Z. Cui[7], A. R. Cukierman[142], W. R. Cunningham[59], F. Curcio[43a,43b], P. Czodrowski[36], M. M. Czurylo[63b], M. J. Da Cunha Sargedas De Sousa[62a], J. V. Da Fonseca Pinto[81b], C. Da Via[100], W. Dabrowski[84a], T. Dado[49], S. Dahbi[33g], T. Dai[105], C. Dallapiccola[102], M. Dam[42], G. D'amen[29], V. D'Amico[76a,76b], J. Damp[99], J. R. Dandoy[127], M. F. Daneri[30], M. Danninger[141], V. Dao[36], G. Darbo[57b], S. Darmora[6], A. Dattagupta[122], S. D'Auria[70a,70b], C. David[155b], T. Davidek[132], D. R. Davis[51], B. Davis-Purcell[34], I. Dawson[93], K. De[8], R. De Asmundis[71a], M. De Beurs[113], S. De Castro[23a,23b], N. De Groot[112], P. de Jong[113], H. De la Torre[106], A. De Maria[14c], A. De Salvo[74a], U. De Sanctis[75a,75b], M. De Santis[75a,75b], A. De Santo[145], J. B. De Vivie De Regie[60], D. V. Dedovich[38], J. Degens[113], A. M. Deiana[44], J. Del Peso[98], F. Del Rio[63a], F. Deliot[134], C. M. Delitzsch[49], M. Della Pietra[71a,71b], D. Della Volpe[56], A. Dell'Acqua[36], L. Dell'Asta[70a,70b], M. Delmastro[4], P. A. Delsart[60], S. Demers[170], M. Demichev[38], S. P. Denisov[37], L. D'Eramo[114], D. Derendarz[85], F. Derue[126], P. Dervan[91], K. Desch[24], K. Dette[154], C. Deutsch[24], P. O. Deviveiros[36], F. A. Di Bello[74a,74b], A. Di Ciaccio[75a,75b], L. Di Ciaccio[4], A. Di Domenico[74a,74b], C. Di Donato[71a,71b], A. Di Girolamo[36], G. Di Gregorio[73a,73b], A. Di Luca[77a,77b,c], B. Di Micco[76a,76b], R. Di Nardo[76a,76b], C. Diaconu[101], F. A. Dias[113], T. Dias Do Vale[141], M. A. Diaz[136a,136b], F. G. Diaz Capriles[24], M. Didenko[161], E. B. Diehl[105], S. Díez Cornell[48], C. Diez Pardos[140], C. Dimitriadi[24,159], A. Dimitrievska[17a], W. Ding[14b], J. Dingfelder[24], I-M. Dinu[27b], S. J. Dittmeier[63b], F. Dittus[36], F. Djama[101], T. Djobava[148b], J. I. Djuvsland[16],

D. Dodsworth[26], C. Doglioni[100,97], J. Dolejsi[132], Z. Dolezal[132], M. Donadelli[81c], B. Dong[62c], J. Donini[40], A. D'Onofrio[14c], M. D'Onofrio[91], J. Dopke[133], A. Doria[71a], M. T. Dova[89], A. T. Doyle[59], E. Drechsler[141], E. Dreyer[167], A. S. Drobac[157], D. Du[62a], T. A. du Pree[113], F. Dubinin[37], M. Dubovsky[28a], E. Duchovni[167], G. Duckeck[108], O. A. Ducu[36,27b], D. Duda[109], A. Dudarev[36], M. D'uffizi[100], L. Duflot[66], M. Dührssen[36], C. Dülsen[169], A. E. Dumitriu[27b], M. Dunford[63a], S. Dungs[49], K. Dunne[47a,47b], A. Duperrin[101], H. Duran Yildiz[3a], M. Düren[58], A. Durglishvili[148b], B. Dutta[48], B. L. Dwyer[114], G. I. Dyckes[17a], M. Dyndal[84a], S. Dysch[100], B. S. Dziedzic[85], B. Eckerova[28a], M. G. Eggleston[51], E. Egidio Purcino De Souza[81b], L. F. Ehrke[56], G. Eigen[16], K. Einsweiler[17a], T. Ekelof[159], Y. El Ghazali[35b], H. El Jarrari[35e], A. El Moussaouy[35a], V. Ellajosyula[159], M. Ellert[159], F. Ellinghaus[169], A. A. Elliot[93], N. Ellis[36], J. Elmsheuser[29], M. Elsing[36], D. Emeliyanov[133], A. Emerman[41], Y. Enari[152], I. Ene[17a], J. Erdmann[49], A. Ereditato[19], P. A. Erland[85], M. Errenst[169], M. Escalier[66], C. Escobar[161], E. Etzion[150], G. Evans[129a], H. Evans[67], M. O. Evans[145], A. Ezhilov[37], S. Ezzarqtouni[35a], F. Fabbri[59], L. Fabbri[23a,23b], G. Facini[165], V. Fadeyev[135], R. M. Fakhrutdinov[37], S. Falciano[74a], P. J. Falke[24], S. Falke[36], J. Faltova[132], Y. Fan[14a], Y. Fang[14a,14d], G. Fanourakis[46], M. Fanti[70a,70b], M. Faraj[62c], A. Farbin[8], A. Farilla[76a], E. M. Farina[72a,72b], T. Farooque[106], S. M. Farrington[52], F. Fassi[35e], D. Fassouliotis[9], M. Faucci Giannelli[75a,75b], W. J. Fawcett[32], L. Fayard[66], O. L. Fedin[37,a], G. Fedotov[37], M. Feickert[160], L. Feligioni[101], A. Fell[138], D. E. Fellers[122], C. Feng[62b], M. Feng[14b], M. J. Fenton[158], A. B. Fenyuk[37], S. W. Ferguson[45], J. Ferrando[48], A. Ferrari[159], P. Ferrari[113], R. Ferrari[72a], D. Ferrere[56], C. Ferretti[105], F. Fiedler[99], A. Filipčič[92], F. Filthaut[112], M. C. N. Fiolhais[129a,129c,b], L. Fiorini[161], F. Fischer[140], W. C. Fisher[106], T. Fitschen[20,66], I. Fleck[140], P. Fleischmann[105], T. Flick[169], L. Flores[127], M. Flores[33d], L. R. Flores Castillo[64a], F. M. Follega[77a,77b], N. Fomin[16], J. H. Foo[154], B. C. Forland[67], A. Formica[134], A. C. Forti[100], E. Fortin[101], A. W. Fortman[61], M. G. Foti[17a], L. Fountas[9], D. Fournier[66], H. Fox[90], P. Francavilla[73a,73b], S. Francescato[61], M. Franchini[23a,23b], S. Franchino[63a], D. Francis[36], L. Franco[4], L. Franconi[19], M. Franklin[61], G. Frattari[74a,74b], A. C. Freegard[93], P. M. Freeman[20], W. S. Freund[81b], E. M. Freundlich[49], D. Froidevaux[36], J. A. Frost[125], Y. Fu[62a], M. Fujimoto[117], E. Fullana Torregrosa[161,*], J. Fuster[161], A. Gabrielli[23a,23b], A. Gabrielli[36], P. Gadow[48], G. Gagliardi[57a,57b], L. G. Gagnon[17a], G. E. Gallardo[125], E. J. Gallas[125], B. J. Gallop[133], R. Gamboa Goni[93], K. K. Gan[118], S. Ganguly[152], J. Gao[62a], Y. Gao[52], F. M. Garay Walls[136a,136b], B. Garcia[29], C. García[161], J. E. García Navarro[161], J. A. García Pascual[14a], M. Garcia-Sciveres[17a], R. W. Gardner[39], D. Garg[79], R. B. Garg[142], S. Gargiulo[54], C. A. Garner[154], V. Garonne[29], S. J. Gasiorowski[137], P. Gaspar[81b], G. Gaudio[72a], P. Gauzzi[74a,74b], I. L. Gavrilenko[37], A. Gavrilyuk[37], C. Gay[162], G. Gaycken[48], E. N. Gazis[10], A. A. Geanta[27b], C. M. Gee[135], J. Geisen[97], M. Geisen[99], C. Gemme[57b], M. H. Genest[60], S. Gentile[74a,74b], S. George[94], W. F. George[20], T. Geralis[46], L. O. Gerlach[55], P. Gessinger-Befurt[36], M. Ghasemi Bostanabad[163], M. Ghneimat[140], A. Ghosal[140], A. Ghosh[158], A. Ghosh[7], B. Giacobbe[23b], S. Giagu[74a,74b], N. Giangiacomi[154], P. Giannetti[73a], A. Giannini[62a], S. M. Gibson[94], M. Gignac[135], D. T. Gil[84b], B. J. Gilbert[41], D. Gillberg[34], G. Gilles[113], N. E. K. Gillwald[48], L. Ginabat[126], D. M. Gingrich[2,ab], M. P. Giordani[68a,68c], P. F. Giraud[134], G. Giugliarelli[68a,68c], D. Giugni[70a], F. Giuli[75a,75b], I. Gkialas[9,i], P. Gkountoumis[10], L. K. Gladilin[37], C. Glasman[98], G. R. Gledhill[122], M. Glisic[122], I. Gnesi[43b,e], Y. Go[29], M. Goblirsch-Kolb[26], D. Godin[107], S. Goldfarb[104], T. Golling[56], M. G. D. Gololo[33g], D. Golubkov[37], J. P. Gombas[106], A. Gomes[129a,129b], R. Goncalves Gama[55], R. Gonçalo[129a,129c], G. Gonella[122], L. Gonella[20], A. Gongadze[38], F. Gonnella[20], J. L. Gonski[41], S. González de la Hoz[161], S. Gonzalez Fernandez[13], R. Gonzalez Lopez[91], C. Gonzalez Renteria[17a], R. Gonzalez Suarez[159], S. Gonzalez-Sevilla[56], G. R. Gonzalvo Rodriguez[161], R. Y. González Andana[52], L. Goossens[36], N. A. Gorasia[20], P. A. Gorbounov[37], B. Gorini[36], E. Gorini[69a,69b], A. Gorišek[92], A. T. Goshaw[51], M. I. Gostkin[38], C. A. Gottardo[112], M. Gouighri[35b], V. Goumarre[48], A. G. Goussiou[137], N. Govender[33c], C. Goy[4], I. Grabowska-Bold[84a], K. Graham[34], E. Gramstad[124], S. Grancagnolo[18], M. Grandi[145], V. Gratchev[37,*], P. M. Gravila[27f], F. G. Gravili[69a,69b], H. M. Gray[17a], C. Grefe[24], I. M. Gregor[48], P. Grenier[142], K. Grevtsov[48], C. Grieco[13], A. A. Grillo[135], K. Grimm[31,m], S. Grinstein[13,r], J-F. Grivaz[66], S. Groh[99], E. Gross[167], J. Grosse-Knetter[55], C. Grud[105], A. Grummer[111], J. C. Grundy[125], L. Guan[105], W. Guan[168], C. Gubbels[162], J. G. R. Guerrero Rojas[161], F. Guescini[109], R. Gugel[99], A. Guida[48], T. Guillemin[4], S. Guindon[36], F. Guo[14a,14d], J. Guo[62c], L. Guo[66], Y. Guo[105], R. Gupta[48], S. Gurbuz[24], G. Gustavino[36], M. Guth[56], P. Gutierrez[119], L. F. Gutierrez Zagazeta[127], C. Gutschow[95], C. Guyot[134], C. Gwenlan[125], C. B. Gwilliam[91], E. S. Haaland[124], A. Haas[116], M. Habedank[48], C. Haber[17a], H. K. Hadavand[8], A. Hadef[99], S. Hadzic[109], M. Haleem[164], J. Haley[120],

J. J. Hall[138], G. D. Hallewell[101], L. Halser[19], K. Hamano[163], H. Hamdaoui[35e], M. Hamer[24], G. N. Hamity[52], J. Han[62b], K. Han[62a], L. Han[14c], L. Han[62a], S. Han[17a], Y. F. Han[154], K. Hanagaki[82], M. Hance[135], D. A. Hangal[41], M. D. Hank[39], R. Hankache[100], E. Hansen[97], J. B. Hansen[42], J. D. Hansen[42], P. H. Hansen[42], K. Hara[156], D. Harada[56], T. Harenberg[169], S. Harkusha[37], Y. T. Harris[125], P. F. Harrison[165], N. M. Hartman[142], N. M. Hartmann[108], Y. Hasegawa[139], A. Hasib[52], S. Haug[19], R. Hauser[106], M. Havranek[131], C. M. Hawkes[20], R. J. Hawkings[36], S. Hayashida[110], D. Hayden[106], C. Hayes[105], R. L. Hayes[162], C. P. Hays[125], J. M. Hays[93], H. S. Hayward[91], F. He[62a], Y. He[153], Y. He[126], M. P. Heath[52], V. Hedberg[97], A. L. Heggelund[124], N. D. Hehir[93], C. Heidegger[54], K. K. Heidegger[54], W. D. Heidorn[80], J. Heilman[34], S. Heim[48], T. Heim[17a], B. Heinemann[48,y], J. G. Heinlein[127], J. J. Heinrich[122], L. Heinrich[36], J. Hejbal[130], L. Helary[48], A. Held[116], S. Hellesund[124], C. M. Helling[162], S. Hellman[47a,47b], C. Helsens[36], R. C. W. Henderson[90], L. Henkelmann[32], A. M. Henriques Correia[36], H. Herde[142], Y. Hernández Jiménez[144], H. Herr[99], M. G. Herrmann[108], T. Herrmann[50], G. Herten[54], R. Hertenberger[108], L. Hervas[36], N. P. Hessey[155a], H. Hibi[83], E. Higón-Rodriguez[161], S. J. Hillier[20], I. Hinchliffe[17a], F. Hinterkeuser[24], M. Hirose[123], S. Hirose[156], D. Hirschbuehl[169], B. Hiti[92], O. Hladik[130], J. Hobbs[144], R. Hobincu[27e], N. Hod[167], M. C. Hodgkinson[138], B. H. Hodkinson[32], A. Hoecker[36], J. Hofer[48], D. Hohn[54], T. Holm[24], M. Holzbock[109], L. B. A. H. Hommels[32], B. P. Honan[100], J. Hong[62c], T. M. Hong[128], Y. Hong[55], J. C. Honig[54], A. Hönle[109], B. H. Hooberman[160], W. H. Hopkins[6], Y. Horii[110], L. A. Horyn[39], S. Hou[147], J. Howarth[59], J. Hoya[89], M. Hrabovsky[121], A. Hrynevich[37], T. Hryn'ova[4], P. J. Hsu[65], S.-C. Hsu[137], Q. Hu[41], S. Hu[62c], Y. F. Hu[14a,14d,ad], D. P. Huang[95], X. Huang[14c], Y. Huang[62a], Y. Huang[14a], Z. Hubacek[131], M. Huebner[24], F. Huegging[24], T. B. Huffman[125], M. Huhtinen[36], S. K. Huiberts[16], R. Hulsken[60], N. Huseynov[12,a], J. Huston[106], J. Huth[61], R. Hyneman[142], S. Hyrych[28a], G. Iacobucci[56], G. Iakovidis[29], I. Ibragimov[140], L. Iconomidou-Fayard[66], P. Iengo[36], R. Iguchi[152], T. Iizawa[56], Y. Ikegami[82], A. Ilg[19], N. Ilic[154], H. Imam[35a], T. Ingebretsen Carlson[47a,47b], G. Introzzi[72a,72b], M. Iodice[76a], V. Ippolito[74a,74b], M. Ishino[152], W. Islam[168], C. Issever[18,48], S. Istin[21a,ae], H. Ito[166], J. M. Iturbe Ponce[64a], R. Iuppa[77a,77b], A. Ivina[167], J. M. Izen[45], V. Izzo[71a], P. Jacka[130,131], P. Jackson[1], R. M. Jacobs[48], B. P. Jaeger[141], C. S. Jagfeld[108], G. Jäkel[169], K. Jakobs[54], T. Jakoubek[167], J. Jamieson[59], K. W. Janas[84a], G. Jarlskog[97], A. E. Jaspan[91], T. Javůrek[36], M. Javurkova[102], F. Jeanneau[134], L. Jeanty[122], J. Jejelava[148a,v], P. Jenni[54,f], S. Jézéquel[4], J. Jia[144], Z. Jia[14c], Y. Jiang[62a], S. Jiggins[52], J. Jimenez Pena[109], S. Jin[14c], A. Jinaru[27b], O. Jinnouchi[153], H. Jivan[33g], P. Johansson[138], K. A. Johns[7], C. A. Johnson[67], D. M. Jones[32], E. Jones[165], R. W. L. Jones[90], T. J. Jones[91], J. Jovicevic[15], X. Ju[17a], J. J. Junggeburth[36], A. Juste Rozas[13,r], S. Kabana[136e], A. Kaczmarska[85], M. Kado[74a,74b], H. Kagan[118], M. Kagan[142], A. Kahn[41], A. Kahn[127], C. Kahra[99], T. Kaji[166], E. Kajomovitz[149], N. Kakati[167], C. W. Kalderon[29], A. Kamenshchikov[154], N. J. Kang[135], Y. Kano[110], D. Kar[33g], K. Karava[125], M. J. Kareem[155b], E. Karentzos[54], I. Karkanias[151], S. N. Karpov[38], Z. M. Karpova[38], V. Kartvelishvili[90], A. N. Karyukhin[37], E. Kasimi[151], C. Kato[62d], J. Katzy[48], S. Kaur[34], K. Kawade[139], K. Kawagoe[88], T. Kawaguchi[110], T. Kawamoto[134], G. Kawamura[55], E. F. Kay[163], F. I. Kaya[157], S. Kazakos[13], V. F. Kazanin[37], Y. Ke[144], J. M. Keaveney[33a], R. Keeler[163], J. S. Keller[34], A. S. Kelly[95], D. Kelsey[145], J. J. Kempster[20], J. Kendrick[20], K. E. Kennedy[41], O. Kepka[130], S. Kersten[169], B. P. Kerševan[92], S. Ketabchi Haghighat[154], M. Khandoga[126], A. Khanov[120], A. G. Kharlamov[37], T. Kharlamova[37], E. E. Khoda[137], T. J. Khoo[18], G. Khoriauli[164], J. Khubua[148b], M. Kiehn[36], A. Kilgallon[122], E. Kim[153], Y. K. Kim[39], N. Kimura[95], A. Kirchhoff[55], D. Kirchmeier[50], C. Kirfel[24], J. Kirk[133], A. E. Kiryunin[109], T. Kishimoto[152], D. P. Kisliuk[154], C. Kitsaki[10], O. Kivernyk[24], M. Klassen[63a], C. Klein[34], L. Klein[164], M. H. Klein[105], M. Klein[91], U. Klein[91], P. Klimek[36], A. Klimentov[29], F. Klimpel[109], T. Klingl[24], T. Klioutchnikova[36], F. F. Klitzner[108], P. Kluit[113], S. Kluth[109], E. Kneringer[78], T. M. Knight[154], A. Knue[54], D. Kobayashi[88], R. Kobayashi[86], M. Kocian[142], T. Kodama[152], P. Kodyš[132], D. M. Koeck[145], P. T. Koenig[24], T. Koffas[34], N. M. Köhler[36], M. Kolb[134], I. Koletsou[4], T. Komarek[121], K. Köneke[54], A. X. Y. Kong[1], T. Kono[117], V. Konstantinides[95], N. Konstantinidis[95], B. Konya[97], R. Kopeliansky[67], S. Koperny[84a], K. Korcyl[85], K. Kordas[151], G. Koren[150], A. Korn[95], S. Korn[55], I. Korolkov[13], N. Korotkova[37], B. Kortman[113], O. Kortner[109], S. Kortner[109], W. H. Kostecka[114], V. V. Kostyukhin[140,37], A. Kotsokechagia[66], A. Kotwal[51], A. Koulouris[36], A. Kourkoumeli-Charalampidi[72a,72b], C. Kourkoumelis[9], E. Kourlitis[6], O. Kovanda[145], R. Kowalewski[163], W. Kozanecki[134], A. S. Kozhin[37], V. A. Kramarenko[37], G. Kramberger[92], P. Kramer[99], M. W. Krasny[126], A. Krasznahorkay[36], J. A. Kremer[99], J. Kretzschmar[91], K. Kreul[18], P. Krieger[154], F. Krieter[108], S. Krishnamurthy[102], A. Krishnan[63b], M. Krivos[132], K. Krizka[17a], K. Kroeninger[49], H. Kroha[109],

J. Kroll[130], J. Kroll[127], K. S. Krowpman[106], U. Kruchonak[38], H. Krüger[24], N. Krumnack[80], M. C. Kruse[51], J. A. Krzysiak[85], A. Kubota[153], O. Kuchinskaia[37], S. Kuday[3a], D. Kuechler[48], J. T. Kuechler[48], S. Kuehn[36], T. Kuhl[48], V. Kukhtin[38], Y. Kulchitsky[37,a], S. Kuleshov[136d,136b], M. Kumar[33g], N. Kumari[101], M. Kuna[60], A. Kupco[130], T. Kupfer[49], O. Kuprash[54], H. Kurashige[83], L. L. Kurchaninov[155a], Y. A. Kurochkin[37], A. Kurova[37], E. S. Kuwertz[36], M. Kuze[153], A. K. Kvam[137], J. Kvita[121], T. Kwan[103], K. W. Kwok[64a], C. Lacasta[161], F. Lacava[74a,74b], H. Lacker[18], D. Lacour[126], N. N. Lad[95], E. Ladygin[38], B. Laforge[126], T. Lagouri[136e], S. Lai[55], I. K. Lakomiec[84a], N. Lalloue[60], J. E. Lambert[119], S. Lammers[67], W. Lampl[7], C. Lampoudis[151], E. Lançon[29], U. Landgraf[54], M. P. J. Landon[93], V. S. Lang[54], J. C. Lange[55], R. J. Langenberg[102], A. J. Lankford[158], F. Lanni[29], K. Lantzsch[24], A. Lanza[72a], A. Lapertosa[57a,57b], J. F. Laporte[134], T. Lari[70a], F. Lasagni Manghi[23b], M. Lassnig[36], V. Latonova[130], T. S. Lau[64a], A. Laudrain[99], A. Laurier[34], M. Lavorgna[71a,71b], S. D. Lawlor[94], Z. Lawrence[100], M. Lazzaroni[70a,70b], B. Le[100], B. Leban[92], A. Lebedev[80], M. LeBlanc[36], T. LeCompte[6], F. Ledroit-Guillon[60], A. C. A. Lee[95], G. R. Lee[16], L. Lee[61], S. C. Lee[147], L. L. Leeuw[33c], B. Lefebvre[155a], H. P. Lefebvre[94], M. Lefebvre[163], C. Leggett[17a], K. Lehmann[141], G. Lehmann Miotto[36], W. A. Leight[102], A. Leisos[151,q], M. A. L. Leite[81c], C. E. Leitgeb[48], R. Leitner[132], K. J. C. Leney[44], T. Lenz[24], S. Leone[73a], C. Leonidopoulos[52], A. Leopold[143], C. Leroy[107], R. Les[106], C. G. Lester[32], M. Levchenko[37], J. Levêque[4], D. Levin[105], L. J. Levinson[167], D. J. Lewis[20], B. Li[14b], B. Li[62b], C. Li[62a], C-Q. Li[62c,62d], H. Li[62a], H. Li[62b], H. Li[62b], J. Li[62c], K. Li[137], L. Li[62c], M. Li[14a,14d], Q. Y. Li[62a], S. Li[62d,62c,d], T. Li[62b], X. Li[48], Z. Li[62b], Z. Li[125], Z. Li[103], Z. Li[91], Z. Liang[14a], M. Liberatore[48], B. Liberti[75a], K. Lie[64c], J. Lieber Marin[81b], K. Lin[106], R. A. Linck[67], R. E. Lindley[7], J. H. Lindon[2], A. Linss[48], E. Lipeles[127], A. Lipniacka[16], T. M. Liss[160,z], A. Lister[162], J. D. Little[4], B. Liu[14a], B. X. Liu[141], D. Liu[62d,62c], J. B. Liu[62a], J. K. K. Liu[32], K. Liu[62d,62c], M. Liu[62a], M. Y. Liu[62a], P. Liu[14a], Q. Liu[62d,137,62c], X. Liu[62a], Y. Liu[48], Y. Liu[14c,14d], Y. L. Liu[105], Y. W. Liu[62a], M. Livan[72a,72b], J. Llorente Merino[141], S. L. Lloyd[93], E. M. Lobodzinska[48], P. Loch[7], S. Loffredo[75a,75b], T. Lohse[18], K. Lohwasser[138], M. Lokajicek[130], J. D. Long[160], I. Longarini[74a,74b], L. Longo[69a,69b], R. Longo[160], I. Lopez Paz[36], A. Lopez Solis[48], J. Lorenz[108], N. Lorenzo Martinez[4], A. M. Lory[108], A. Lösle[54], X. Lou[47a,47b], X. Lou[14a,14d], A. Lounis[66], J. Love[6], P. A. Love[90], J. J. Lozano Bahilo[161], G. Lu[14a,14d], M. Lu[79], S. Lu[127], Y. J. Lu[65], H. J. Lubatti[137], C. Luci[74a,74b], F. L. Lucio Alves[14c], A. Lucotte[60], F. Luehring[67], I. Luise[144], O. Lundberg[143], B. Lund-Jensen[143], N. A. Luongo[122], M. S. Lutz[150], D. Lynn[29], H. Lyons[91], R. Lysak[130], E. Lytken[97], F. Lyu[14a], V. Lyubushkin[38], T. Lyubushkina[38], H. Ma[29], L. L. Ma[62b], Y. Ma[95], D. M. Mac Donell[163], G. Maccarrone[53], J. C. MacDonald[138], R. Madar[40], W. F. Mader[50], J. Maeda[83], T. Maeno[29], M. Maerker[50], V. Magerl[54], J. Magro[68a,68c], D. J. Mahon[41], C. Maidantchik[81b], A. Maio[129a,129b,129d], K. Maj[84a], O. Majersky[28a], S. Majewski[122], N. Makovec[66], V. Maksimovic[15], B. Malaescu[126], Pa. Malecki[85], V. P. Maleev[37], F. Malek[60], D. Malito[43a,43b], U. Mallik[79], C. Malone[32], S. Maltezos[10], S. Malyukov[38], J. Mamuzic[161], G. Mancini[53], J. P. Mandalia[93], I. Mandić[92], L. Manhaes de Andrade Filho[81a], I. M. Maniatis[151], M. Manisha[134], J. Manjarres Ramos[50], D. C. Mankad[167], K. H. Mankinen[97], A. Mann[108], A. Manousos[78], B. Mansoulie[134], S. Manzoni[36], A. Marantis[151,q], G. Marchiori[5], M. Marcisovsky[130], L. Marcoccia[75a,75b], C. Marcon[97], M. Marinescu[20], M. Marjanovic[119], Z. Marshall[17a], S. Marti-Garcia[161], T. A. Martin[165], V. J. Martin[52], B. Martin dit Latour[16], L. Martinelli[74a,74b], M. Martinez[13,r], P. Martinez Agullo[161], V. I. Martinez Outschoorn[102], P. Martinez Suarez[13], S. Martin-Haugh[133], V. S. Martoiu[27b], A. C. Martyniuk[95], A. Marzin[36], S. R. Maschek[109], L. Masetti[99], T. Mashimo[152], J. Masik[100], A. L. Maslennikov[37], L. Massa[23b], P. Massarotti[71a,71b], P. Mastrandrea[73a,73b], A. Mastroberardino[43a,43b], T. Masubuchi[152], T. Mathisen[159], A. Matic[108], N. Matsuzawa[152], J. Maurer[27b], B. Maček[92], D. A. Maximov[37], R. Mazini[147], I. Maznas[151], M. Mazza[106], S. M. Mazza[135], C. Mc Ginn[29], J. P. Mc Gowan[103], S. P. Mc Kee[105], T. G. McCarthy[109], W. P. McCormack[17a], E. F. McDonald[104], A. E. McDougall[113], J. A. Mcfayden[145], G. Mchedlidze[148b], M. A. McKay[44], R. P. Mckenzie[33g], D. J. Mclaughlin[95], K. D. McLean[163], S. J. McMahon[133], P. C. McNamara[104], R. A. McPherson[163,t], J. E. Mdhluli[33g], S. Meehan[36], T. Megy[40], S. Mehlhase[108], A. Mehta[91], B. Meirose[45], D. Melini[149], B. R. Mellado Garcia[33g], A. H. Melo[55], F. Meloni[48], A. Melzer[24], E. D. Mendes Gouveia[129a], A. M. Mendes Jacques Da Costa[20], H. Y. Meng[154], L. Meng[90], S. Menke[109], M. Mentink[36], E. Meoni[43a,43b], C. Merlassino[125], L. Merola[71a,71b], C. Meroni[70a], G. Merz[105], O. Meshkov[37], J. K. R. Meshreki[140], J. Metcalfe[6], A. S. Mete[6], C. Meyer[67], J-P. Meyer[134], M. Michetti[18], R. P. Middleton[133], L. Mijović[52], G. Mikenberg[167], M. Mikestikova[130], M. Mikuž[92], H. Mildner[138], A. Milic[154], C. D. Milke[44], D. W. Miller[39], L. S. Miller[34], A. Milov[167],

D. A. Milstead[47a,47b], T. Min[14c], A. A. Minaenko[37], I. A. Minashvili[148b], L. Mince[59], A. I. Mincer[116], B. Mindur[84a], M. Mineev[38], Y. Minegishi[152], Y. Mino[86], L. M. Mir[13], M. Miralles Lopez[161], M. Mironova[125], T. Mitani[166], A. Mitra[165], V. A. Mitsou[161], O. Miu[154], P. S. Miyagawa[93], Y. Miyazaki[88], A. Mizukami[82], J. U. Mjörnmark[97], T. Mkrtchyan[63a], M. Mlynarikova[114], T. Moa[47a,47b], S. Mobius[55], K. Mochizuki[107], P. Moder[48], P. Mogg[108], A. F. Mohammed[14a,14d], S. Mohapatra[41], G. Mokgatitswane[33g], B. Mondal[140], S. Mondal[131], K. Mönig[48], E. Monnier[101], L. Monsonis Romero[161], J. Montejo Berlingen[36], M. Montella[118], F. Monticelli[89], N. Morange[66], A. L. Moreira De Carvalho[129a], M. Moreno Llácer[161], C. Moreno Martinez[13], P. Morettini[57b], S. Morgenstern[165], D. Mori[141], M. Morii[61], M. Morinaga[152], V. Morisbak[124], A. K. Morley[36], A. P. Morris[95], L. Morvaj[36], P. Moschovakos[36], B. Moser[113], M. Mosidze[148b], T. Moskalets[54], P. Moskvitina[112], J. Moss[31,n], E. J. W. Moyse[102], S. Muanza[101], J. Mueller[128], D. Muenstermann[90], R. Müller[19], G. A. Mullier[97], J. J. Mullin[127], D. P. Mungo[70a,70b], J. L. Munoz Martinez[13], F. J. Munoz Sanchez[100], M. Murin[100], W. J. Murray[133,165], A. Murrone[70a,70b], J. M. Muse[119], M. Muškinja[17a], C. Mwewa[29], A. G. Myagkov[37,a], A. J. Myers[8], A. A. Myers[128], G. Myers[67], M. Myska[131], B. P. Nachman[17a], O. Nackenhorst[49], A. Nag[50], K. Nagai[125], K. Nagano[82], J. L. Nagle[29], E. Nagy[101], A. M. Nairz[36], Y. Nakahama[82], K. Nakamura[82], H. Nanjo[123], F. Napolitano[63a], R. Narayan[44], E. A. Narayanan[111], I. Naryshkin[37], M. Naseri[34], C. Nass[24], G. Navarro[22a], J. Navarro-Gonzalez[161], R. Nayak[150], P. Y. Nechaeva[37], F. Nechansky[48], T. J. Neep[20], A. Negri[72a,72b], M. Negrini[23b], C. Nellist[112], C. Nelson[103], K. Nelson[105], S. Nemecek[130], M. Nessi[36,g], M. S. Neubauer[160], F. Neuhaus[99], J. Neundorf[48], R. Newhouse[162], P. R. Newman[20], C. W. Ng[128], Y. S. Ng[18], Y. W. Y. Ng[158], B. Ngair[35e], H. D. N. Nguyen[107], R. B. Nickerson[125], R. Nicolaidou[134], D. S. Nielsen[42], J. Nielsen[135], M. Niemeyer[55], N. Nikiforou[11], V. Nikolaenko[37,a], I. Nikolic-Audit[126], K. Nikolopoulos[20], P. Nilsson[29], H. R. Nindhito[56], A. Nisati[74a], N. Nishu[2], R. Nisius[109], S. J. Noacco Rosende[89], T. Nobe[152], D. L. Noel[32], Y. Noguchi[86], I. Nomidis[126], M. A. Nomura[29], M. B. Norfolk[138], R. R. B. Norisam[95], J. Novak[92], T. Novak[48], O. Novgorodova[50], L. Novotny[131], R. Novotny[111], L. Nozka[121], K. Ntekas[158], E. Nurse[95], F. G. Oakham[34,ab], J. Ocariz[126], A. Ochi[83], I. Ochoa[129a], J. P. Ochoa-Ricoux[136a], S. Oda[88], S. Odaka[82], S. Oerdek[159], A. Ogrodnik[84a], A. Oh[100], C. C. Ohm[143], H. Oide[153], R. Oishi[152], M. L. Ojeda[48], Y. Okazaki[86], M. W. O'Keefe[91], Y. Okumura[152], A. Olariu[27b], L. F. Oleiro Seabra[129a], S. A. Olivares Pino[136e], D. Oliveira Damazio[29], D. Oliveira Goncalves[81a], J. L. Oliver[158], M. J. R. Olsson[158], A. Olszewski[85], J. Olszowska[85,*], Ö.O. Öncel[54], D. C. O'Neil[141], A. P. O'Neill[19], A. Onofre[129a,129e], P. U. E. Onyisi[11], R. G. Oreamuno Madriz[114], M. J. Oreglia[39], G. E. Orellana[89], D. Orestano[76a,76b], N. Orlando[13], R. S. Orr[154], V. O'Shea[59], R. Ospanov[62a], G. Otero y Garzon[30], H. Otono[88], P. S. Ott[63a], G. J. Ottino[17a], M. Ouchrif[35d], J. Ouellette[29], F. Ould-Saada[124], M. Owen[59], R. E. Owen[133], K. Y. Oyulmaz[21a], V. E. Ozcan[21a], N. Ozturk[8], S. Ozturk[21d], J. Pacalt[121], H. A. Pacey[32], K. Pachal[51], A. Pacheco Pages[13], C. Padilla Aranda[13], S. Pagan Griso[17a], G. Palacino[67], S. Palazzo[52], S. Palestini[36], M. Palka[84b], J. Pan[170], D. K. Panchal[11], C. E. Pandini[113], J. G. Panduro Vazquez[94], P. Pani[48], G. Panizzo[68a,68c], L. Paolozzi[56], C. Papadatos[107], S. Parajuli[44], A. Paramonov[6], C. Paraskevopoulos[10], D. Paredes Hernandez[64b], B. Parida[167], T. H. Park[154], A. J. Parker[31], M. A. Parker[32], F. Parodi[57a,57b], E. W. Parrish[114], V. A. Parrish[52], J. A. Parsons[41], U. Parzefall[54], B. Pascual Dias[107], L. Pascual Dominguez[150], V. R. Pascuzzi[17a], F. Pasquali[113], E. Pasqualucci[74a], S. Passaggio[57b], F. Pastore[94], P. Pasuwan[47a,47b], J. R. Pater[100], A. Pathak[168], J. Patton[91], T. Pauly[36], J. Pearkes[142], M. Pedersen[124], R. Pedro[129a], S. V. Peleganchuk[37], O. Penc[130], C. Peng[64b], H. Peng[62a], M. Penzin[37], B. S. Peralva[81a], A. P. Pereira Peixoto[60], L. Pereira Sanchez[47a,47b], D. V. Perepelitsa[29], E. Perez Codina[155a], M. Perganti[10], L. Perini[70a,70b,*], H. Pernegger[36], S. Perrella[36], A. Perrevoort[112], O. Perrin[40], K. Peters[48], R. F. Y. Peters[100], B. A. Petersen[36], T. C. Petersen[42], E. Petit[101], V. Petousis[131], C. Petridou[151], A. Petrukhin[140], M. Pettee[17a], N. E. Pettersson[36], K. Petukhova[132], A. Peyaud[134], R. Pezoa[136f], L. Pezzotti[36], G. Pezzullo[170], T. Pham[104], P. W. Phillips[133], M. W. Phipps[160], G. Piacquadio[144], E. Pianori[17a], F. Piazza[70a,70b], R. Piegaia[30], D. Pietreanu[27b], A. D. Pilkington[100], M. Pinamonti[68a,68c], J. L. Pinfold[2], C. Pitman Donaldson[95], D. A. Pizzi[34], L. Pizzimento[75a,75b], A. Pizzini[113], M.-A. Pleier[29], V. Plesanovs[54], V. Pleskot[132], E. Plotnikova[38], G. Poddar[4], R. Poettgen[97], R. Poggi[56], L. Poggioli[126], I. Pogrebnyak[106], D. Pohl[24], I. Pokharel[55], S. Polacek[132], G. Polesello[72a], A. Poley[141,155a], R. Polifka[131], A. Polini[23b], C. S. Pollard[125], Z. B. Pollock[118], V. Polychronakos[29], D. Ponomarenko[37], L. Pontecorvo[36], S. Popa[27a], G. A. Popeneciu[27d], L. Portales[4], D. M. Portillo Quintero[155a], S. Pospisil[131], P. Postolache[27c], K. Potamianos[125], I. N. Potrap[38], C. J. Potter[32], H. Potti[1], T. Poulsen[48], J. Poveda[161], G. Pownall[48], M. E. Pozo Astigarraga[36], A. Prades Ibanez[161], P. Pralavorio[101], M. M. Prapa[46],

J. A. Pretel[54], D. Price[100], M. Primavera[69a], M. A. Principe Martin[98], M. L. Proffitt[137], N. Proklova[37], K. Prokofiev[64c], G. Proto[75a,75b], S. Protopopescu[29], J. Proudfoot[6], M. Przybycien[84a], D. Pudzha[37], P. Puzo[66], D. Pyatiizbyantseva[37], J. Qian[105], Y. Qin[100], T. Qiu[93], A. Quadt[55], M. Queitsch-Maitland[24], G. Rabanal Bolanos[61], D. Rafanoharana[54], F. Ragusa[70a,70b], J. A. Raine[56], S. Rajagopalan[29], K. Ran[14a,14d], V. Raskina[126], D. F. Rassloff[63a], S. Rave[99], B. Ravina[59], I. Ravinovich[167], M. Raymond[36], A. L. Read[124], N. P. Readioff[138], D. M. Rebuzzi[72a,72b], G. Redlinger[29], K. Reeves[45], D. Reikher[150], A. Reiss[99], A. Rej[140], C. Rembser[36], A. Renardi[48], M. Renda[27b], M. B. Rendel[109], A. G. Rennie[59], S. Resconi[70a], M. Ressegotti[57a,57b], E. D. Resseguie[17a], S. Rettie[95], B. Reynolds[118], E. Reynolds[17a], M. Rezaei Estabragh[169], O. L. Rezanova[37], P. Reznicek[132], E. Ricci[77a,77b], R. Richter[109], S. Richter[47a,47b], E. Richter-Was[84b], M. Ridel[126], P. Rieck[116], P. Riedler[36], M. Rijssenbeek[144], A. Rimoldi[72a,72b], M. Rimoldi[48], L. Rinaldi[23a,23b], T. T. Rinn[160], M. P. Rinnagel[108], G. Ripellino[143], I. Riu[13], P. Rivadeneira[48], J. C. Rivera Vergara[163], F. Rizatdinova[120], E. Rizvi[93], C. Rizzi[56], B. A. Roberts[165], B. R. Roberts[17a], S. H. Robertson[103,t], M. Robin[48], D. Robinson[32], C. M. Robles Gajardo[136f], M. Robles Manzano[99], A. Robson[59], A. Rocchi[75a,75b], C. Roda[73a,73b], S. Rodriguez Bosca[63a], Y. Rodriguez Garcia[22a], A. Rodriguez Rodriguez[54], A. M. Rodríguez Vera[155b], S. Roe[36], J. T. Roemer[158], A. R. Roepe-Gier[119], J. Roggel[169], O. Røhne[124], R. A. Rojas[163], B. Roland[54], C. P. A. Roland[67], J. Roloff[29], A. Romaniouk[37], M. Romano[23b], A. C. Romero Hernandez[160], N. Rompotis[91], M. Ronzani[116], L. Roos[126], S. Rosati[74a], B. J. Rosser[127], E. Rossi[4], E. Rossi[71a,71b], L. P. Rossi[57b], L. Rossini[48], R. Rosten[118], M. Rotaru[27b], B. Rottler[54], D. Rousseau[66], D. Rousso[32], G. Rovelli[72a,72b], A. Roy[160], A. Rozanov[101], Y. Rozen[149], X. Ruan[33g], A. J. Ruby[91], T. A. Ruggeri[1], F. Rühr[54], A. Ruiz-Martinez[161], A. Rummler[36], Z. Rurikova[54], N. A. Rusakovich[38], H. L. Russell[163], L. Rustige[40], J. P. Rutherfoord[7], E. M. Rüttinger[138], K. Rybacki[90], M. Rybar[132], E. B. Rye[124], A. Ryzhov[37], J. A. Sabater Iglesias[56], P. Sabatini[161], L. Sabetta[74a,74b], H. F-W. Sadrozinski[135], F. Safai Tehrani[74a], B. Safarzadeh Samani[145], M. Safdari[142], S. Saha[103], M. Sahinsoy[109], A. Sahu[169], M. Saimpert[134], M. Saito[152], T. Saito[152], D. Salamani[36], G. Salamanna[76a,76b], A. Salnikov[142], J. Salt[161], A. Salvador Salas[13], D. Salvatore[43a,43b], F. Salvatore[145], A. Salzburger[36], D. Sammel[54], D. Sampsonidis[151], D. Sampsonidou[62d,62c], J. Sánchez[161], A. Sanchez Pineda[4], V. Sanchez Sebastian[161], H. Sandaker[124], C. O. Sander[48], I. G. Sanderswood[90], J. A. Sandesara[102], M. Sandhoff[169], C. Sandoval[22b], D. P. C. Sankey[133], A. Sansoni[53], C. Santoni[40], H. Santos[129a,129b], S. N. Santpur[17a], A. Santra[167], K. A. Saoucha[138], J. G. Saraiva[129a,129d], J. Sardain[101], O. Sasaki[82], K. Sato[156], C. Sauer[63b], F. Sauerburger[54], E. Sauvan[4], P. Savard[154,ab], R. Sawada[152], C. Sawyer[133], L. Sawyer[96], I. Sayago Galvan[161], C. Sbarra[23b], A. Sbrizzi[23a,23b], T. Scanlon[95], J. Schaarschmidt[137], P. Schacht[109], D. Schaefer[39], U. Schäfer[99], A. C. Schaffer[66], D. Schaile[108], R. D. Schamberger[144], E. Schanet[108], C. Scharf[18], N. Scharmberg[100], V. A. Schegelsky[37], D. Scheirich[132], F. Schenck[18], M. Schernau[158], C. Scheulen[55], C. Schiavi[57a,57b], Z. M. Schillaci[26], E. J. Schioppa[69a,69b], M. Schioppa[43a,43b], B. Schlag[99], K. E. Schleicher[54], S. Schlenker[36], K. Schmieden[99], C. Schmitt[99], S. Schmitt[48], L. Schoeffel[134], A. Schoening[63b], P. G. Scholer[54], E. Schopf[125], M. Schott[99], J. Schovancova[36], S. Schramm[56], F. Schroeder[169], H-C. Schultz-Coulon[63a], M. Schumacher[54], B. A. Schumm[135], Ph. Schune[134], A. Schwartzman[142], T. A. Schwarz[105], Ph. Schwemling[134], R. Schwienhorst[106], A. Sciandra[135], G. Sciolla[26], F. Scuri[73a], F. Scutti[104], C. D. Sebastiani[91], K. Sedlaczek[49], P. Seema[18], S. C. Seidel[111], A. Seiden[135], B. D. Seidlitz[29], T. Seiss[39], C. Seitz[48], J. M. Seixas[81b], G. Sekhniaidze[71a], S. J. Sekula[44], L. Selem[4], N. Semprini-Cesari[23a,23b], S. Sen[51], V. Senthilkumar[161], L. Serin[66], L. Serkin[68a,68b], M. Sessa[76a,76b], H. Severini[119], S. Sevova[142], F. Sforza[57a,57b], A. Sfyrla[56], E. Shabalina[55], R. Shaheen[143], J. D. Shahinian[127], N. W. Shaikh[47a,47b], D. Shaked Renous[167], L. Y. Shan[14a], M. Shapiro[17a], A. Sharma[36], A. S. Sharma[1], S. Sharma[48], P. B. Shatalov[37], K. Shaw[145], S. M. Shaw[100], P. Sherwood[95], L. Shi[95], C. O. Shimmin[170], Y. Shimogama[166], J. D. Shinner[94], I. P. J. Shipsey[125], S. Shirabe[56], M. Shiyakova[38], J. Shlomi[167], M. J. Shochet[39], J. Shojaii[104], D. R. Shope[143], S. Shrestha[118], E. M. Shrif[33g], M. J. Shroff[163], P. Sicho[130], A. M. Sickles[160], E. Sideras Haddad[33g], O. Sidiropoulou[36], A. Sidoti[23b], F. Siegert[50], Dj. Sijacki[15], F. Sili[89], J. M. Silva[20], M. V. Silva Oliveira[36], S. B. Silverstein[47a], S. Simion[66], R. Simoniello[36], N. D. Simpson[97], S. Simsek[21a], S. Sindhu[55], P. Sinervo[154], V. Sinetckii[37], S. Singh[141], S. Singh[154], S. Sinha[48], S. Sinha[33g], M. Sioli[23a,23b], I. Siral[122], S. Yu. Sivoklokov[37,*], J. Sjölin[47a,47b], A. Skaf[55], E. Skorda[97], P. Skubic[119], M. Slawinska[85], V. Smakhtin[167], B. H. Smart[133], J. Smiesko[132], S. Yu. Smirnov[37], Y. Smirnov[37], L. N. Smirnova[37,a], O. Smirnova[97], E. A. Smith[39], H. A. Smith[125], R. Smith[142], M. Smizanska[90], K. Smolek[131], A. Smykiewicz[85], A. A. Snesarev[37], H. L. Snoek[113], S. Snyder[29], R. Sobie[163,t], A. Soffer[150], C. A. Solans Sanchez[36], E. Yu. Soldatov[37],

U. Soldevila[161], A. A. Solodkov[37], S. Solomon[54], A. Soloshenko[38], K. Solovieva[54], O. V. Solovyanov[37], V. Solovyev[37], P. Sommer[138], H. Son[157], A. Sonay[13], W. Y. Song[155b], A. Sopczak[131], A. L. Sopio[95], F. Sopkova[28b], V. Sothilingam[63a], S. Sottocornola[72a,72b], R. Soualah[115c], Z. Soumaimi[35e], D. South[48], S. Spagnolo[69a,69b], M. Spalla[109], M. Spangenberg[165], F. Spanò[94], D. Sperlich[54], G. Spigo[36], M. Spina[145], S. Spinali[90], D. P. Spiteri[59], M. Spousta[132], E. J. Staats[34], A. Stabile[70a,70b], R. Stamen[63a], M. Stamenkovic[113], A. Stampekis[20], M. Standke[24], E. Stanecka[85], B. Stanislaus[17a], M. M. Stanitzki[48], M. Stankaityte[125], B. Stapf[48], E. A. Starchenko[37], G. H. Stark[135], J. Stark[101], D. M. Starko[155b], P. Staroba[130], P. Starovoitov[63a], S. Stärz[103], R. Staszewski[85], G. Stavropoulos[46], J. Steentoft[159], P. Steinberg[29], A. L. Steinhebel[122], B. Stelzer[141,155a], H. J. Stelzer[128], O. Stelzer-Chilton[155a], H. Stenzel[58], T. J. Stevenson[145], G. A. Stewart[36], M. C. Stockton[36], G. Stoicea[27b], M. Stolarski[129a], S. Stonjek[109], A. Straessner[50], J. Strandberg[143], S. Strandberg[47a,47b], M. Strauss[119], T. Strebler[101], P. Strizenec[28b], R. Ströhmer[164], D. M. Strom[122], L. R. Strom[48], R. Stroynowski[44], A. Strubig[47a,47b], S. A. Stucci[29], B. Stugu[16], J. Stupak[119], N. A. Styles[48], D. Su[142], S. Su[62a], W. Su[62c,62d,137], X. Su[62a,66], K. Sugizaki[152], V. V. Sulin[37], M. J. Sullivan[91], D. M. S. Sultan[77a,77b], L. Sultanaliyeva[37], S. Sultansoy[3b], T. Sumida[86], S. Sun[105], S. Sun[168], O. Sunneborn Gudnadottir[159], M. R. Sutton[145], M. Svatos[130], M. Swiatlowski[155a], T. Swirski[164], I. Sykora[28a], M. Sykora[132], T. Sykora[132], D. Ta[99], K. Tackmann[48,s], A. Taffard[158], R. Tafirout[155a], R. H. M. Taibah[126], R. Takashima[87], K. Takeda[83], E. P. Takeva[52], Y. Takubo[82], M. Talby[101], A. A. Talyshev[37], K. C. Tam[64b], N. M. Tamir[150], A. Tanaka[152], J. Tanaka[152], R. Tanaka[66], J. Tang[62c], Z. Tao[162], S. Tapia Araya[80], S. Tapprogge[99], A. Tarek Abouelfadl Mohamed[106], S. Tarem[149], K. Tariq[62b], G. Tarna[27b], G. F. Tartarelli[70a], P. Tas[132], M. Tasevsky[130], E. Tassi[43a,43b], G. Tateno[152], Y. Tayalati[35e], G. N. Taylor[104], W. Taylor[155b], H. Teagle[91], A. S. Tee[168], R. Teixeira De Lima[142], P. Teixeira-Dias[94], J. J. Teoh[113], K. Terashi[152], J. Terron[98], S. Terzo[13], M. Testa[53], R. J. Teuscher[154,t], N. Themistokleous[52], T. Theveneaux-Pelzer[18], O. Thielmann[169], D. W. Thomas[94], J. P. Thomas[20], E. A. Thompson[48], P. D. Thompson[20], E. Thomson[127], E. J. Thorpe[93], Y. Tian[55], V. Tikhomirov[37,a], Yu. A. Tikhonov[37], S. Timoshenko[37], E. X. L. Ting[1], P. Tipton[170], S. Tisserant[101], S. H. Tlou[33g], A. Tnourji[40], K. Todome[23a,23b], S. Todorova-Nova[132], S. Todt[50], M. Togawa[82], J. Tojo[88], S. Tokár[28a], K. Tokushuku[82], R. Tombs[32], M. Tomoto[82,110], L. Tompkins[142], P. Tornambe[102], E. Torrence[122], H. Torres[50], E. Torró Pastor[161], M. Toscani[30], C. Tosciri[39], D. R. Tovey[138], A. Traeet[16], I. S. Trandafir[27b], C. J. Treado[116], T. Trefzger[164], A. Tricoli[29], I. M. Trigger[155a], S. Trincaz-Duvoid[126], D. A. Trischuk[162], B. Trocmé[60], A. Trofymov[66], C. Troncon[70a], F. Trovato[145], L. Truong[33c], M. Trzebinski[85], A. Trzupek[85], F. Tsai[144], M. Tsai[105], A. Tsiamis[151], P. V. Tsiareshka[37], A. Tsirigotis[151,q], V. Tsiskaridze[144], E. G. Tskhadadze[148a], M. Tsopoulou[151], Y. Tsujikawa[86], I. I. Tsukerman[37], V. Tsulaia[17a], S. Tsuno[82], O. Tsur[149], D. Tsybychev[144], Y. Tu[64b], A. Tudorache[27b], V. Tudorache[27b], A. N. Tuna[36], S. Turchikhin[38], I. Turk Cakir[3a], R. Turra[70a], P. M. Tuts[41], S. Tzamarias[151], P. Tzanis[10], E. Tzovara[99], K. Uchida[152], F. Ukegawa[156], P. A. Ulloa Poblete[136c], G. Unal[36], M. Unal[11], A. Undrus[29], G. Unel[158], K. Uno[152], J. Urban[28b], P. Urquijo[104], G. Usai[8], R. Ushioda[153], M. Usman[107], Z. Uysal[21b], V. Vacek[131], B. Vachon[103], K. O. H. Vadla[124], T. Vafeiadis[36], C. Valderanis[108], E. Valdes Santurio[47a,47b], M. Valente[155a], S. Valentinetti[23a,23b], A. Valero[161], A. Vallier[101], J. A. Valls Ferrer[161], T. R. Van Daalen[137], P. Van Gemmeren[6], S. Van Stroud[95], I. Van Vulpen[113], M. Vanadia[75a,75b], W. Vandelli[36], M. Vandenbroucke[134], E. R. Vandewall[120], D. Vannicola[150], L. Vannoli[57a,57b], R. Vari[74a], E. W. Varnes[7], C. Varni[17a], T. Varol[147], D. Varouchas[66], K. E. Varvell[146], M. E. Vasile[27b], L. Vaslin[40], G. A. Vasquez[163], F. Vazeille[40], D. Vazquez Furelos[13], T. Vazquez Schroeder[36], J. Veatch[55], V. Vecchio[100], M. J. Veen[113], I. Veliscek[125], L. M. Veloce[154], F. Veloso[129a,129c], S. Veneziano[74a], A. Ventura[69a,69b], A. Verbytskyi[109], M. Verducci[73a,73b], C. Vergis[24], M. Verissimo De Araujo[81b], W. Verkerke[113], J. C. Vermeulen[113], C. Vernieri[142], P. J. Verschuuren[94], M. Vessella[102], M. L. Vesterbacka[116], M. C. Vetterli[141,ab], A. Vgenopoulos[151], N. Viaux Maira[136f], T. Vickey[138], O. E. Vickey Boeriu[138], G. H. A. Viehhauser[125], L. Vigani[63b], M. Villa[23a,23b], M. Villaplana Perez[161], E. M. Villhauer[52], E. Vilucchi[53], M. G. Vincter[34], G. S. Virdee[20], A. Vishwakarma[52], C. Vittori[23a,23b], I. Vivarelli[145], V. Vladimirov[165], E. Voevodina[109], M. Vogel[169], P. Vokac[131], J. Von Ahnen[48], E. Von Toerne[24], B. Vormwald[36], V. Vorobel[132], K. Vorobev[37], M. Vos[161], J. H. Vossebeld[91], M. Vozak[113], L. Vozdecky[93], N. Vranjes[15], M. Vranjes Milosavljevic[15], V. Vrba[131,*], M. Vreeswijk[113], R. Vuillermet[36], O. Vujinovic[99], I. Vukotic[39], S. Wada[156], C. Wagner[102], W. Wagner[169], S. Wahdan[169], H. Wahlberg[89], R. Wakasa[156], M. Wakida[110], V. M. Walbrecht[109], J. Walder[133], R. Walker[108], W. Walkowiak[140], A. M. Wang[61], A. Z. Wang[168], C. Wang[62a], C. Wang[62c], H. Wang[17a], J. Wang[64a], P. Wang[44], R.-

J. Wang[99], R. Wang[61], R. Wang[6], S. M. Wang[147], S. Wang[62b], T. Wang[62a], W. T. Wang[79], W. X. Wang[62a], X. Wang[14c], X. Wang[160], X. Wang[62c], Y. Wang[62d], Z. Wang[105], Z. Wang[62d,51,62c], Z. Wang[105], A. Warburton[103], R. J. Ward[20], N. Warrack[59], A. T. Watson[20], M. F. Watson[20], G. Watts[137], B. M. Waugh[95], A. F. Webb[11], C. Weber[29], M. S. Weber[19], S. A. Weber[34], S. M. Weber[63a], C. Wei[62a], Y. Wei[125], A. R. Weidberg[125], J. Weingarten[49], M. Weirich[99], C. Weiser[54], T. Wenaus[29], B. Wendland[49], T. Wengler[36], N. S. Wenke[109], N. Wermes[24], M. Wessels[63a], K. Whalen[122], A. M. Wharton[90], A. S. White[61], A. White[8], M. J. White[1], D. Whiteson[158], L. Wickremasinghe[123], W. Wiedenmann[168], C. Wiel[50], M. Wielers[133], N. Wieseotte[99], C. Wiglesworth[42], L. A. M. Wiik-Fuchs[54], D. J. Wilbern[119], H. G. Wilkens[36], D. M. Williams[41], H. H. Williams[127], S. Williams[32], S. Willocq[102], P. J. Windischhofer[125], F. Winklmeier[122], B. T. Winter[54], M. Wittgen[142], M. Wobisch[96], A. Wolf[99], R. Wölker[125], J. Wollrath[158], M. W. Wolter[85], H. Wolters[129a,129c], V. W. S. Wong[162], A. F. Wongel[48], S. D. Worm[48], B. K. Wosiek[85], K. W. Woźniak[85], K. Wraight[59], J. Wu[14a,14d], S. L. Wu[168], X. Wu[56], Y. Wu[62a], Z. Wu[134,62a], J. Wuerzinger[125], T. R. Wyatt[100], B. M. Wynne[52], S. Xella[42], L. Xia[14c], M. Xia[14b], J. Xiang[64c], X. Xiao[105], M. Xie[62a], X. Xie[62a], I. Xiotidis[145], D. Xu[14a], H. Xu[62a], H. Xu[62a], L. Xu[62a], R. Xu[127], T. Xu[62a], W. Xu[105], Y. Xu[14b], Z. Xu[62b], Z. Xu[142], B. Yabsley[146], S. Yacoob[33a], N. Yamaguchi[88], Y. Yamaguchi[153], H. Yamauchi[156], T. Yamazaki[17a], Y. Yamazaki[83], J. Yan[62c], S. Yan[125], Z. Yan[25], H. J. Yang[62c,62d], H. T. Yang[17a], S. Yang[62a], T. Yang[64c], X. Yang[62a], X. Yang[14a], Y. Yang[44], Z. Yang[62a,105], W-M. Yao[17a], Y. C. Yap[48], H. Ye[14c], J. Ye[44], S. Ye[29], X. Ye[62a], I. Yeletskikh[38], M. R. Yexley[90], P. Yin[41], K. Yorita[166], C. J. S. Young[54], C. Young[142], M. Yuan[105], R. Yuan[62b,j], X. Yue[63a], M. Zaazoua[35e], B. Zabinski[85], G. Zacharis[10], E. Zaid[52], T. Zakareishvili[148b], N. Zakharchuk[34], S. Zambito[36], D. Zanzi[54], O. Zaplatilek[131], S. V. Zeißner[49], C. Zeitnitz[169], J. C. Zeng[160], D. T. Zenger Jr[26], O. Zenin[37], T. Ženiš[28a], S. Zenz[93], S. Zerradi[35a], D. Zerwas[66], B. Zhang[14c], D. F. Zhang[138], G. Zhang[14b], J. Zhang[6], K. Zhang[14a,14d], L. Zhang[14c], M. Zhang[160], R. Zhang[168], S. Zhang[105], X. Zhang[62c], X. Zhang[62b], Z. Zhang[66], H. Zhao[137], P. Zhao[51], T. Zhao[62b], Y. Zhao[135], Z. Zhao[62a], A. Zhemchugov[38], Z. Zheng[142], D. Zhong[160], B. Zhou[105], C. Zhou[168], H. Zhou[7], N. Zhou[62c], Y. Zhou[7], C. G. Zhu[62b], C. Zhu[14a,14d], H. L. Zhu[62a], H. Zhu[14a], J. Zhu[105], Y. Zhu[62a], X. Zhuang[14a], K. Zhukov[37], V. Zhulanov[37], D. Zieminska[67], N. I. Zimine[38], S. Zimmermann[54,*], J. Zinsser[63b], M. Ziolkowski[140], L. Živković[15], A. Zoccoli[23a,23b], K. Zoch[56], T. G. Zorbas[138], O. Zormpa[46], W. Zou[41], L. Zwalinski[36]

[1] Department of Physics, University of Adelaide, Adelaide, Australia
[2] Department of Physics, University of Alberta, Edmonton, AB, Canada
[3] [(a)]Department of Physics, Ankara University, Ankara, Turkey; [(b)]Division of Physics, TOBB University of Economics and Technology, Ankara, Turkey
[4] LAPP, Univ. Savoie Mont Blanc, CNRS/IN2P3, Annecy, France
[5] APC, Université Paris Cité, CNRS/IN2P3, Paris, France
[6] High Energy Physics Division, Argonne National Laboratory, Argonne, IL, USA
[7] Department of Physics, University of Arizona, Tucson, AZ, USA
[8] Department of Physics, University of Texas at Arlington, Arlington, TX, USA
[9] Physics Department, National and Kapodistrian University of Athens, Athens, Greece
[10] Physics Department, National Technical University of Athens, Zografou, Greece
[11] Department of Physics, University of Texas at Austin, Austin, TX, USA
[12] Institute of Physics, Azerbaijan Academy of Sciences, Baku, Azerbaijan
[13] Institut de Física d'Altes Energies (IFAE), Barcelona Institute of Science and Technology, Barcelona, Spain
[14] [(a)]Institute of High Energy Physics, Chinese Academy of Sciences, Beijing, China; [(b)]Physics Department, Tsinghua University, Beijing, China; [(c)]Department of Physics, Nanjing University, Nanjing, China; [(d)]University of Chinese Academy of Science (UCAS), Beijing, China
[15] Institute of Physics, University of Belgrade, Belgrade, Serbia
[16] Department for Physics and Technology, University of Bergen, Bergen, Norway
[17] [(a)]Physics Division, Lawrence Berkeley National Laboratory, Berkeley, CA, USA; [(b)]University of California, Berkeley, CA, USA
[18] Institut für Physik, Humboldt Universität zu Berlin, Berlin, Germany
[19] Albert Einstein Center for Fundamental Physics and Laboratory for High Energy Physics, University of Bern, Bern, Switzerland

[20] School of Physics and Astronomy, University of Birmingham, Birmingham, UK
[21] [(a)]Department of Physics, Bogazici University, Istanbul, Turkey; [(b)]Department of Physics Engineering, Gaziantep University, Gaziantep, Turkey; [(c)]Department of Physics, Istanbul University, Istanbul, Turkey; [(d)]Istinye University, Sariyer, Istanbul, Turkey
[22] [(a)]Facultad de Ciencias y Centro de Investigaciónes, Universidad Antonio Nariño, Bogotá, Colombia; [(b)]Departamento de Física, Universidad Nacional de Colombia, Bogotá, Colombia
[23] [(a)]Dipartimento di Fisica e Astronomia A. Righi, Università di Bologna, Bologna, Italy; [(b)]INFN Sezione di Bologna, Bologna, Italy
[24] Physikalisches Institut, Universität Bonn, Bonn, Germany
[25] Department of Physics, Boston University, Boston, MA, USA
[26] Department of Physics, Brandeis University, Waltham, MA, USA
[27] [(a)]Transilvania University of Brasov, Brasov, Romania; [(b)]Horia Hulubei National Institute of Physics and Nuclear Engineering, Bucharest, Romania; [(c)]Department of Physics, Alexandru Ioan Cuza University of Iasi, Iasi , Romania; [(d)]Physics Department, National Institute for Research and Development of Isotopic and Molecular Technologies, Cluj-Napoca, Romania; [(e)]University Politehnica Bucharest, Bucharest, Romania; [(f)]West University in Timisoara, Timisoara, Romania
[28] [(a)]Faculty of Mathematics, Physics and Informatics, Comenius University, Bratislava, Slovak Republic; [(b)]Department of Subnuclear Physics, Institute of Experimental Physics of the Slovak Academy of Sciences, Kosice, Slovak Republic
[29] Physics Department, Brookhaven National Laboratory, Upton, NY, USA
[30] Universidad de Buenos Aires, Facultad de Ciencias Exactas y Naturales, Departamento de Física, y CONICET, Instituto de Física de Buenos Aires (IFIBA), Buenos Aires, Argentina
[31] California State University, Long Beach, CA, USA
[32] Cavendish Laboratory, University of Cambridge, Cambridge, UK
[33] [(a)]Department of Physics, University of Cape Town, Cape Town, South Africa; [(b)]iThemba Labs, Western Cape, South Africa; [(c)]Department of Mechanical Engineering Science, University of Johannesburg, Johannesburg , South Africa; [(d)]National Institute of Physics, University of the Philippines Diliman (Philippines), Quezon City , Philippines; [(e)]University of South Africa, Department of Physics, Pretoria, South Africa; [(f)]University of Zululand, Kwadlangezwa, South Africa; [(g)]School of Physics, University of the Witwatersrand, Johannesburg, South Africa
[34] Department of Physics, Carleton University, Ottawa, ON, Canada
[35] [(a)]Faculté des Sciences Ain Chock, Réseau Universitaire de Physique des Hautes Energies - Université Hassan II, Casablanca, Morocco; [(b)]Faculté des Sciences, Université Ibn-Tofail, Kenitra, Morocco; [(c)]Faculté des Sciences Semlalia, Université Cadi Ayyad, LPHEA-Marrakech, Marrakesh, Morocco; [(d)]LPMR, Faculté des Sciences, Université Mohamed Premier, Oujda, Morocco; [(e)]Faculté des sciences, Université Mohammed V, Rabat, Morocco; [(f)]Institute of Applied Physics, Mohammed VI Polytechnic University, Ben Guerir, Morocco
[36] CERN, Geneva, Switzerland
[37] Affiliated with an institute covered by a cooperation agreement with CERN, Geneva, Switzerland
[38] Affiliated with an international laboratory covered by a cooperation agreement with CERN, Geneva, Switzerland
[39] Enrico Fermi Institute, University of Chicago, Chicago, IL, USA
[40] LPC, Université Clermont Auvergne, CNRS/IN2P3, Clermont-Ferrand, France
[41] Nevis Laboratory, Columbia University, Irvington, NY, USA
[42] Niels Bohr Institute, University of Copenhagen, Copenhagen, Denmark
[43] [(a)]Dipartimento di Fisica, Università della Calabria, Rende, Italy; [(b)]INFN Gruppo Collegato di Cosenza, Laboratori Nazionali di Frascati, Italy
[44] Physics Department, Southern Methodist University, Dallas, TX, USA
[45] Physics Department, University of Texas at Dallas, Richardson, TX, USA
[46] National Centre for Scientific Research "Demokritos", Agia Paraskevi, Greece
[47] [(a)]Department of Physics, Stockholm University, Sweden; [(b)]Oskar Klein Centre, Stockholm, Sweden
[48] Deutsches Elektronen-Synchrotron DESY, Hamburg and Zeuthen, Germany
[49] Fakultät Physik , Technische Universität Dortmund, Dortmund, Germany
[50] Institut für Kern- und Teilchenphysik, Technische Universität Dresden, Dresden, Germany
[51] Department of Physics, Duke University, Durham, NC, USA
[52] SUPA-School of Physics and Astronomy, University of Edinburgh, Edinburgh, UK
[53] INFN e Laboratori Nazionali di Frascati, Frascati, Italy

[54] Physikalisches Institut, Albert-Ludwigs-Universität Freiburg, Freiburg, Germany
[55] II. Physikalisches Institut, Georg-August-Universität Göttingen, Göttingen, Germany
[56] Département de Physique Nucléaire et Corpusculaire, Université de Genève, Geneve, Switzerland
[57] [(a)]Dipartimento di Fisica, Università di Genova, Genoa, Italy; [(b)]INFN Sezione di Genova, Genoa, Italy
[58] II. Physikalisches Institut, Justus-Liebig-Universität Giessen, Giessen, Germany
[59] SUPA-School of Physics and Astronomy, University of Glasgow, Glasgow, UK
[60] LPSC, Université Grenoble Alpes, CNRS/IN2P3, Grenoble INP, Grenoble, France
[61] Laboratory for Particle Physics and Cosmology, Harvard University, Cambridge, MA, USA
[62] [(a)]Department of Modern Physics and State Key Laboratory of Particle Detection and Electronics, University of Science and Technology of China, Hefei, China; [(b)]Institute of Frontier and Interdisciplinary Science and Key Laboratory of Particle Physics and Particle Irradiation (MOE), Shandong University, Qingdao, China; [(c)]School of Physics and Astronomy, Shanghai Jiao Tong University, Key Laboratory for Particle Astrophysics and Cosmology (MOE), SKLPPC, Shanghai, China; [(d)]Tsung-Dao Lee Institute, Shanghai, China
[63] [(a)]Kirchhoff-Institut für Physik, Ruprecht-Karls-Universität Heidelberg, Heidelberg, Germany; [(b)]Physikalisches Institut, Ruprecht-Karls-Universität Heidelberg, Heidelberg, Germany
[64] [(a)]Department of Physics, Chinese University of Hong Kong, Shatin N.T., Hong Kong, China; [(b)]Department of Physics, University of Hong Kong, Hong Kong, China; [(c)]Department of Physics and Institute for Advanced Study, Hong Kong University of Science and Technology, Clear Water Bay, Kowloon, Hong Kong, China
[65] Department of Physics, National Tsing Hua University, Hsinchu, Taiwan
[66] IJCLab, Université Paris-Saclay, CNRS/IN2P3, 91405 Orsay, France
[67] Department of Physics, Indiana University, Bloomington, IN, USA
[68] [(a)]INFN Gruppo Collegato di Udine, Sezione di Trieste, Udine, Italy; [(b)]ICTP, Trieste, Italy; [(c)]Dipartimento Politecnico di Ingegneria e Architettura, Università di Udine, Udine, Italy
[69] [(a)]INFN Sezione di Lecce, Lecce, Italy; [(b)]Dipartimento di Matematica e Fisica, Università del Salento, Lecce, Italy
[70] [(a)]INFN Sezione di Milano, Milan, Italy; [(b)]Dipartimento di Fisica, Università di Milano, Milan, Italy
[71] [(a)]INFN Sezione di Napoli, Naples, Italy; [(b)]Dipartimento di Fisica, Università di Napoli, Naples, Italy
[72] [(a)]INFN Sezione di Pavia, Pavia, Italy; [(b)]Dipartimento di Fisica, Università di Pavia, Pavia, Italy
[73] [(a)]INFN Sezione di Pisa, Pisa, Italy; [(b)]Dipartimento di Fisica E. Fermi, Università di Pisa, Pisa, Italy
[74] [(a)]INFN Sezione di Roma, Rome, Italy; [(b)]Dipartimento di Fisica, Sapienza Università di Roma, Rome, Italy
[75] [(a)]INFN Sezione di Roma Tor Vergata, Rome, Italy; [(b)]Dipartimento di Fisica, Università di Roma Tor Vergata, Rome, Italy
[76] [(a)]INFN Sezione di Roma Tre, Rome, Italy; [(b)]Dipartimento di Matematica e Fisica, Università Roma Tre, Rome, Italy
[77] [(a)]INFN-TIFPA, Trento, Italy; [(b)]Università degli Studi di Trento, Trento, Italy
[78] Universität Innsbruck, Department of Astro and Particle Physics, Innsbruck, Austria
[79] University of Iowa, Iowa City, IA, USA
[80] Department of Physics and Astronomy, Iowa State University, Ames, IA, USA
[81] [(a)]Departamento de Engenharia Elétrica, Universidade Federal de Juiz de Fora (UFJF), Juiz de Fora , Brazil; [(b)]Universidade Federal do Rio De Janeiro COPPE/EE/IF, Rio de Janeiro, Brazil; [(c)]Instituto de Física, Universidade de São Paulo, São Paulo, Brazil; [(d)]Rio de Janeiro State University, Rio de Janeiro, Brazil
[82] KEK, High Energy Accelerator Research Organization, Tsukuba, Japan
[83] Graduate School of Science, Kobe University, Kobe, Japan
[84] [(a)]AGH University of Science and Technology, Faculty of Physics and Applied Computer Science, Kraków , Poland; [(b)]Marian Smoluchowski Institute of Physics, Jagiellonian University, Kraków, Poland
[85] Institute of Nuclear Physics Polish Academy of Sciences, Kraków, Poland
[86] Faculty of Science, Kyoto University, Kyoto, Japan
[87] Kyoto University of Education, Kyoto, Japan
[88] Research Center for Advanced Particle Physics and Department of Physics, Kyushu University, Fukuoka, Japan
[89] Instituto de Física La Plata, Universidad Nacional de La Plata and CONICET, La Plata, Argentina
[90] Physics Department, Lancaster University, Lancaster, UK
[91] Oliver Lodge Laboratory, University of Liverpool, Liverpool, UK
[92] Department of Experimental Particle Physics, Jožef Stefan Institute and Department of Physics, University of Ljubljana, Ljubljana, Slovenia
[93] School of Physics and Astronomy, Queen Mary University of London, London, UK

[94] Department of Physics, Royal Holloway University of London, Egham, UK
[95] Department of Physics and Astronomy, University College London, London, UK
[96] Louisiana Tech University, Ruston, LA, USA
[97] Fysiska institutionen, Lunds universitet, Lund, Sweden
[98] Departamento de Física Teorica C-15 and CIAFF, Universidad Autónoma de Madrid, Madrid, Spain
[99] Institut für Physik, Universität Mainz, Mainz, Germany
[100] School of Physics and Astronomy, University of Manchester, Manchester, UK
[101] CPPM, Aix-Marseille Université, CNRS/IN2P3, Marseille, France
[102] Department of Physics, University of Massachusetts, Amherst, MA, USA
[103] Department of Physics, McGill University, Montreal, QC, Canada
[104] School of Physics, University of Melbourne, Parkville, VIC, Australia
[105] Department of Physics, University of Michigan, Ann Arbor, MI, USA
[106] Department of Physics and Astronomy, Michigan State University, East Lansing, MI, USA
[107] Group of Particle Physics, University of Montreal, Montreal, QC, Canada
[108] Fakultät für Physik, Ludwig-Maximilians-Universität München, Munich, Germany
[109] Max-Planck-Institut für Physik (Werner-Heisenberg-Institut), Munich, Germany
[110] Graduate School of Science and Kobayashi-Maskawa Institute, Nagoya University, Nagoya, Japan
[111] Department of Physics and Astronomy, University of New Mexico, Albuquerque, NM, USA
[112] Institute for Mathematics, Astrophysics and Particle Physics, Radboud University/Nikhef, Nijmegen, The Netherlands
[113] Nikhef National Institute for Subatomic Physics and University of Amsterdam, Amsterdam, The Netherlands
[114] Department of Physics, Northern Illinois University, DeKalb, IL, USA
[115] [(a)]New York University Abu Dhabi, Abu Dhabi, United Arab Emirates; [(b)]United Arab Emirates University, Al Ain, United Arab Emirates; [(c)]University of Sharjah, Sharjah, United Arab Emirates
[116] Department of Physics, New York University, New York, NY, USA
[117] Ochanomizu University, Otsuka, Bunkyo-ku, Tokyo, Japan
[118] Ohio State University, Columbus, OH, USA
[119] Homer L. Dodge Department of Physics and Astronomy, University of Oklahoma, Norman, OK, USA
[120] Department of Physics, Oklahoma State University, Stillwater, OK, USA
[121] Palacký University, Joint Laboratory of Optics, Olomouc, Czech Republic
[122] Institute for Fundamental Science, University of Oregon, Eugene, OR, USA
[123] Graduate School of Science, Osaka University, Osaka, Japan
[124] Department of Physics, University of Oslo, Oslo, Norway
[125] Department of Physics, Oxford University, Oxford, UK
[126] LPNHE, Sorbonne Université, Université Paris Cité, CNRS/IN2P3, Paris, France
[127] Department of Physics, University of Pennsylvania, Philadelphia, PA, USA
[128] Department of Physics and Astronomy, University of Pittsburgh, Pittsburgh, PA, USA
[129] [(a)]Laboratório de Instrumentação e Física Experimental de Partículas-LIP, Lisbon, Portugal; [(b)]Departamento de Física, Faculdade de Ciências, Universidade de Lisboa, Lisbon, Portugal; [(c)]Departamento de Física, Universidade de Coimbra, Coimbra, Portugal; [(d)]Centro de Física Nuclear da Universidade de Lisboa, Lisbon, Portugal; [(e)]Departamento de Física, Universidade do Minho, Braga, Portugal; [(f)]Departamento de Física Teórica y del Cosmos, Universidad de Granada, Granada, Spain; [(g)]Instituto Superior Técnico, Universidade de Lisboa, Lisbon, Portugal
[130] Institute of Physics of the Czech Academy of Sciences, Prague, Czech Republic
[131] Czech Technical University in Prague, Prague, Czech Republic
[132] Charles University, Faculty of Mathematics and Physics, Prague, Czech Republic
[133] Particle Physics Department, Rutherford Appleton Laboratory, Didcot, UK
[134] IRFU, CEA, Université Paris-Saclay, Gif-sur-Yvette, France
[135] Santa Cruz Institute for Particle Physics, University of California Santa Cruz, Santa Cruz, CA, USA
[136] [(a)]Departamento de Física, Pontificia Universidad Católica de Chile, Santiago, Chile; [(b)]Millennium Institute for Subatomic physics at high energy frontier (SAPHIR), Santiago, Chile; [(c)]Instituto de Investigación Multidisciplinario en Ciencia y Tecnología y Departamento de Física, Universidad de La Serena, La Serena, Chile; [(d)]Department of Physics, Universidad Andres Bello, Santiago, Chile; [(e)]Instituto de Alta Investigación, Universidad de Tarapacá, Arica, Chile ; [(f)]Departamento de Física, Universidad Técnica Federico Santa María, Valparaiso, Chile
[137] Department of Physics, University of Washington, Seattle, WA, USA

[138] Department of Physics and Astronomy, University of Sheffield, Sheffield, UK
[139] Department of Physics, Shinshu University, Nagano, Japan
[140] Department Physik, Universität Siegen, Siegen, Germany
[141] Department of Physics, Simon Fraser University, Burnaby, BC, Canada
[142] SLAC National Accelerator Laboratory, Stanford, CA, USA
[143] Department of Physics, Royal Institute of Technology, Stockholm, Sweden
[144] Departments of Physics and Astronomy, Stony Brook University, Stony Brook, NY, USA
[145] Department of Physics and Astronomy, University of Sussex, Brighton, UK
[146] School of Physics, University of Sydney, Sydney, Australia
[147] Institute of Physics, Academia Sinica, Taipei, Taiwan
[148] [(a)]E. Andronikashvili Institute of Physics, Iv. Javakhishvili Tbilisi State University, Tbilisi, Georgia; [(b)]High Energy Physics Institute, Tbilisi State University, Tbilisi, Georgia; [(c)]University of Georgia, Tbilisi, Georgia
[149] Department of Physics, Technion, Israel Institute of Technology, Haifa, Israel
[150] Raymond and Beverly Sackler School of Physics and Astronomy, Tel Aviv University, Tel Aviv, Israel
[151] Department of Physics, Aristotle University of Thessaloniki, Thessaloniki, Greece
[152] International Center for Elementary Particle Physics and Department of Physics, University of Tokyo, Tokyo, Japan
[153] Department of Physics, Tokyo Institute of Technology, Tokyo, Japan
[154] Department of Physics, University of Toronto, Toronto, ON, Canada
[155] [(a)]TRIUMF, Vancouver, BC, Canada; [(b)]Department of Physics and Astronomy, York University, Toronto, ON, Canada
[156] Division of Physics and Tomonaga Center for the History of the Universe, Faculty of Pure and Applied Sciences, University of Tsukuba, Tsukuba, Japan
[157] Department of Physics and Astronomy, Tufts University, Medford, MA, USA
[158] Department of Physics and Astronomy, University of California Irvine, Irvine, CA, USA
[159] Department of Physics and Astronomy, University of Uppsala, Uppsala, Sweden
[160] Department of Physics, University of Illinois, Urbana, IL, USA
[161] Instituto de Física Corpuscular (IFIC), Centro Mixto Universidad de Valencia - CSIC, Valencia, Spain
[162] Department of Physics, University of British Columbia, Vancouver, BC, Canada
[163] Department of Physics and Astronomy, University of Victoria, Victoria, BC, Canada
[164] Fakultät für Physik und Astronomie, Julius-Maximilians-Universität Würzburg, Würzburg, Germany
[165] Department of Physics, University of Warwick, Coventry, UK
[166] Waseda University, Tokyo, Japan
[167] Department of Particle Physics and Astrophysics, Weizmann Institute of Science, Rehovot, Israel
[168] Department of Physics, University of Wisconsin, Madison, WI, USA
[169] Fakultät für Mathematik und Naturwissenschaften, Fachgruppe Physik, Bergische Universität Wuppertal, Wuppertal, Germany
[170] Department of Physics, Yale University, New Haven, CT, USA

[a] Also Affiliated with an institute covered by a cooperation agreement with CERN, Geneva, Switzerland
[b] Also at Borough of Manhattan Community College, City University of New York, New York, NY, USA
[c] Also at Bruno Kessler Foundation, Trento, Italy
[d] Also at Center for High Energy Physics, Peking University, Beijing, China
[e] Also at Centro Studi e Ricerche Enrico Fermi, Rome, Italy
[f] Also at CERN, Geneva, Switzerland
[g] Also at Département de Physique Nucléaire et Corpusculaire, Université de Genève, Geneva, Switzerland
[h] Also at Departament de Fisica de la Universitat Autonoma de Barcelona, Barcelona, Spain
[i] Also at Department of Financial and Management Engineering, University of the Aegean, Chios, Greece
[j] Also at Department of Physics and Astronomy, Michigan State University, East Lansing, MI, USA
[k] Also at Department of Physics and Astronomy, University of Louisville, Louisville, KY, USA
[l] Also at Department of Physics, Ben Gurion University of the Negev, Beer Sheva, Israel
[m] Also at Department of Physics, California State University, East Bay, USA
[n] Also at Department of Physics, California State University, Sacramento, USA
[o] Also at Department of Physics, King's College London, London, UK
[p] Also at Department of Physics, University of Fribourg, Fribourg, Switzerland

[q] Also at Hellenic Open University, Patras, Greece
[r] Also at Institucio Catalana de Recerca i Estudis Avancats, ICREA, Barcelona, Spain
[s] Also at Institut für Experimentalphysik, Universität Hamburg, Hamburg, Germany
[t] Also at Institute of Particle Physics (IPP), Montreal, Canada
[u] Also at Institute of Physics, Azerbaijan Academy of Sciences, Baku, Azerbaijan
[v] Also at Institute of Theoretical Physics, Ilia State University, Tbilisi, Georgia
[w] Also at Instituto de Fisica Teorica, IFT-UAM/CSIC, Madrid, Spain
[x] Also at Physics Department, An-Najah National University, Nablus, Palestine
[y] Also at Physikalisches Institut, Albert-Ludwigs-Universität Freiburg, Freiburg, Germany
[z] Also at The City College of New York, New York, NY, USA
[aa] Also at The Collaborative Innovation Center of Quantum Matter (CICQM), Beijing, China
[ab] Also at TRIUMF, Vancouver, BC, Canada
[ac] Also at Università di Napoli Parthenope, Naples, Italy
[ad] Also at University of Chinese Academy of Sciences (UCAS), Beijing, China
[ae] Also at Yeditepe University, Physics Department, Istanbul, Turkey
[*] Deceased